Alexander Königseder, BSc

Investigation of the Thermal Runaway in Lithium Ion batteries

MASTERARBEIT

zur Erlangung des akademischen Grades

Master of Science

Masterstudium Umweltsystemwissenschaften-
Naturwissenschaftliche Technologien

eingereicht an der

Technischen Universität Graz

Laborbetreuung: Dipl.-Ing. Michael Lammer
Betreuer und Beurteilung: Assoc. Prof. Dipl.-Ing. Dr.techn. Viktor Hacker

Institut für Chemische Verfahrenstechnik und Umwelttechnik
der Technischen Universität Graz

Graz, März 2017

Zusammenfassung

Lithium-Ionen-Akkumulatoren zeichnen sich durch ihre hohe Energiedichte, Zellspannung und Zyklenfestigkeit aus und sind mittlerweile der dominierende Energiespeicher für tragbare und mobile Anwendungen wie Smartphones, Laptops und Elektromobilität. Jedoch gibt es erhebliche Sicherheitsbedenken bezüglich der thermischen Stabilität dieses Batterietypes. Im Zuge dieser Arbeit wurden neun unterschiedliche Lithium-Ionen-Zellen mit zwei verschiedenen Kathodenmaterialien $LiNi_{0.8}Co_{0.15}Al_{0.05}O_2$ (NCA) und $LiNi_{1/3}Mn_{1/3}Co_{1/3}O_2$ (NMC) hinsichtlich deren thermischen Verhaltens untersucht. Die zylindrischen Zellen des Formates 18650 wurden dazu in einem Rohrreaktor einer thermischen Rampe unterworfen. Mit Thermoelementen wurde die Temperatur im Reaktor, am Probenhalter, und an der Zelle gemessen. Die Zellspannung wurde aufgezeichnet und die von den Zellen emittierten Gase analysiert. Während des Aufheizens finden in den Zellen exotherme Zersetzungreaktionen statt, welche zu einer beschleunigten Erwärmung führen. Ohne ausreichende Wärmeabfuhr führt dies zu der Entstehung von brennbaren und potentiell toxischen Gasen und letztendlich zu der Zerstörung der Zelle. Zelltemperaturen von über 780 °C und gemittelte Aufheizraten von über 140 °C min^{-1} wurden während des thermischen Durchgehens der Zellen gemessen. Das dabei emittierte Gas mit einem Volumen von bis zu 5,9 Liter enthielt Kohlendioxid, Kohlenmonoxid, Wasserstoff und in geringerem Umfang kurzkettige Kohlenwasserstoffe.

Abstract

Lithium ion (Li-ion) batteries are characterized by their high energy density, cell voltage and good cycle stability. Despite their widespread use for mobile applications and in the field of electro mobility there are still safety concerns regarding the thermal instability of this battery type. In this work the thermal behavior of nine types of 18650 format Li-ion batteries with $LiNi_{0.8}Co_{0.15}Al_{0.05}O_2$ (NCA) and $LiNi_{1/3}Mn_{1/3}Co_{1/3}O_2$ (NMC) positive electrode materials were investigated during thermal ramp experiments inside a tubular reactor. Thermocouples were used to measure the temperature of the reactor, sample holder and the cell. In addition the cell voltage was measured and the gases emitted by the cells were investigated. During the slow heat up, the cell constituents undergo several exothermic degradation processes. This exothermic reactions lead to a self promoting heating and can end in violent disintegration of the cell accompanied by a significant heat generation and the release of flammable and potentially toxic gases. Cell temperatures as high as 780 °C have been measured with averaged heating rates as high as 140 °C min^{-1} during thermal runaway. The amount of gas emitted was as high as 5.9 liters and mainly consisted of carbon dioxide, carbon monoxide, hydrogen and small quantities of short chained hydrocarbons.

EIDESSTATTLICHE ERKLÄRUNG
AFFIDAVIT

Ich erkläre an Eides statt, dass ich die vorliegende Arbeit selbstständig verfasst, andere als die angegebenen Quellen/Hilfsmittel nicht benutzt, und die den benutzten Quellen wörtlich und inhaltlich entnommenen Stellen als solche kenntlich gemacht habe. Das in TUGRAZonline hochgeladene Textdokument ist mit der vorliegenden Masterarbeit identisch.

I declare that I have authored this thesis independently, that I have not used other than the declared sources/resources, and that I have explicitly indicated all material which has been quoted either literally or by content from the sources used. The text document uploaded to TUGRAZonline is identical to the present master's thesis.

_____   _____
Datum / Date   Unterschrift / Signature

Acknowledgements

First of all I would like to thank Assoc. Prof. Dipl.-Ing. Dr. techn. Viktor Hacker for giving me the chance to be a part of his aspiring research team. It was very enriching for me to get a deep insight into the academic research routine and the daily duties that accompany it. I would also like to thank Univ.-Prof. Dipl.-Ing. Dr. techn. Matthäus Siebenhofer in his function as head of the Institute of Chemical Engineering and Environmental Technology at the University of Technology Graz.

My special thanks goes to Dipl.-Ing. Michael Lammer who gave me opportunity to work with him on the project ISALIB and write this thesis. With his pleasant and precise nature he made it very easy for me to work with him and I was able to gain a lot from our collaborative work. He always had an ear for me and took the time to discuss relevant issues.

I would also like to thank the whole staff at the Institute of Chemical Engineering and Environmental Technology and especially the members of the fuel cell group under Prof. Hacker. They made me feel immediately as a part of the team and made my time there a memorable one.

Content

1   INTRODUCTION

Climate change and its effects on nature and humanity is coming more and more into the focus of the public eye. The consequences of constantly increasing greenhouse gas emissions in the atmosphere such as rising temperature and sea levels, acidification of the oceans, extended droughts as well as more frequent floodings can be attributed to the anthropogenic burning of fossil fuels [1]. As a result political leaders pass bills and make international agreements to significantly cut down carbon emissions. In order to keep the impact of climate change moderate, new ways of energy production and utilization must be found. For that reason scientists and companies around the world are looking for alternative ways to produce and store the energy of renewable resources. These technologies have to overcome the various advantages of fossil fuels while competing with their relatively low price. The advantages of fossil fuels are mainly their easy availability, well established infrastructure, high energy density and good transportability. Most renewables such as wind, hydro and solar power have the disadvantage of not being available constantly and everywhere. Therefore one of the main bottle necks for the development of a sustainable energy system is the storage of electricity from alternative, delocalized sources. Great expectations and intense research effort is put into a hydrogen based system for energy storage and utilization. Hydrogen can be easily produced by electrolysis of water and the well-developed natural gas infrastructure can be used for distribution. Nevertheless the overall efficiency of the hydrogen generation with electrolysis is still moderate. Some work is also done to develop compressed air energy storage systems (CAES) where a turbine compresses air into a compartment and generates electricity when expanding it again. But the associated heat generation is limiting the process significantly. For small to medium applications an additional technology has gained remarkable momentum over the last two decades. This technology is the electrochemical energy storage in lithium ion batteries.

Since its market introduction in the early 1990s the Li-ion battery technology was a real success story and has enabled the production of smartphones and tablets with big screens and high processor power in the first place. Pristine, conventional battery types wouldn´t be able to provide sufficient energy for those applications. Nowadays Li-ion batteries are largely used in portable devices such as smartphones, notebooks and tablets, power tools, camcorders, small scale household energy storage and to a constantly increasing amount in the transportation sector for hybrid or fully electric vehicles. Figure 1 gives an overview of the impressive development of the Li-ion market and the shares of the main applications.
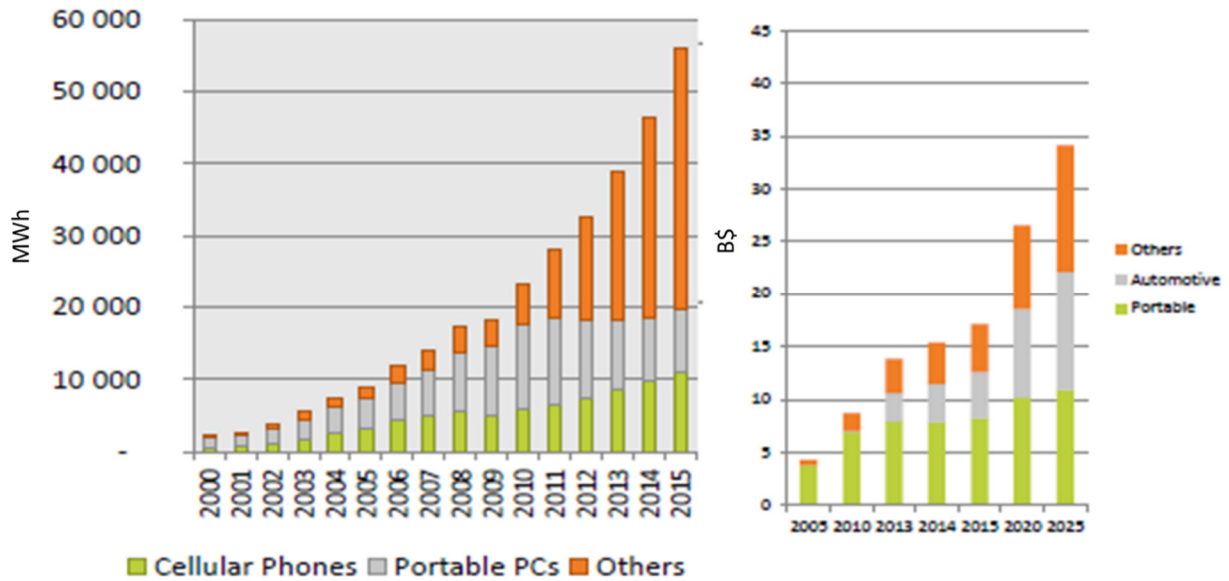
Figure 1: Worldwide sales development of Li-ion batteries in MWh/sold per year (left) and development and outlook of the worldwide market up to 2025 in B$ on the right side [2].

With a constant increase in capacity and the start of mass production by different competitors the prices have dropped significantly while the production amount grew annually. Li-ion batteries have several advantages over conventional nickel metal hydride (NiMH) or lead acid batteries, making them the technology of choice especially for portable applications where high volumetric energy density is needed. They have a higher nominal voltage due to their anode and cathode materials, higher capacity and energy density as well as almost no memory effect and a longer shelf life. They can be charged and discharged quickly with rates several times their capacity. For usage as power supply for automotive applications high gravimetric energy and power is needed to maximize range and acceleration. Figure 2 gives an overview of the specific energy and power of several technologies for automotive applications as well as the desired goals for hybrid electric vehicles (HEV), plug in hybrid electric vehicles (PHEV) and electric vehicles (EV). The specific energy of batteries (the capacity for storing energy per kilogram of weight) is still only around 1-2 percent of the specific energy of gasoline. Unless there is a major breakthrough, batteries will continue to limit the driving range of electric vehicles to some 250 to 300 kilometers between charges [3]. Specific power is especially important in hybrid vehicles because they charge/discharge a small amount of energy quickly. In pure electric vehicles specific energy is more important, though. It has to be the goal of the industry to strongly increase the nominal energy densities of the whole battery packs since the packs make up around 25 percent of the weight of the whole car, thus limiting the range even more [3]. It can be clearly seen that the internal combustion (IC) engine still has the best characteristics regarding specific energy as well as specific power. But the efficiency of combustion engines is limited by Carnot's theorem. Because much heat is generated which can´t be used, their efficiency is normally only around 40 percent. The good energy result is mostly due to the high specific energies of the liquid fuels which are near to 13.000 Wh/kg [3].
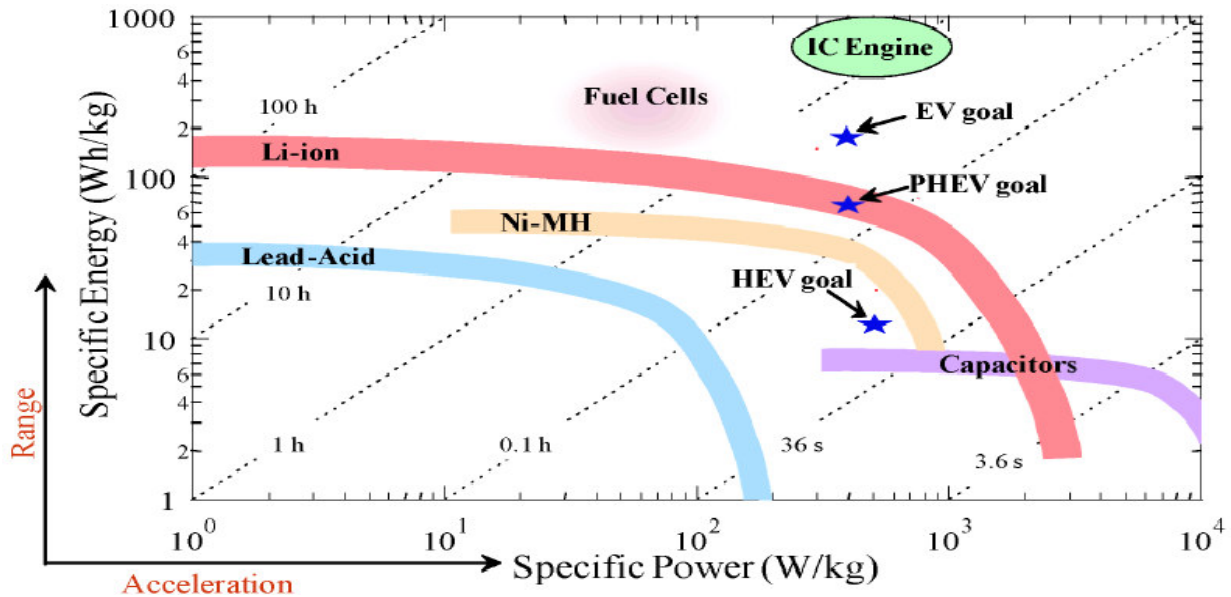
Figure 2: Ragone plot comparing several electrochemical energy storage technologies with the traditional internal combustion engine. More specific energy increases the range while a higher specific power leads to a better acceleration of automotive applications [4].

Despite all their favorable features it must be noted that batteries contain both the fuel (negative electrode) as well as the oxidizer (positive electrode) emerged in an often flammable electrolyte and closely packed in a sealed containment. With this unavoidable construction form comes an immanent risk for direct reactions between fuel and oxidizer. During normal operating conditions Li-ion batteries electrochemically convert this energy into electricity and can be regarded as relatively safe. Nevertheless there have been some serious incidents and accidents related to the self heating of Li-ion batteries. In 2006 Sony had to recall almost as many as 6 million Li-ion laptop batteries after numerous reports of spontaneous self-igniting accumulators used in Apple and Dell notebooks [5]. Several fire incidents have been reported onboard cargo and passenger airplanes which can be traced back to the overheating of batteries [6]. There are serious safety concerns especially under abnormal or abusive conditions such as increased temperatures, short circuits, mechanical damage, overcharge or underdischarge. Under these exceptional conditions the cells can develop a significant amount of heat which in the worst case can lead to a catastrophic, self-promoting event called thermal runaway (TR). Thermal runaway is an event where the cell materials are inadvertently able to react directly inside the cell which leads to an undesirable amount of heat generated by the cell. Thermal runaway can be triggered by abusive conditions or by internal failures and might happen spontaneously even several days after the provoking event [7]. If the exothermic heat generation in the cell is higher than the heat that is dissipated by the surface of the cell, it will heat up to a point where an exothermic breakdown of its constituents occurs. The rapid thermally induced degeneration of the cell material is accompanied by the production of flammable and toxic gases [6]. The possibilities to stop this positive-feedback loop event are very limited and represent a major challenge for battery management systems.

1.1 Working principle and structure of Li-ion batteries

Li-ion batteries are mostly produced as prismatic, cylindrical or pouch cells with metals or polymers used as housing material. A clear distinction is made between Li-ion batteries and lithium polymer batteries. The main difference between them is the electrolyte which is in a liquid (Li-ion) or in a polymer state (Li-polymer). Despite the type of electrolyte both technologies are quite similar and the cell design has little influence on the mode of operation. This work solely investigates cylindrical Li-ion cells in the 18650 format, therefore the following brief introduction to the working principles and state of the art will deal with this type of batteries only.

A standard, rechargeable 18650 Li-ion battery consists of a positive (cathode) and negative (anode) electrode isolated by a separator and wetted with the ion conducting electrolyte. These basic main parts are coiled and built into a stainless steel can closed with a cap acting as positive terminal. The cell itself has a diameter of 18 mm and an overall length of 65 mm with manufacturer dependent tolerances of +/- 0.5 mm. The design configuration of such a cell can be seen in Figure 3.
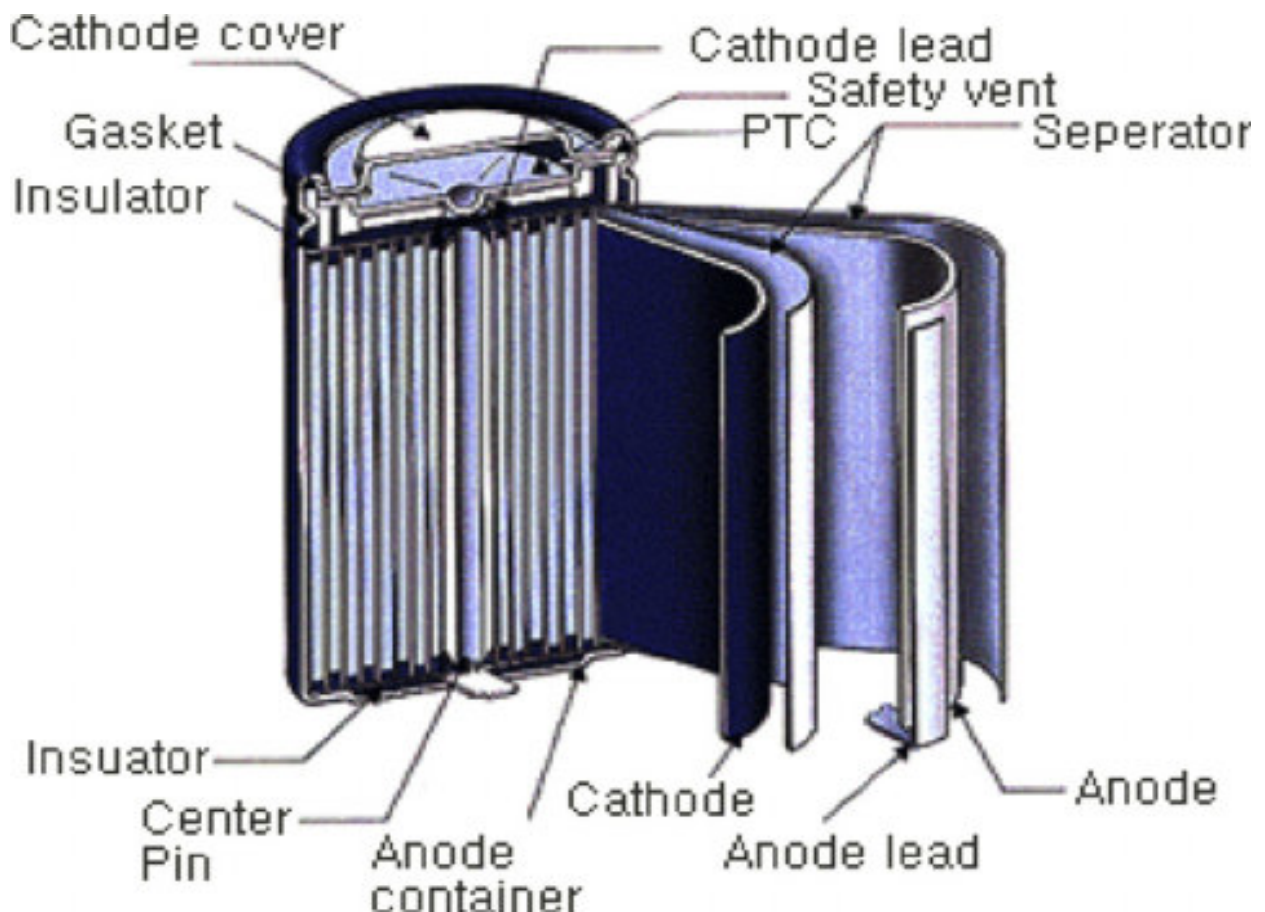
Figure 3: Design configuration of a standardized cylindrical Li-ion cell [8].

Small conductive leads are used to connect the electrodes to the casing and the cathode cover which closes the cell housing. The cathode cover typically also contains a safety vent which allows the safe release of gases when pressure builds up inside the cell. A positive temperature coefficient (PTC) disk in the cap is limiting the current flow when it gets heated up in consequence of unnatural high discharge rates.

When charging a Li-ion battery the Li^+ ions move from the positive electrode which typically consist of a lithium metal oxide through the separator into the graphite based negative electrode, arranging between the oppositely charged carbon layers. Both electrodes allow the ions to move in and out of their structure. This reversible process is called insertion or intercalation of Li^+ ions. While discharging, the ions move back from the negative electrode to the positive one, therefore forcing the electrons over a closed external circuit where electric work is executed. Figure 4 illustrates the movement of the lithium ions inside the cell, the electron movement in the external circuit and it is also showing the intercalation of the ions between the graphite and cobalt oxide layers.
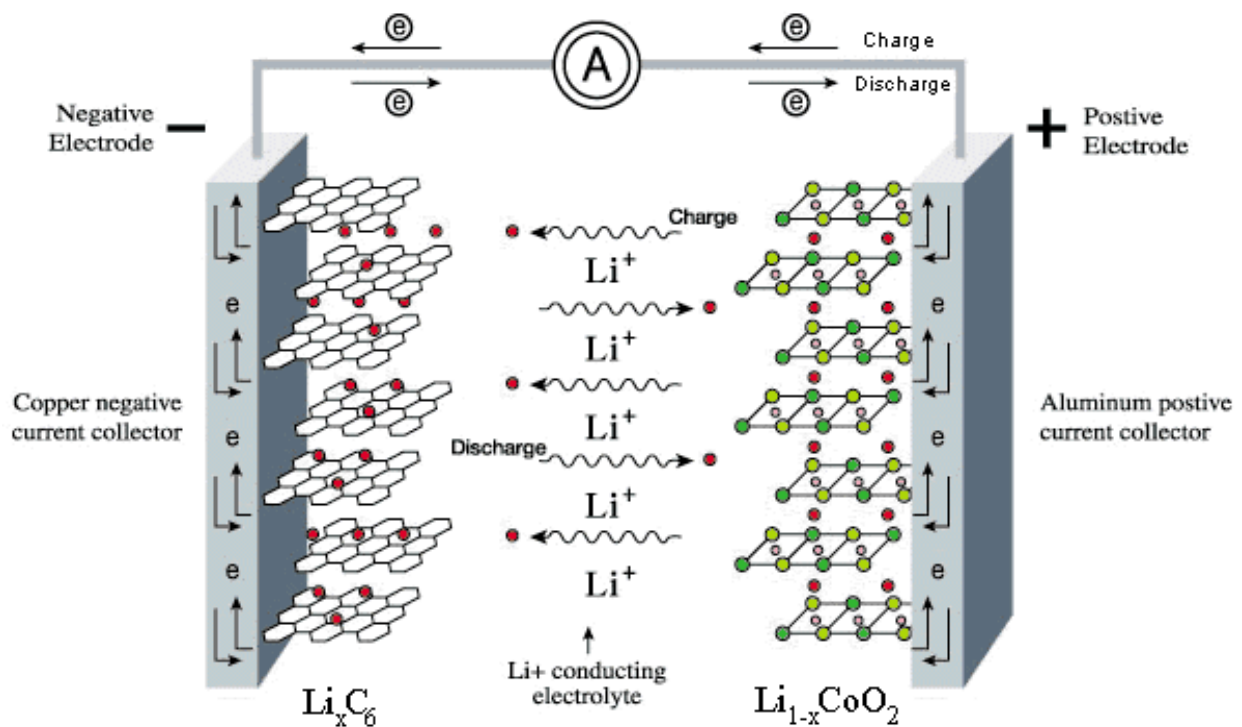
Figure 4: Schematic illustration of a $LiCoO_2$/C battery showing the reversible intercalation of Li-ions in the electrode or cathode structure [9].

Negative electrode (Anode): $Li^+ + e^- + C_6 \rightarrow LiC_6$ (Eq. 1)

Positive electrode (Cathode): $LiCoO_2 \rightarrow CoO_2 + Li^+ + e^-$ (Eq. 2)

Overall: $Li_{1-x}CoO_2 + Li_xC_n \leftrightarrow LiCoO_2 + {}_nC$ (Eq. 3)
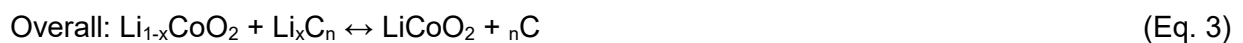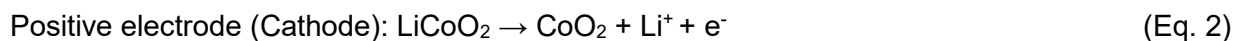
As in all batteries, the basic manner of function in Li-ion batteries is based on redox reactions between the two electrodes (Eq. 1-3). When discharged the positive electrode acts as electron - acceptor while the negative electrode acts as electron donor. The cell voltage is a result of the difference in Gibbs free energy of the Li^+ ions between the two electrodes and decreases during discharge, as the equilibrium electrode potentials are a result of the lithium concentration [10]. This process has its limits which are defined mainly by the cathode materials. Materials such as $Li_{0.0}FePO_4$ are fully delithiated when charged completely to a State of Charge (SoC) of 100 percent while $Li_{0.5}CoO_2$ still has half of its lithium ions intercalated between the cathode layers.

LIBs are typically charged by a constant current/constant voltage (CC/CV) mode at a voltage around 4.20 V. Their typical (nominal) voltage is 3.70 V. The end of discharge is reached when the negative electrode is depleted of freely available lithium ions and cell voltage drops to the cutoff voltage of around 2.75 V. Overcharging and underdischarging has to be prevented by monitoring systems in order to avoid irreversible damage to the cells.

The positive electrode (typically referred to as cathode) consist of an aluminum foil acting as current collector and carrier of the cathode active material. Binder materials such as polyvinylidene fluoride (PVDF) are used to increase the stability of the active material on the current collector foil of the cathode. To increase the electrical conductivity between the active material and the current collector foil, additives are blended in. It is assumed, that 2.5–5% of carbon black is used as conducting agent for cathodes [11]. There are several different cathode active materials used in today´s batteries with very distinct properties which have a major influence on cell performance and safety [5]. Most commercial available cathode materials are transition metal oxides such as $LiCoO_2$, $Li(NiMnCo)O_2$ and $Li(NiCoAl)O_2$.

Figure 5 displays spider web diagrams of some of the most common cathode materials for automotive applications and gives a good overview of the strengths and weaknesses of each material. The cathode materials are evaluated regarding their specific energy (how much energy the battery can store per kilogram of weight), specific power (how much power the battery can store per kilogram mass), safety, performance (peak power at low temperatures, SoC measurements and thermal management), life span (charge and discharge cycles as well as overall battery age) and cost [3].
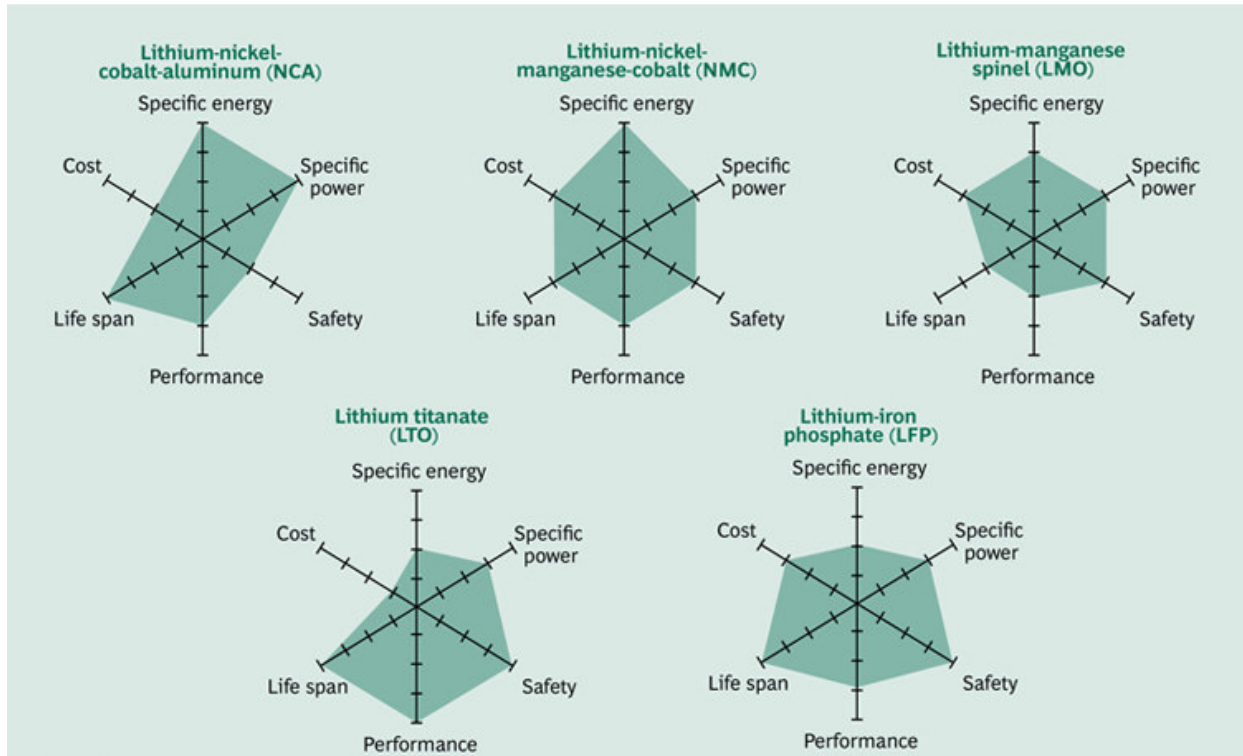
Figure 5: Spider web diagrams of common cathode materials for automotive applications regarding their performance aspects; the further the shapes extend among a given axis the better/higher the value [3].

As can be seen from Figure 5 every cathode material has tradeoffs and isn´t superior in all six categories. There are always drawbacks and compromises to be made when choosing a material for a certain application. For example the lithium nickel cobalt aluminum (NCA) cathode material has a very high specific energy and power combined with a long life span. But because of its high cost and poor safety performance it is not well suited for large automotive uses. Lithium iron phosphate (LFP) is regarded as a very safe and cost effective material but is seriously lacking capability and performance. While lithium cobalt oxide (LCO) is still the most common cathode material for small applications, it also has the drawback of including large amounts of high cost cobalt as well as having a very low thermal stability and is therefore not well suited for large scale automotive applications and not included in the figure above.

The thermal response of cathode active materials at elevated temperatures were investigated with accelerated rate calorimetry (ARC) by numerous research groups [7, 12, 13, 14, 15].
The accelerated rate calorimetry measurements at elevated temperatures are an excellent tool to precisely show chemical and thermal instabilities of single cell components or complete cells. Generally it can be said that cathode materials that are prone to evolve oxygen when decomposed show stronger thermal responses. They show lower thermal runaway onset temperatures and higher heating rates. Car manufacturers have to decide if they are willing to choose a rather unstable but high performance battery type which will oblige them to invest more in the (active) cooling of the battery packs and a more sophisticated battery management system or if they are

going for a lower energy battery type such as lithium iron phosphate (LFP) which is significantly safer and cheaper but will limit the range of the vehicle. It has to be mentioned that safety is, next to costs, the most important aspect for electric cars today. Since the technology is still emerging, a catastrophic battery fire event could turn public opinion against it and set back the technology substantially. Due to the high influence of cathode materials for battery performance and safety, extensive research is done to develop advanced materials which deliver high performance, long cycle life while having a high thermal stability. The cost factor plays a major role in developing new cathodes since almost 50 percent of manufacturing costs derive solely from the purchase of resources for active cathode materials [3]. Although the extensive research efforts from many different university and industrial players, it is believed that several cathode chemistries will coexist for the next few years and no major breakthrough will alter the contemporary market diversity [3].

The negative electrode (referred to as anode) consists of a copper foil with the active material attached to it. Although many different carbonaceous materials like coke and tailored carbon spherical particles such as meso-carbon micro beads (MCMB) can act as negative electrode material, mostly pure graphite is used as anode with variations in morphology, particle size, active material layer thickness and small fractions of stability enhancing materials blended in [7]. The materials are chosen to have high capacity, high rate capability, low irreversible loss during cycling, low expansion of the material during charge/discharge and good thermal stability. Equally to cathode materials also anode materials react with the electrolyte which leads to degradation reactions when thermally stressed. When cells are initially charged in the factory after assembling, some of the lithium incorporated in the cathode is irreversibly lost on the anode surface to form the solid electrolyte interface (SEI) because of complex reduction reactions between the electrolyte, SEI-improving additives such as vinylene carbonate (VC) and the carbonaceous anode material. This loss can be roughly as high as 10 percent of the initial capacity [11]. The SEI is lowering the ion conductivity on the anode and is limiting the capacity. But a well-developed solid electrolyte interface is necessary to prevent further electrolyte reduction. Similar to cathodes also anode materials are under extensive research to make them more stable while increasing the capacity. Silicon has the ability to incorporate lithium tightly but owing to its increase in size during this intercalation it is not well suited for standardized cells. Some manufacturers already add small amounts of Si to the graphite to achieve slight increases in capacity. Due to the low cost of anode materials and their abundance the reduction of costs for anode materials is not as important as for the cathode active materials [3].

The separator is a thin polymer foil between the entire anode and cathode surface and allows for ion conductivity between both electrodes while preventing electronic conductivity (short circuits) even under abusive conditions. Materials for separators in liquid electrolyte cells must be chemically stable, have a homogeneous permeability to ensure uniform current distribution and a porosity below 1 μm to prevent penetration of particles from the electrodes and hold sufficient electrolyte [10]. Common separator materials are thin sheets of polypropylene (PP) and polyethylene (PE) layers which are mostly arranged in a PE-PP or PP-PE-PP sandwich layout [11]. Separators must be resistant to thermal shrinkage to prevent short circuits. PE closes its pores at a temperature near 130 °C to interrupt further ion conductivity while the separator remains mechanically stable until the melting point of PP at around 165 °C [6]. To increase the mechanical stability and strength of the separator without sacrificing the ion conductivity and cell performance, Al_2O_3 nano-particle coated separators have been developed and are used by several manufacturers [3].

The electrolyte enables ion conductivity between the electrodes as a result of the dissolved ionic salts. The Li^+ cations act as charge carrier between the electrodes when the battery is charged/discharged. Li-ion based batteries use non-aqueous electrolytes with lithium salts such as $LiPF_6$, $LiBF_6$, $LiClO_4$ [10]. The conductive salts contain a non coordinating anion with extensive charge delocalization. For best conductivity the anions should be big, highly dissociated and have a high mobility. Big anions are favored because the wide distance between anion charge centers and Li^+ cations in the salt weakens the coulomb forces. The mobility of big anions is small however [10].

Most electrolytes use a mixture of linear and cyclic carbonates. Typically ethylene carbonate (EC), ethyl methyl carbonate (EMC) and dimethyl carbonate (DMC) is used in various ratios. Customarily $LiPF_6$ is used for most commercially available Li-ion cells in a concentration range between 1-1.2 M [11].

Several safety devices are used internal or external of Li-ion cells and battery packs to either prevent a catastrophic event from happening or minimize the severity of the outcome if it occurs [5]:

- **Cell vent or tear-off tab**: A burst opening in the top cap of the cell which ensures a safe release of gases and electrolyte when the internal cell pressure reaches a certain level. The venting of the gases also leads to a cooling of the cell due to the Joule-Thomson effect which may prevent the cell from going into thermal runaway.
- **Shutdown separator**: The separator between anode and cathode prevents ionic conduction if the cell gets heated up. Thus further charge or discharge is limited due to the melting and blocking of its ion permeable pores.
- **PTC disks**: The positive temperature coefficient disks in the cell's head space limits the current due to a sharply higher resistance when heated up.
- **Current Interrupt Device**: Terminates the current flow permanently if a certain cell pressure is reached.
- **Diodes**: They might be used to block reversed polarity or as bypass diodes to protect weak cells.
- **Battery Management Systems (BMS)**: The BMS protects the cells of a battery pack or module against over-/undervoltage, high current charging or discharging and excess temperature. It is also vital to make sure the single cells in a module are all balanced and no additional stress is applied to cells of poor performance.

As mentioned earlier there are several failure modes for Li-ion batteries which compromise the safety of the technology. They must be fully understood and their probability of event must be minimized to ensure the user´s health and prevent them from physical or financial harm. Catastrophic battery failures also have the potential to hinder the development of the emerging electric vehicle market via bad publicity. Production related spontaneous internal failures are called field failures and mainly arise from internal short circuits due to contamination or bad production practice. These field failures are rare since serious manufacturers perform X-ray inspection and high-potentiometer testing before shipping and sale. Most battery failures happen because of abusive or abnormal working conditions and environments. To fully understand and evaluate the behavior and the processes happening inside the cell or battery pack several abuse tests have been established. They can be grouped into three major categories [5]:

- **Thermal abuse:** thermal stability, thermal ramp experiments, elevated temperature storage and thermal shock cycling.
- **Electrical abuse:** over-/underdischarge, over-/undervoltage, short circuit and voltage reversal.
- **Mechanical abuse:** nail penetration, crush, drop, vibrational and mechanical shock tests.

Most failure modes of LIBs are accompanied by a significant heat generation which can lead to a severe thermal runaway event and even one failing cell can lead to the destruction of a whole battery module. Hence it is well recognized that thermal tests are the most important ones to understand, evaluate and improve battery safety [5]. Batteries and their single components are tested by methods such as differential scanning calorimetry (DSC), accelerating rate calorimetry (ARC) and thermal ramp experiments. In thermal ramp experiments defined external heating of the cells is performed until cell failure. Although thermal ramp experiments are not as sensitive to display slight exothermic or endothermic processes as ARC or DSC, they are a good way to investigate the thermal stability of complete cells [7]. They are performed under atmospheric pressure to minimize the interferences for cell venting and thermal runaway. Due to the quasi-adiabatic conditions, endothermic and exothermic feedback behavior of the cells can be measured and reproducible data can be collected. The thermal behavior is highly influenced by the reactions of the electrolyte with active cell materials. Figure 6 illustrates the basic processes that are involved in the thermal degradation of cylindrical Li-ion batteries. The several decomposition reactions which take place when cells are heated up or used outside their operating limits are mostly exothermic and contribute to an increase in self-heating [6]. Venting of electrolyte or ejecta is cooling the cells due to the Joule-Thomson effect and removes unreacted material from the cell and is therefore mitigating the reaction potential. When the exothermic reactions produce more heat than can be dissipated by active cooling, convection, radiation or material and gas ejection, the cells go into the self-promoting thermal runaway. Safety has to be addressed on the cell, battery pack, module and the whole vehicle level since a failure on one level is likely to proceed to the higher levels (domino effect). Due to the safety concerns when upscaling batteries and the high number of single cells in automotive battery packs the thermal analysis of complete Li-ion batteries and studying the influence of one failing cell for the whole battery is crucial [5].
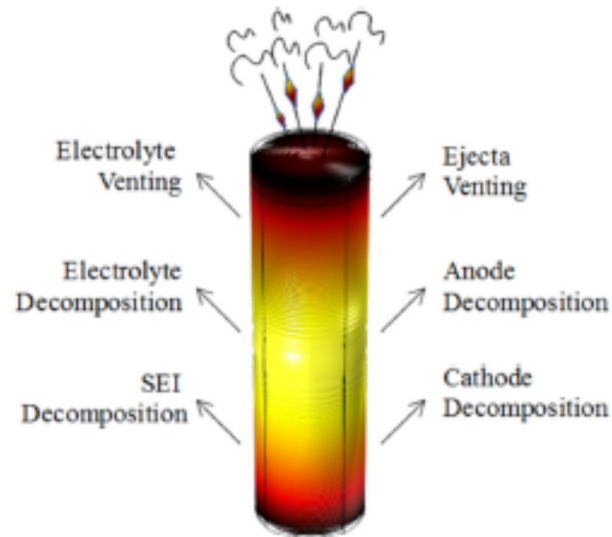
Figure 6: Thermal reactions contributing to thermal runaway [12].

The aim of this work is to identify, characterize and evaluate the intrinsic risks that are present in 18650 format Li-ion batteries. Especially the critical temperatures which trigger a self-accelerating thermal runaway event and the associated gas emissions were investigated. Therefore different cells, from various manufacturers, with different electrode chemistries were tested under defined testing conditions. The results should help to provide fundamental data to better understand the main failure modes and reactions in order to allow for the safe use of LIBs in the automotive sector and contribute to better market acceptance of this emerging technology.

2 EXPERIMENTAL METHOD

2.1 Batteries tested

All nine battery classes used in the experiments were commercially purchased, new Li-ion cells of the 18650 format. Primarily state of the art, high capacity batteries with $Li(Ni_{0.8}Co_{0.15}Al_{0.05})O_2$ (NCA) and $Li(Ni_{1/3}Mn_{1/3}Co_{1/3})O_2$ (NMC) cathode chemistries where purchased from leading manufacturers in this market segment. The new cells were charged to the desired State of Charge (SoC) using a Battery Test System (BaSyTec, Type CTS-LAB, Basytec GmbH). All batteries where charged using a constant current/constant voltage (CC/CV) mode where the current is kept constant until the battery voltage is approaching the maximum charging voltage. When this voltage is reached, it is kept constant and the current is reduced until it falls below the minimum charging current of 50 mA. In this way a complete and safe charge of the cells is guaranteed. Every charging cycle was preceded by a discharge process where the batteries were discharged with a rate of 1 C. The discharge was stopped after the cells reached their assorted discharge cut off voltage between 2.5 to 2.75 V. After charging, the shrinkage foil was removed from the battery shell and the bare steel cells were weighed before mounted inside the test reactor. The basic information of the tested cells are summarized in Table 1.

Table 1: Information on the tested 18650 Li-ion batteries.

Cell type	Nominal capacity / mAh	Cathode material	Cell mass / g*	Volumetric energy density / Wh L^{-1}	Gravimetric energy density / Wh kg^{-1}
NCR18650B	3350	$Li(NiCoAl)O_2$	45.32	729.1	266.1
NCR18650BF	3350	$Li(NiCoAl)O_2$	44.88	729.1	268.7
NCR18650GA	3300	$Li(NiCoAl)O_2$	46.75	718.3	254.1
ICR18650-32A	3200	$Li(NiCoAl)O_2$	48.64	725.5	247.6
INR18650-35E	3500	$Li(NiCoAl)O_2$	47.68	761.8	264.3
INR18650MJ1	3500	$Li(NiCoAl)O_2$	46.31	769.2	274.7
LG18650HE4	2500	$Li(NiMnCo)O_2$	45.48	544.1	197.9
ICR18650-26F	2600	$Li(NiMnCo)O_2$	44.14	581.6	218.0
US18650VTC5A	2500	$Li(NiMnCo)O_2$	47.48	544.1	189.6

*Cell mass as mean value of at least 6 different cell measurements, max. deviation of 0.15 g

Volumetric and Gravimetric energy densities calculated with nominal voltage and capacity according to the data sheets of the manufacturer, real values may be significantly lower, cell volume is 16.5 cm^3 [11].

To perfectly understand the reactions taking place inside the cell before and during thermal runaway it would be highly beneficial to know the exact composition and mass split of the various components and parts inside every single cell type. Battery manufacturers typically are very reluctant when it comes to providing detailed information about the composition of their products. Sophisticated analytical studies would be necessary in order to evaluate the exact composition and structure of every cell type. This is not the purpose of this work and was done to some extend in a previous project within our department [11, 13].

2.2 Setup of the test rig

All of the experiments were executed inside a heated, tubular, stainless steel reactor located inside a fume hood (Figure 7).
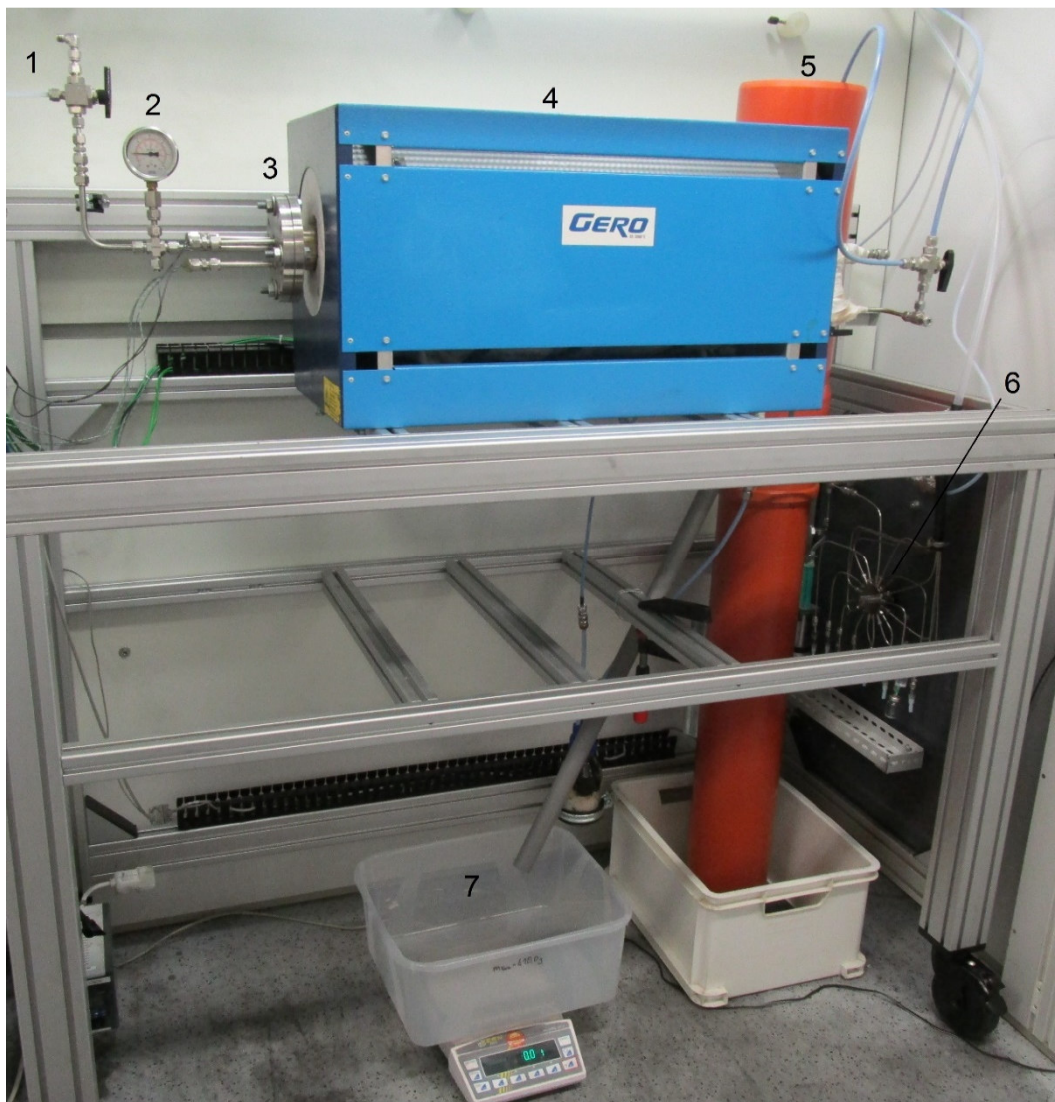
Figure 7: Complete test rig under the fume hood, 1) inert gas inlet, 2) manometer, 3) flange with inlets, 4) tube furnace, 5) water displacement tubing, 6) 16 port gas sampling valve, 7) water displacement scale.

The tubular, stainless steel test-reactor was equipped with a 12 hole DN 60 flange on the front side and a 8 mm pipe on the rear (outlet) side. It had an overall length of 775 mm, an outside diameter of 60 mm and a wall thickness of 3.5 mm which added up to a total reactor volume of 1680 mL. The flange, which allowed for easy access and fast sample preparation, was attached with four M10*50 mm screws and a gasket disk (SIGRAFLEX HD Graphite, V20011Z31) was used to ensure gas tightness. A manometer (WIKAI, 1-5 bar) was mounted on the inlet side of the reactor to indicate any potential pressure build-up. The reactor was placed horizontally inside an electrically powered tube furnace (GERO RES-E230/3, 3kVA, 30–3000 °C). The heating of the oven was realized using either the GERO RES AC-power supply (for quick pre-heating) or a DC-power supply unit (TTi EX, 300 W) for a controlled slower heating rate. In the standardized experiments the power supply was set to a voltage of 35.2 V and a current of 2.10 A. This corresponded to a heating power of 74.27 W. Various attempts showed a slow and controlled heating that allowed a good and insightful experimental procedure with this heating values. To minimize heat loss the front and the end of the reactor were insulated using ceramic wool. For the piping of the vent gas tubings, 6 mm and 8 mm stainless steel pipes were equipped with tube fittings to connect the reactor outlet to the analytical devices respectively. According to the design of experiment the gas stream from the reactor was directed to the gas sampling valve, gas volume measuring device (water displacement), optical gas cell or simply the exhaust using manually operated ball valves, check valves and T-piece adapter (FITOK, 316 stainless steel). Septums acted as grommets and allowed for sealing of the reactor while connecting the cables for online measurements of temperature and voltage in the inside. All relevant parameters were controlled and recorded using a Data Acquisition Controller (National Instruments daQ 9178 with NI9472, NI9421, NI9221, NI9213 I/O modules). The rate of data recording was set to 8 Hz for all experiments. A customized LabVIEW (National Instruments) program was used as controlling interface and provided time-resolved, online visualization which made the test progress observable. The LabVIEW program made it possible to control the inert gas stream, the gas sampling process, the pipe heating and data acquisition of all relevant temperatures, the gas flow, the time and mode of gas sampling, cell voltage and the gas volume. Inert materials were chosen because of the reaction potential of the cell constituents and the off-gas stream. After closing of the reactor with the flange, the whole apparatus was flushed with nitrogen in favour of ensuring a constant and reproducible, non-flammable, inert atmosphere inside the whole testing equipment. The inert gas (N_2, 5.0 purity) rate was regulated using a mass flow controller (Bronkhorst,F-201CV-1KO, 0-1000 mL min^{-1}). The complete experimental equipment was built into a fume hood for safety reasons. A complete piping and instrumentation diagram of the test rig and its periphery can be seen in Figure 8.
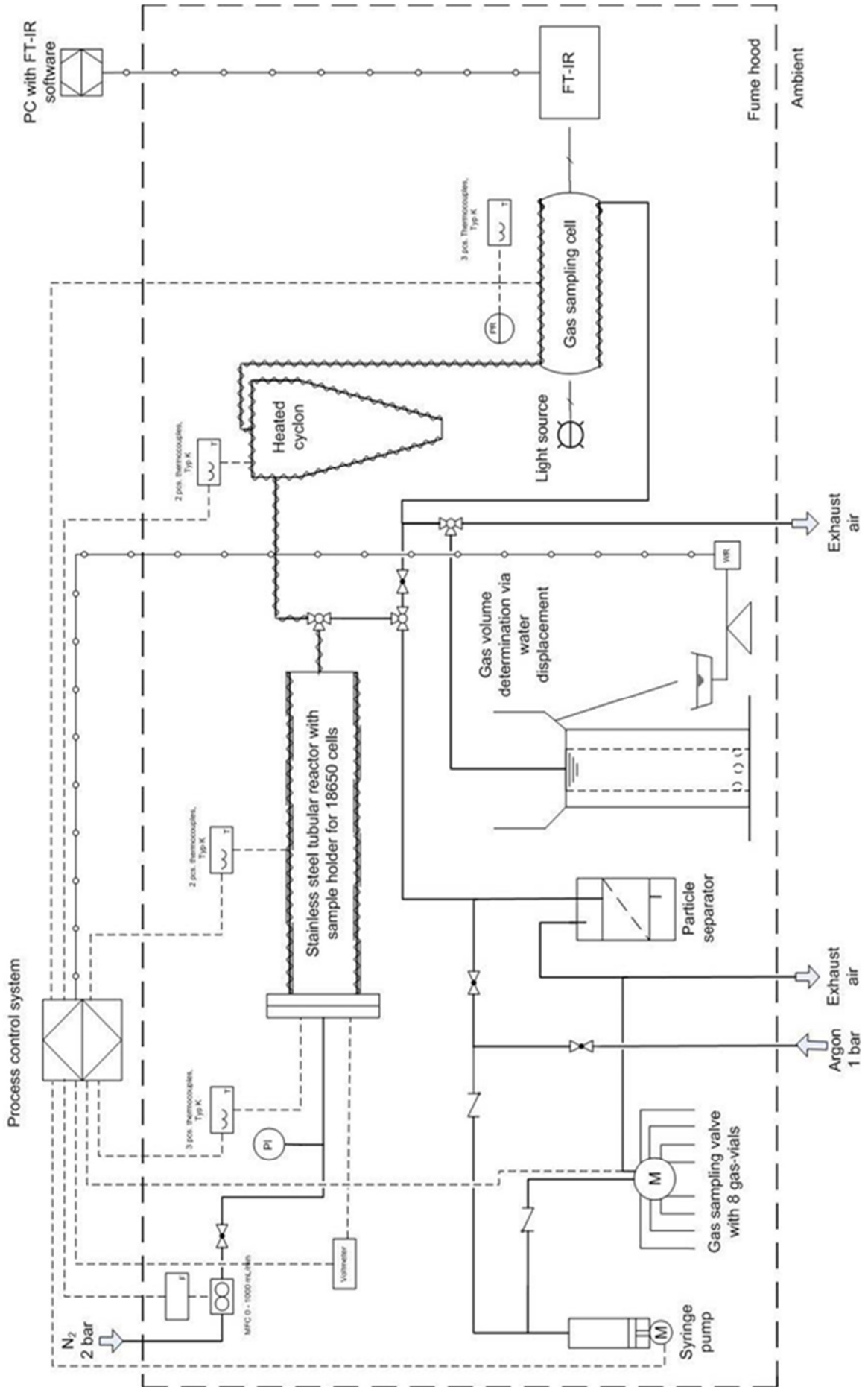
Figure 8: Piping and instrumentation diagram of the test rig and its periphery.

2.3 Test procedure

A typical experiment started with conditioning the cell to the desired state of charge. The heat shrinkage foil was then removed and the cell was weighed on a lab scale (Kern 57-2, d=0.01g). After conditioning and weighing of the cell, three type K thermocouples were placed on the front, middle and end section of the cells in order to achieve high temporal and spatial resolution. The cell and the thermocouples were wrapped with glass fiber band and everything was secured and held in place by a steel wire (Figure 9). The band also served as thermal insulation against the steel sample holder allowing for uniform heat exposure over the whole cell surface. Two steel plates were fitted in the sample holder to ensure the cell position in the sample holder even after violent cell rupturing. The plates also served as conducting assistance for cell voltage measurements. The upper part of the sample holder was also equipped with a type K thermocouple and adjusted onto the lower part to close the sample holder. To obtain relevant and reliable data a good sample holder design is crucial and a defined thermal insulation of the cell from the sample holder is needed to evaluate the self heating process taking place inside the cell.
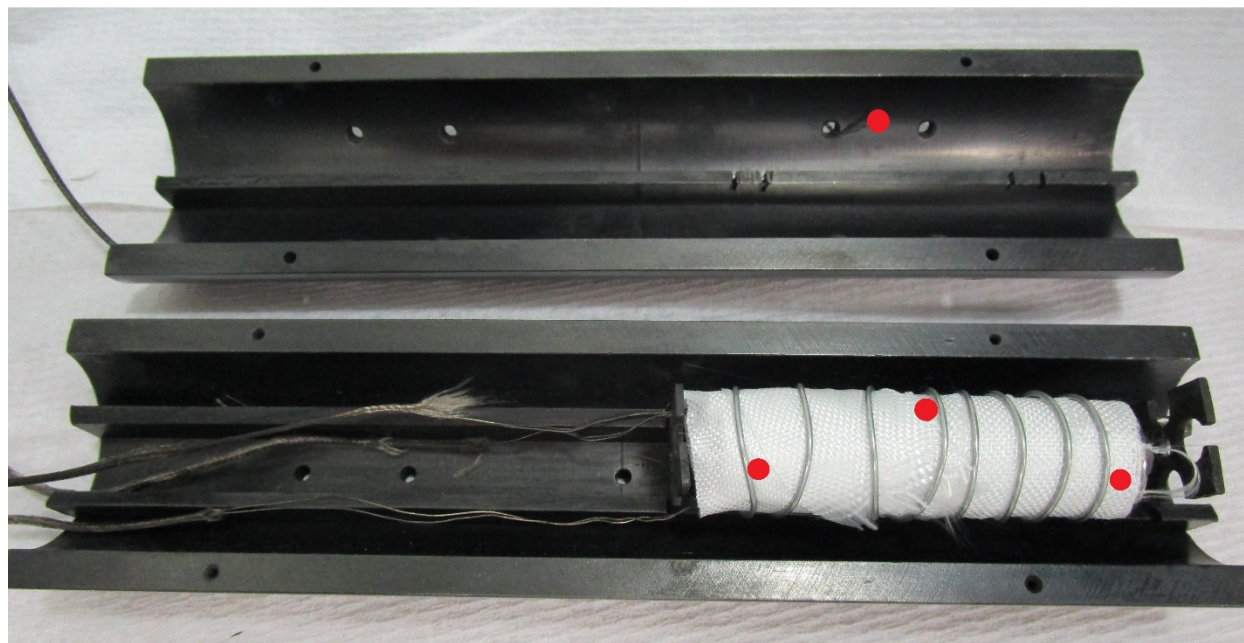
Figure 9: Stainless steel sample cell holder, containing an insulated cell and thermocouples (red dots indicate their positions).

The complete sample holder was carefully inserted into the tubular reactor. A wad of ceramic fiber tissue filter media was inserted at the outlet to hold back most of the ejected particular matter and therefore to protect the affiliated instruments. Stainless steel pipes were used as spacers to ensure the sample holder was situated in the same place inside the reactor for each experiment. The reactor then was closed with the flange and flushed with nitrogen. After preheating of the oven to 80 °C with AC-power supply the heating was switched to DC-power and the test was initiated with the beginning of data recording.

The reactor began to heat with a defined heating rate according to the chosen power input. All experiments were conducted until the thermal runaway of the cells took place. After the consumption of all reactants the cell cooled down again. Data acquisition was switched off after the cells cooled down to a temperature level similar to that of the oven. After the whole system cooled down to room temperature the reactor and the sample holder were dismantled and cleaned. The remainings of the cell were weighed in order to determine the mass loss (Δm) which emerged from the violent ejection of cell constituents.

Initially a differential cell test was performed on each cell type. With this design of experiment the influence of the state of charge and consequently the lithiation state of the electrodes on the thermal response of the cells to the thermal ramp heating was investigated. For the differential cell test a fully charged (100 % SoC) and a fully discharged cell (0 % SoC) were mounted behind one another into the sample holder and a thermal ramp test was executed on both cells simultaneously. The discharged cell had the same thermal properties and for that reason acted as reference for the charged one. Additionally the open circuit voltage (OCV) of the charged cell was recorded over the whole test procedure.

After the basic thermal performance of a charged and a discharged cell as well as the voltage were tested during the thermal ramp experiment, the fully charged cells were investigated further with several single cell tests. During this single cell test, gas samples were taken over a bypass system from the reactor off-gas. For this purpose the reactor was continuously flushed with 250 mL min^{-1} N_2. For the advanced investigation of the thermal behavior and the gas emissions of the cells, at least three identical thermal ramp tests were conducted in an uniform manner. This uniform execution provided sufficient data for the analysis and supplied information about the reproducibility of the experiments as well as the uniformity of the individual cells of the same type.

2.4 Gaschromatography and gas volume measurement

For qualitative and quantitative analysis of the gases, emitted by the cells at different stages of the thermal runaway process, a gas chromatograph (Agilent 3000A, Micro GC) was used. The two-channel GC was equipped with 2 independent columns to detect a wide range of analytes. After each column a separate thermal conductivity detector (TCD) was used to determine the respective gases according to their elution order. Channel A consisted of a 5 Å molecular sieve column (320 µm diameter, 12 µm stationary phase thickness, 10 m length) which was preceded by a PLOT U (320 µm diameter, 12 µm stationary phase thickness, 3 m length) column. The column A was heated to 110 °C and analyte injection took place in a backflush mode with argon as carrier gas. Channel B has been equipped with a PLOT U (320 µm diameter, 30 µm stationary phase thickness, 8 m length) column which was heated up to 80 °C and ran in a fixed volume

injection mode with helium as carrier gas. For one analysis run 500 µL of gaseous sample was drawn from the attached gas vial into the sample injector which was kept at 100 °C. The injector added 10 µL sample onto the heated columns which were set to 2.8 bar carrier gas pressure. The running time for channel A was set to 70 sec with a backflush time of 9.5 sec while channel B had a running time of 60 seconds. This gas chromatography method was established based on a reliable procedure used in previous experiments. The method was adjusted and verified with commercially purchased analytical test gases. The exact specification of the used gases was summarized in Table 2.

Table 2: Specifications of the gases used for the gas chromatography.

Element	Description	Composition
Carrier gas channel A	Analytical argon gas	Purity: 99.999 % inlet pressure 5.5 bar
Carrier gas channel B	Analytical helium gas	Purity: 99.999 % inlet pressure 5.5 bar
Test gas 1	Air Liquide crystal mix 1	H_2: 88 vol. % CH_4: 0.3 vol. % CO_2: 0.4 vol. % CO: 0.2 vol. % N_2: rest
Test gas 2	Air Liquide crystal mix 2	H_2: 72 vol. % CH_4: 1.5 vol. % CO_2: 3.0 vol. % CO: 2.5 vol. % N_2: rest
Test gas 3	Air Liquide crystal mix 3	H_2: 30 vol. % CH_4: 15 vol. % CO_2: 30 vol. % CO: 12 vol. % N_2: rest
Test gas 4	Linde C2 calibration gas 1	C_2H_2: 1 vol. % C_2H_4: 1 vol. % C_2H_6: 1 vol. % N_2: rest
Test gas 5	Linde C2 calibration gas 2	C_2H_2: 5 vol. % C_2H_4: 5 vol. % C_2H_6: 5 vol. % N_2: rest

For sample taking an electrical actuated syringe pump was utilized to draw a predefined volume of the off-gas, over a bypass line, into the gas sampling vials. Combined with an electrically controlled 16-port valve (SD16MWE-15D, Vici AG, Switzerland), this allowed the in-situ sample collection of 8 gas samples at freely defined moments. The 8 gas vials (5 mL glass vials) where sealed with a septum, equipped with an expansion reservoir for gas exchange and attached to the valve outlets. Before the experiments all the piping and the vials where flushed with inert gas (Ar, 5.0 purity). At specific points of interest the syringe pump flushed the off-gas line twice before directing 30 mL of gas sample into one of the respective vials. Due to the constant flow of inert gas through the reactor, the gas sample taken at a specific time corresponded to the generated gas of the cell at this moment. Immediately after the sampling, the vials were transferred to the gas chromatograph and 3 analytical runs were performed on each sample.

The gas samples were taken simultaneously during the three thermal investigation experiments in an uniform way. Figure 10 illustrates the moments at which the 8 gas samples were drawn from the reactor over a bypass system and transferred into the corresponding gas sample vials. The points of sampling where consistent for every experiment in order to allow the comparison of the different cell types. Shortly before the 1st venting and the thermal runaway event as well as periodically after these events, samples were taken. These points were deliberately chosen to give information about the gas evolution from the cell. Because of the constant flushing of the reactor system with inert gas the samples gave a precise account of the vented gases at this points.

The gas samples were taken:

1. Shortly before the 1st venting of the cell was anticipated
2. Immediately after the 1st venting of the cell had taken place
3. Two minutes after the 1st venting event
4. Right before the thermal runaway of the cell
5. Immediately after the thermal runaway event
6. 60 seconds after the thermal runaway event
7. 120 seconds after the thermal runaway event
8. 300 seconds after the thermal runaway event
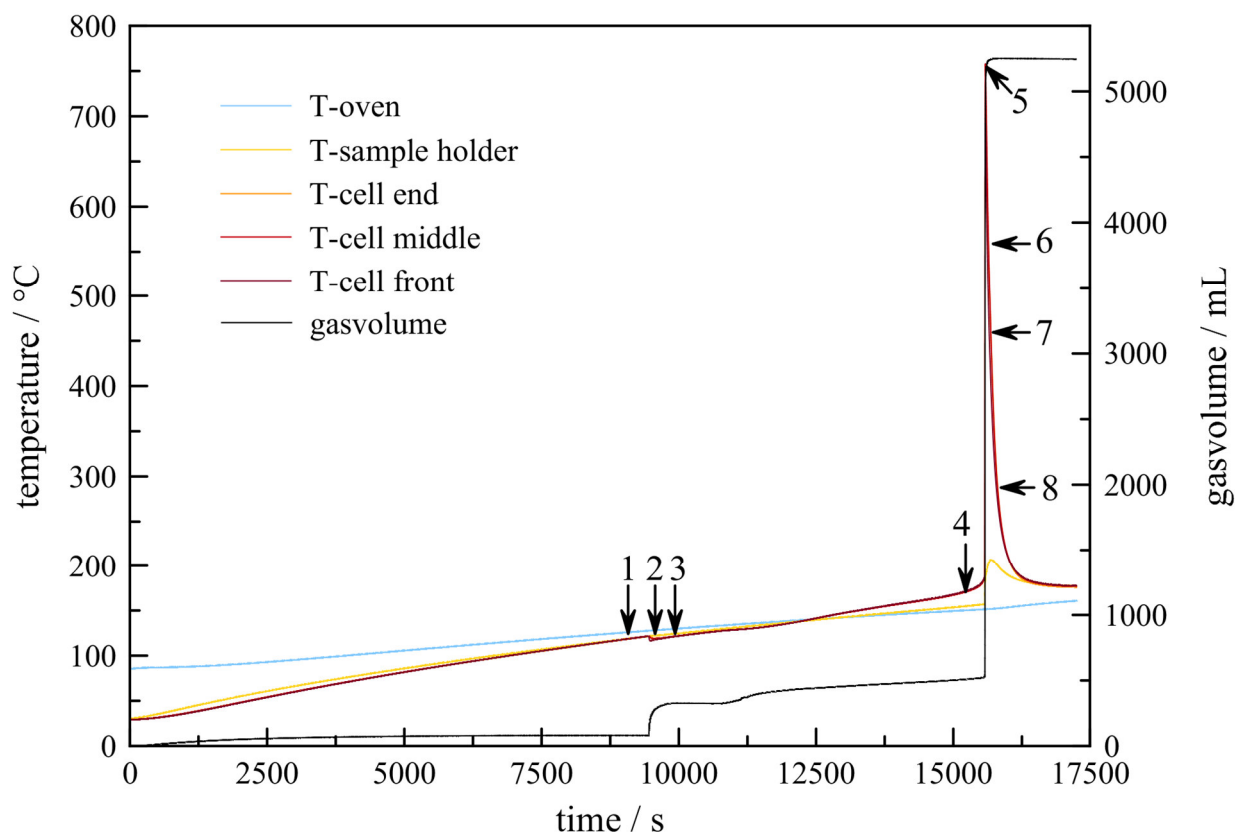
Figure 10: Temperature vs. time plot of a thermal ramp experiment, the points of sample taking for the gas analysis are indicated by numbers, the development of the gas volume is plotted on the right axis vs. the time of the experiment.

To evaluate the volume of gas that is evolving during different stages of the thermal ramp experiment a method had to be found which does not lead to a pressure build-up inside the reactor. Therefore gas volume was evaluated by water displacement combined with a scale to monitor the gas generation. The gas volume measurement was performed independently from the thermal and gas analysis in an separate experiment where no constant inert gas flow was applied over the test duration. With the water displacement apparatus the gases emitted by the cells and the thermally induced increase of the gasvolume inside the reactor could be measured and plotted almost simultaneously to its generation. The main processes leading to gas generation were gas volume increase because of temperature increase, the first venting of the electrolyte and the gas evolution due to the rapid thermal runaway incident. The progression of the gas evolution during the experiment is also plottend in Figure 10.

The rising temperature of the reactor led to a slow increase in gasvolume until the 1st venting event where a significant gas evolution can be seen as a steep surge in the gasvolume curve. With increasing cell and oven temperatures also the thermally induced increase of the gasvolume was amplified. Simultaneously with the thermal ramp event a large amount of gas evolved and was recorded as displaced water. The net value of evolved gasvolume was determined by substracting the value before the venting or thermal runaway event from the value after the distinctive event.

The water displacement apparatus is a custom build system consisting of two PVC pipes telescoped into each other and fixed on a base plate. Holes on the bottom of the inner tube connected both pipes with each other and defined the measureable gas volume to 10 L. The whole apparatus was filled up with water and the inner tube was connected to the gas outlet of the reactor. When pressure builds up inside the reactor due to gas evolution it forces the water level inside the inner tube downwards which leads to an upward lift of the water level in the outer pipe. The basic concept of the apparatus is illustrated in Figure 11. The displaced water from the outer tube runs off through an outlet onto the scale (Kern PRS 12200, max. 12 200 g, d=0.1 g) which is connected to the data acquisition. The volume of the displaced water equals the volume of gas evolution. The scale values are recorded simultaneously to the thermal ramp tests.
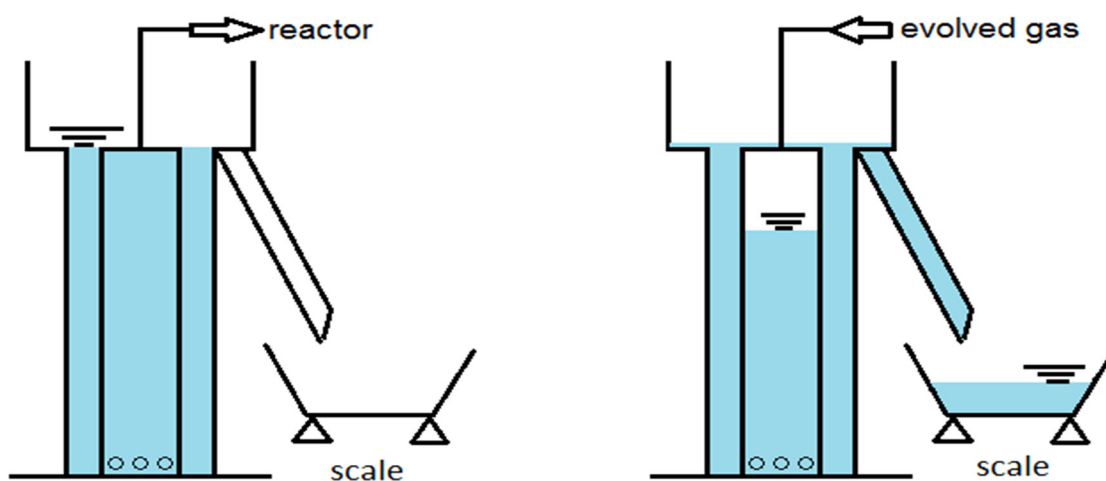
Figure 11: Scheme of the custom built water displacement apparatus which allowed for determination of the evolving gas volume. The water level before the experiment (left) and the water level after gas evolution (right) are illustrated.

3   EXPERIMENTAL RESULTS

The data of the numerous thermal ramp experiments of all nine cell types were recorded and used to display and investigate the thermal runaway process. These experiments were executed as described under *Test procedure*. Some experiments were conducted using variations from the standard procedures in order to allow new insights and identify potential relationships. These variations are mentioned in the respective results.

3.1   Evaluation of the experimental data

For the evaluation and interpretation of the experiments the data, which was obtained in the different thermal ramp tests, was compiled into plots. Initially the temperatures of the oven, the cell and the sample holder were plotted over time. This temperature vs. time plots gave a good overview of the temperature profiles for the duration of the whole experiment. The cell temperatures indicated the exothermic and endothermic events that took place at the corresponding time. Figure 12 shows the temperature of the cell in the end, middle and front position as well as the oven and the sample holder temperatures. The venting event which is accompanied by a slight endothermic cooling around 125 °C and the sharp peak which marks the thermal runaway process can be clearly seen as distinct deviation from the oven temperature slope.
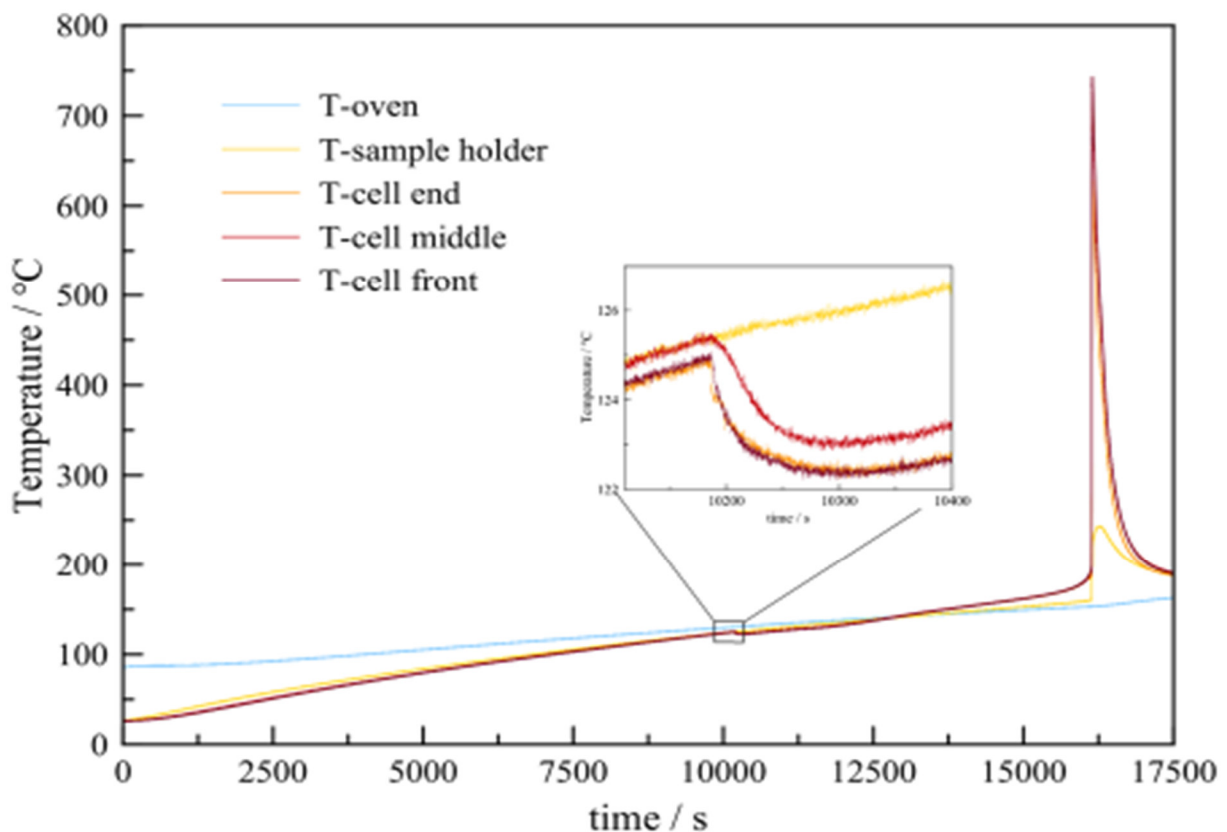
Figure 12: Temperature vs. time plot of a NCR18650B experiment, the cut out shows a detailed view of the endothermic 1st venting event.

After the slow heating of the oven and consequently of the sample holder and the cell, the first event of interest was the venting of the cell. The temperature and time at which the 1st venting took place were evaluated for every single thermocouple. The temperature difference ΔT and the corresponding time difference Δt were evaluated from the moment of which the venting took place until the moment at which the temperature began to rise again (Figure 12). The temperature difference ΔT was used to calculate the amount of heat (Q_{vent}) that got dissipated by the venting (Eq. 4 – where m is the cell mass, c_p is the heat capacity of the cell 1.04 J g^{-1} K^{-1} according to [14]). The amount of heat generated by the thermal runaway (Q_{TR}) was calculated from the thermal runaway temperature (T_{TR}), which was defined as the temperature where the cell experiences a heating rate of 2 °C min^{-1}, until the maximum cell temperature (T_{max}) (Eq. 5).

$$m \times c_p \times \Delta T_{vent} = Q_{vent}$$ (Eq. 4)

$$m \times c_p \times \Delta T_{TR} = Q_{TR}$$ (Eq. 5)
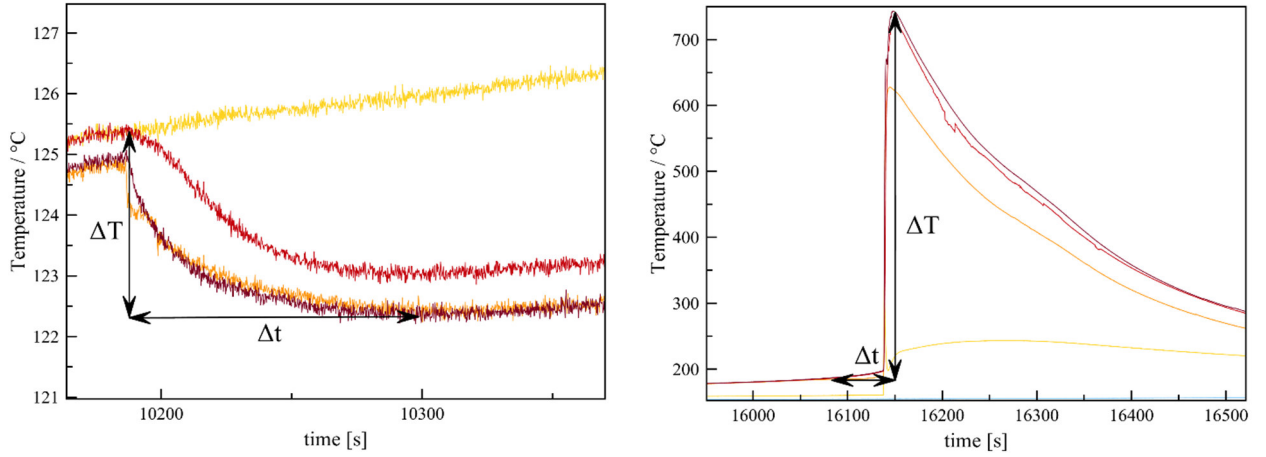
Figure 13: Magnified sections of Figure 12, endothermic venting event (left) and the exothermic runaway reaction (right).

Figure 13 shows a slight drop of the cell temperature at a corresponding temperature of about 125 °C (left) and the significant runaway peak (right). It can be clearly observed that the thermocouples which are located on the front, middle and end position of the cell surface show slightly different temperature behavior. It is therefore important to look at every single temperature signal and evaluate them discretely. The temperature differences before and immediately after a venting or thermal runaway event as well as the respective time differences were used to calculate the rate at which the venting (Eq. 6) and the thermal runaway process (Eq. 7) took place.

$$\frac{dT}{dt} = \frac{T2-T1}{t2-t1} = \frac{\Delta T}{\Delta t} = venting\ rate$$ (Eq. 6)

$$\frac{dT}{dt} = \frac{T2-T1}{t2-t1} = \frac{\Delta T}{\Delta t} = TR\ rate$$ (Eq. 7)

$$\frac{dT}{dt} = \frac{T2-T1}{t2-t1} = heating\ rate\ cell$$ (Eq. 8)

The heating rates of every single thermocouple were also calculated (Eq. 8) over the whole test duration and plotted against the respective cell temperature. With this so called rate-plots even subtle changes of the cell temperature could be visualized. The slightly distorted temperature signals from the thermocouples were inevitable and are an imminent result of the sensitive temperature measurement with high temporal resolution. To display the underlying global trend of the self heating of the cell the temperature rate curves were smoothed on a moving average basis. Figure 14 displays such a temperature rate-plot of a standard experiment. At the beginning of the experiment the heating rate is respectively low and the heating of the cell is mainly a consequence of the oven heating. With increasing cell temperature the difference between cell and oven temperature is decreasing and the heating rate of the cell is approaching the heating rate of the oven which is around 0.5 °C min^{-1}. A steep drop of the heating rate is indicating the endothermic venting event and the following fluctuations are first stirrings of intracellular reactions of the cells constituents. The following thermal runaway event leads to a massive rise of the heating rate, which remains constantly high, until the cell reaches its maximum temperature and cools down again.
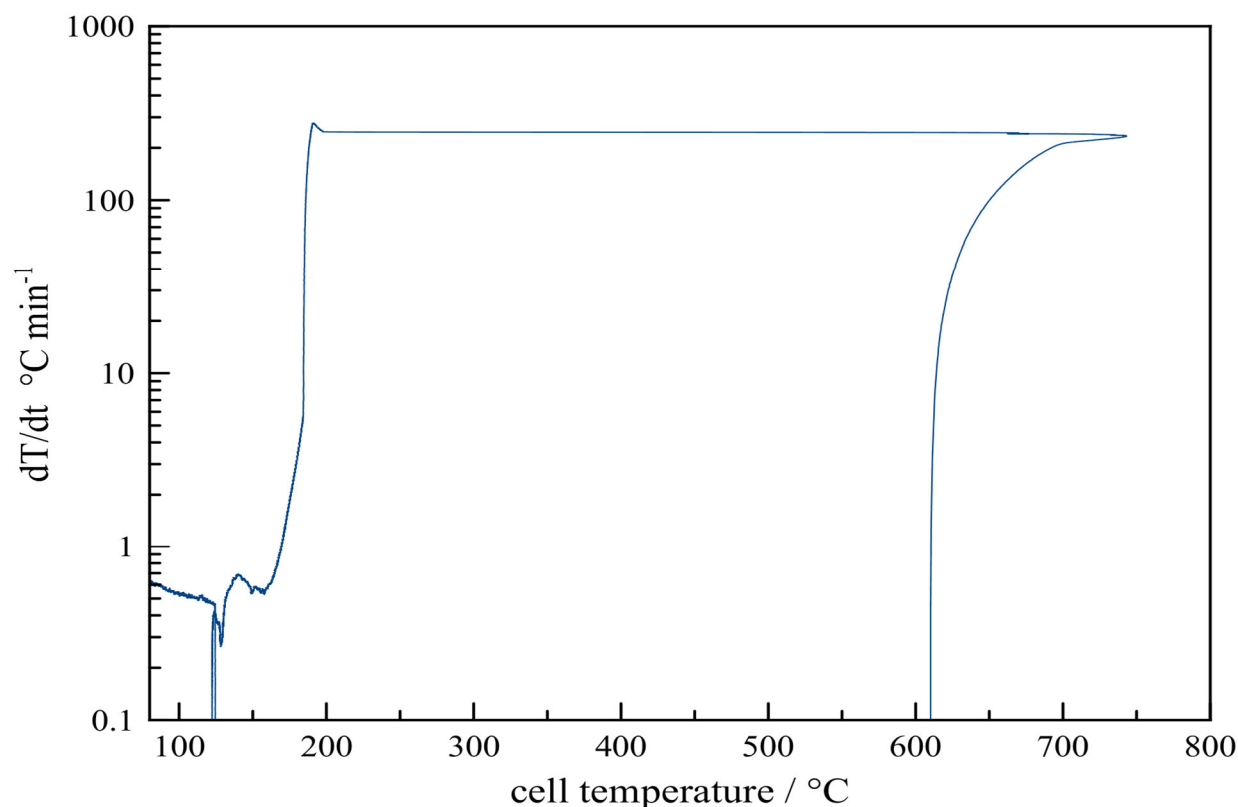
Figure 14: Rate-plot of a standard experiment, the heating rate of one of the cell thermocouples is plotted against the respective cell temperature.

With the help of this rate plots the thermal response of the cell to external heating can be divided into three stages [7, 13]:

- **Heat up (stage 1):** This first stage lasts from the beginning of the experiment, when the cell still has room temperature, until it reaches the onset temperature (T_{onset}). In this phase the cell itself generated no significant amount of heat. The increase in temperature was a consequence of the slow, forced, heating by the oven. The 1st venting of the cell normally took place in this stage and was prolongating the increase in temperature. The temperature at which an acceleration of the cells surface temperature could be observed is called onset temperature (T_{onset}) and could be identified in the rate plot as the point from which the heating rate started to increase persistently.

- **Accelerated heating (stage 2):** T_{onset} marks the end of stage 1 and the beginning of the accelerated heating stage 2. In this stage the cell is becoming a heat source because of the beginning, exothermic, degradation processes inside the cell. These processes are highly temperature dependent and begin to accelerate exponentially with rising temperatures. In the logarithmic plot this stage presents itself as an almost linear, constant growth rate. The transition from stage 2 to stage 3 is hard to estimate as no standard or consensus can be found in the current scientific discussion and literature. The definition of the thermal runaway temperature as well as the onset temperature are very dependend on the sensitivity of the method used for investigation. Therefore it was decided that the thermal runaway temperature (T_{TR}) which marks the beginning of stage 3 is defined as temperature at which the heating rate of the cell reaches 2 °C min^{-1}. At this heating rate a strong acceleration of the cells temperature could be observed which consequently led to the thermal runaway of the cell.

- **Thermal runaway (stage 3):** In this stage the rapid thermal runaway was happening. Beginning with a heating rate of 2 °C min^{-1} the cells temperature was rising evermore in a rapid way. The actual thermal runaway (deflagration) event took place in the course of a few seconds and was accompanied by violent venting. Under ambient conditions were atmospheric oxygen is available the high temperatures would lead to an ignition of the venting gases. The thermal runaway process ended when all the reactants had been consumed. In the plot this can be seen by the reaching of the maximum cell temperature (T_{max}) and the subsequent cooling of the cell.

Figure 15 displays the rate-plot divided into the three stages which lead to and took place in the thermal runaway of a Li-ion battery.
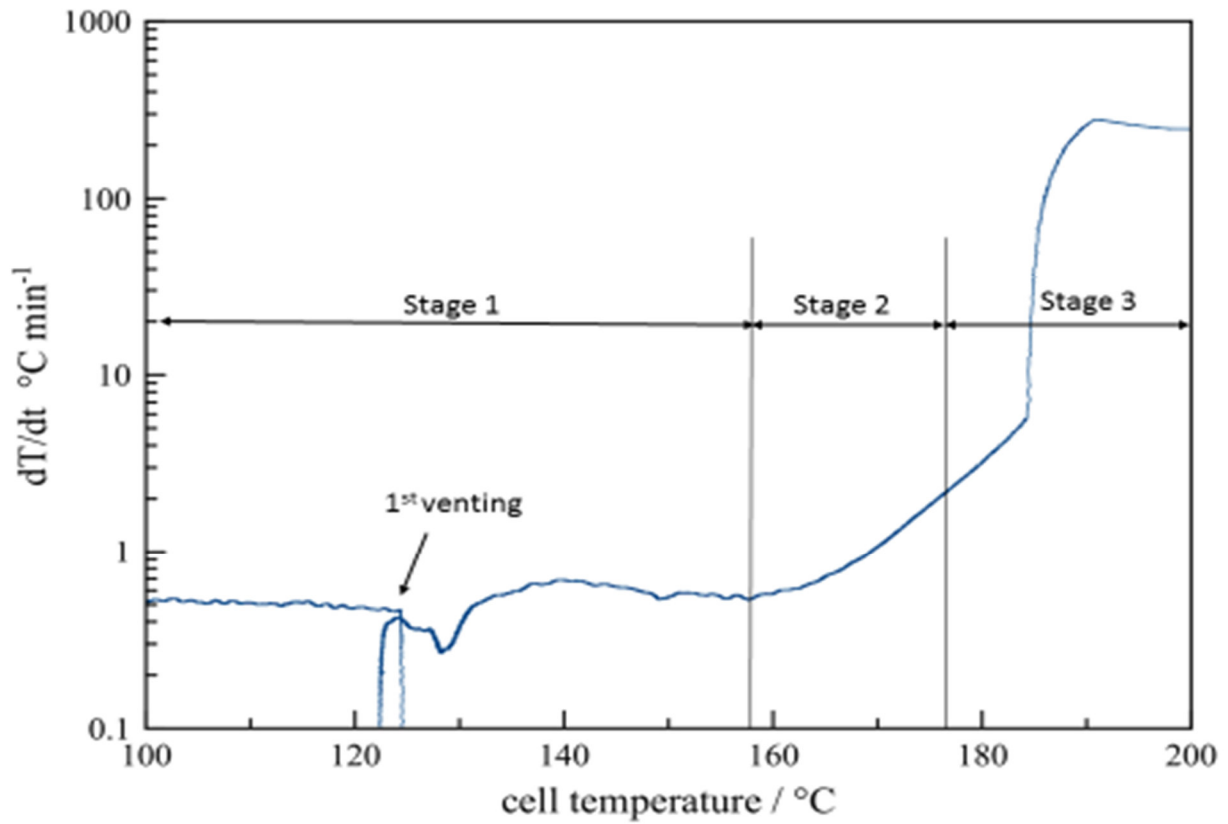
Figure 15: Cut-out of the rate-plot from Figure 14, the heating rate of the cell is plotted over the cell temperature, the three stages in which the heating of the cell can be divided are indicated as well as the venting event which leads to a temporary cooling and consequently to a brief negative heating rate.

3.2 NCR18650B

The NCR18650B cell has a nominal capacity of 3350 mAh at a nominal voltage of 3.60 V. The average weight of the tested cells was 45.32 ± 0.11 g. The nominal, volumetric energy density was calculated to be 729.1 Wh L^{-1} and the gravimetric energy density as 266.1 Wh g^{-1}. The cell has a high capacity with a relatively low, continuous discharge current of 4.875 A. It is well suited for applications which require a long run time at relatively low power consumption. The cathode material of this cell is Li(Ni$_{0.8}$Co$_{0.15}$Al$_{0.05}$)O$_2$ and the anode consists of high density graphite.

3.2.1 Differential celltest NCR18650B

Figure 16 displays the differencial cell test of the NCR18650B cell. With the beginning of the experiment the voltage was steady at 4.15 V and dropped rapidly to 1.60 V at a cell temperature of 99.95 °C. At 109.10 °C the voltage dropped further to 0.88 V and showed an oscillating behavior with highest and lowest voltage values between 0.88 V and 1.61 V until a plateau was reached with 2.11 V. This voltage remained constant until the 1st venting event of the charged cell at a temperature of 126.40 °C. With the venting of the cell the voltage dropped to a low of 0.3 V from which it slowly grew again to 0.79 V at a cell temperature of 156.08 °C. At a cell temperature greater than 162 °C the cells voltage was de facto no longer perceptible.
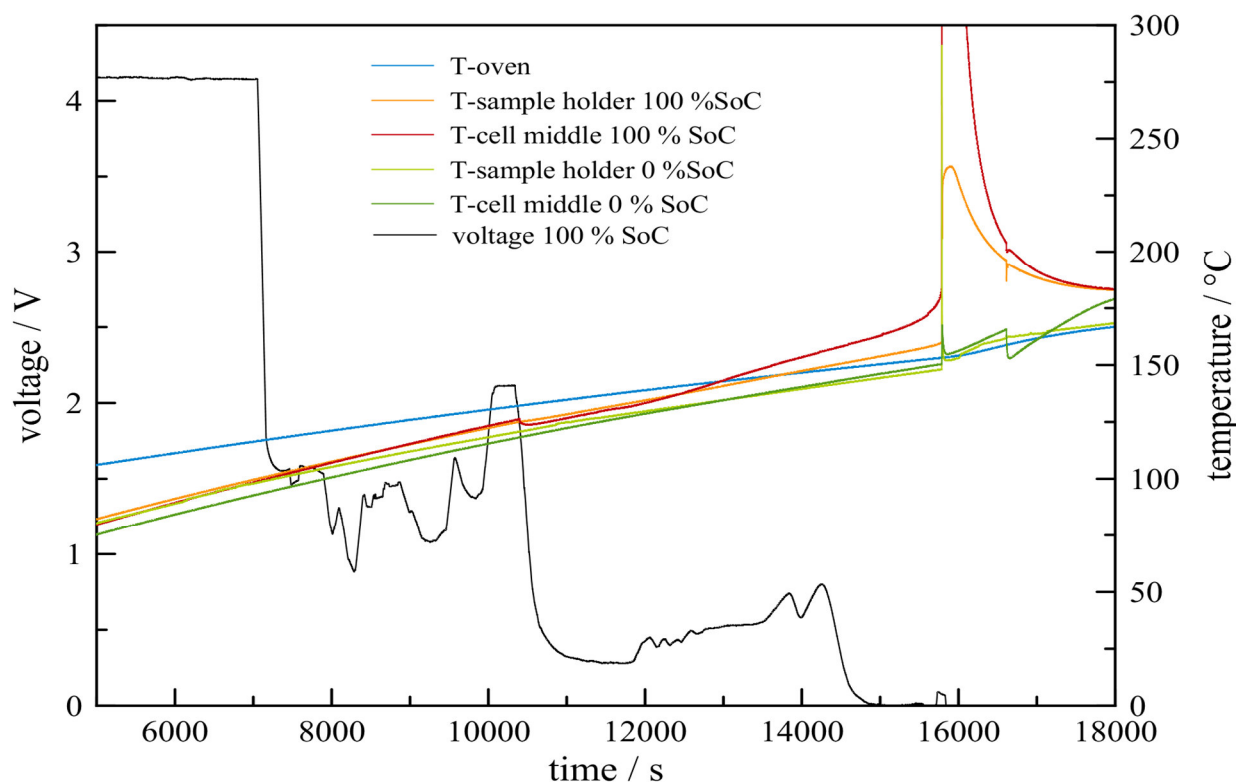
Figure 16: Temperature vs. time plot of the differential cell test experiment of the NCR18650B cell, the cell and sample holder temperatures of each cell as well as the oven temperature and the cell voltage of the charged cell are plotted over the time.

The temperature of the oven amounted close to 80 °C at the beginning of the experiment and increased slowly due to the constant heating by the DC power supply. The sample holder temperature started at 27 °C and approached the oven temperature with a quickening pace. This heating eased with a decreasing temperature difference between oven and sample holder temperature. At a cell temperature around 140 °C the cell and sample holder temperature exceeded the oven temperature which is an indication that the cell became a heat source. As mentioned before the charged cell vented at a cell temperature of 125.70 °C with a drop in temperature of $\approx$ 3 K. After the 1st venting the cell temperature started to rise again with an increasing gradient while the uncharged cell showed no venting and its temperature was increasing slowly with a gradient similar to the sample holder. At a cell temperature of 169.27 °C the charged cell reached the thermal runaway temperature and it's temperature climbed sharply which also led to a quick warming of the sample holder and the uncharged cell. This heat input raised the uncharged cell temperature sustainably by roughly 5 K and consequently also the uncharged cell experienced an explicit venting event at a cell temperature of 165.47 °C which lowered the can temperature by 12.44 K to 153.03 °C. The experiment was continued until the cells temperatures settled and all temperature values stayed constant for a prolonged period of time and no further changes were expected.

3.2.2 Thermal investigation NCR18650B

After the first differential test of the NCR18650B cell the cell type was investigated further for it's thermal properties. Figure 17 displays a standard thermal ramp experiment of a NCR18650B cell over the whole test duration. As described under Test procedure the oven was preheated to 80 °C and then the data acquisition was started. The oven temperature is almost linear ascending over the whole experiment duration. Only after the thermal runaway of the cell the gradient of the oven temperature curve is slightly increasing due to the extensive heat from the runaway event. The same is true for the sample holder temperature which is steadily increasing until the thermal runaway event which also led to a quick temperature rise. The cell is mainly exposed to heat by the sample holder and therefore the temperatures of the cell advanced similar to that of the sample holder with a slight backlog. At a cell temperature of approximately 120 °C the cell temperatures surpassed that of the sample holder which is an indication for developing exothermic processes inside the cell.
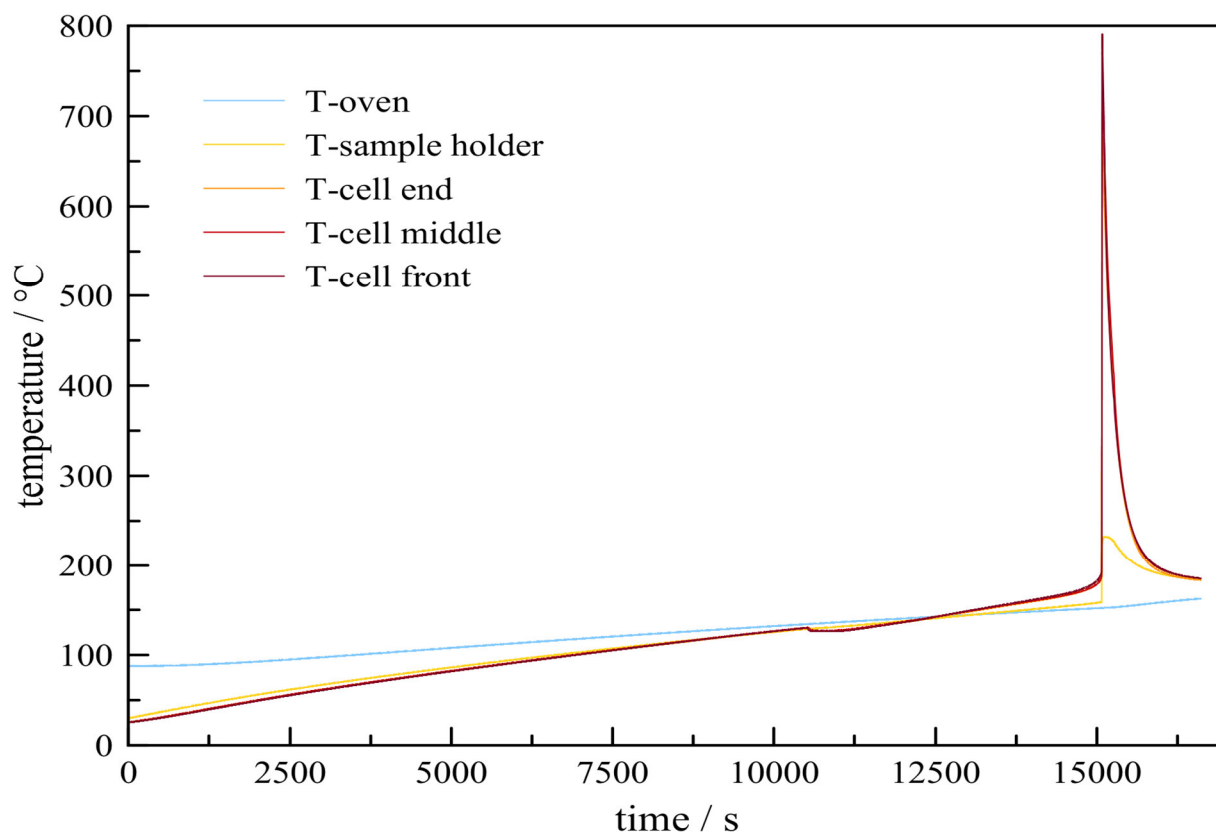
Figure 17: Temperature vs. time plot of the NCR18650B 1 thermal ramp experiment.

A slight offset between the three temperature signals was noticed for the heat up phase until the 1st venting event. The thermocouple in the middle position indicated a 0.6 K higher temperature in this area. The first venting took place at a cell temperature of 130.27 °C after 10518 s of runtime. The venting lowered the cells temperature by 3.40 K and as a consequence dissipated 160.4 J of heat. This drop in the temperature was only temporary and the cell temperature constantly increased after the venting event. The heat distribution over the cell's surface was changing after the venting with the temperature on the front being significantly higher than in the middle or at the end of the cell.

At an averaged cell temperature of 143 °C the cell temperature was exceeding the ovens temperature and already acted as heat source. The heating rate was accelerating permanently and stronger after the onset temperature of 158.63 °C. At a cell temperature of 174.13 °C the highly exothermic thermal runaway led to a temperature increase up to a maximum temperature (T_{max}) of 677.10, 728.80 and 790.92 °C at the end, middle and front position of the cell respectively. This heat generation between the thermal runaway temperature (T_{TR}) and the maximum cell temperature was taking place with an averaged rate of 142.42 °C min^{-1} and was responsible for a heat generation of 26.31 kJ. This experimental results as well as the results of the two other thermal ramp tests of the same cell type are summarized in Table 3.

Table 3: Summary of the key thermal indicators of three identical thermal ramp experiments of the NCR18650B cell.

experiment	Δm / g	T_{vent} / °C	Q_{vent} / KJ	T_{onset} / °C	T_{TR} / °C	T_{max} / °C	TR_{Rate} / °C min^{-1}	Q_{TR} / kJ
NCR18650B 1	17.73	130.27	0.16	158.63	174.13	731.94	142.42	26.31
NCR18650B 2	17.17	131.49	0.15	156.40	172.30	626.53	108.77	21.38
NCR18650B 3	16.29	131.28	0.17	158.03	172.76	698.93	114.90	24.72

3.2.3 Gas analysis NCR18650B

During the three distinctive experiments, which were conducted for the thermal characterization and investigation of the NCR18650B cell, gas samples were drawn from the reactor and analyzed with a gas chromatograph as described under 2.4. The moments at which the samples where taken are displayed in Figure 10. The composition of the gas samples added details to the processes, taking place during the thermal ramp tests. Figure 18 shows that before the first venting no significant amount of gas was emitted by the cell and the detected gas consisted mostly of the inert, flushing gas nitrogen.

	1	2	3	4	5	6	7	8
N2 / %	99.95	99.39	98.64	99.00	24.95	35.20	63.49	86.25
CO2 / %	0.05	0.61	1.22	0.56	7.90	7.40	5.56	2.65
CO / %	0.00	0.00	0.00	0.00	53.81	44.22	21.75	7.05
H2 / %	0.00	0.00	0.00	0.20	11.77	11.92	8.13	3.91
CH4 / %	0.00	0.00	0.00	0.00	0.86	0.89	0.76	0.00
C2H2 / %	0.00	0.00	0.00	0.00	0.28	0.00	0.00	0.00
C2H4 / %	0.00	0.00	0.00	0.11	0.33	0.28	0.20	0.01
C2H6 / %	0.00	0.00	0.15	0.12	0.10	0.10	0.11	0.13
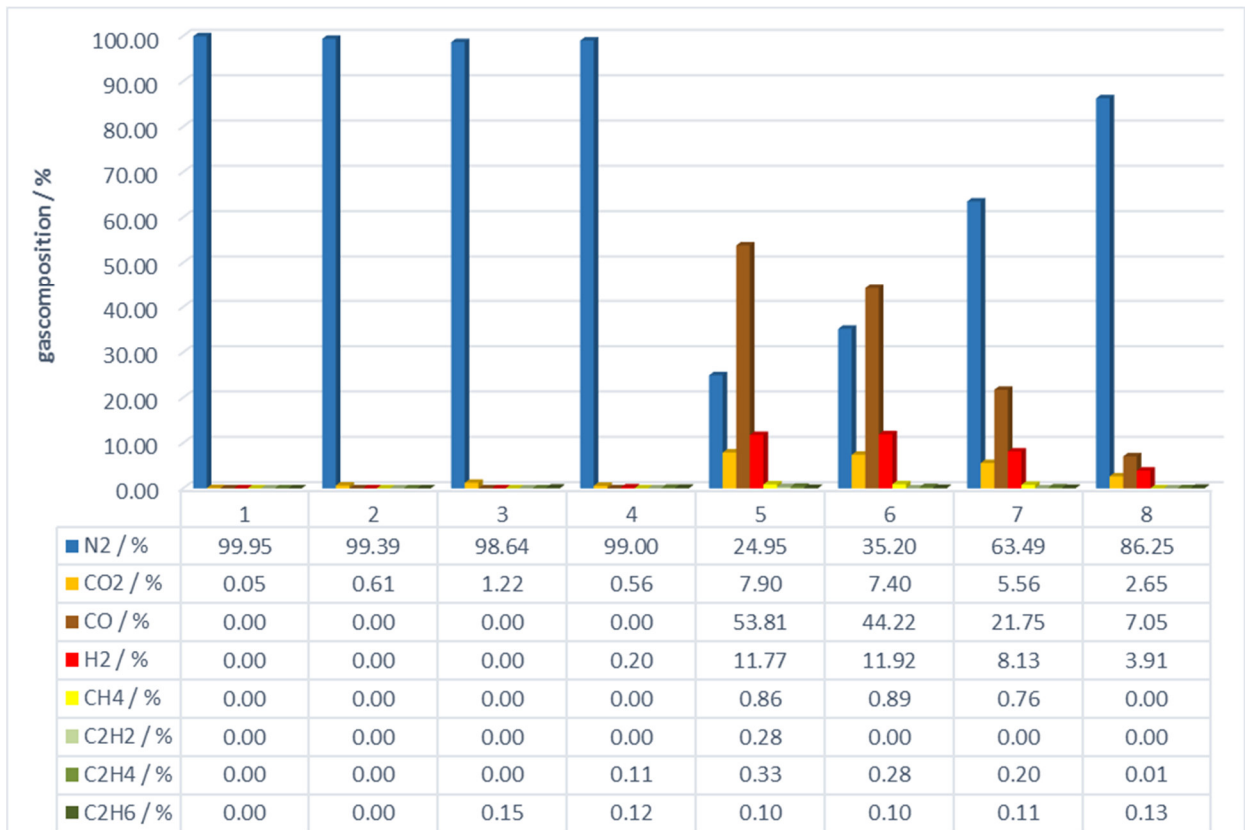
Figure 18: Gas composition of the eight samples taken from the reactor at specific moments during the NCR18650B 2 experiment.

After the first venting event small quantities of CO_2 and C_2H_6 were detected. These vented gases where displaced by the inert gas and only minor gas formation was measured before the thermal runaway. Directly after the thermal runaway a diverse composition of the vented gases could be noticed which was increasingly diluted by the flushing gas with advancing time. Therefore it is evident that the gas sample 5, which was taken directly after the thermal runaway event, was the most significant one and provided information about the degradation reactions taking place. In Table 4 the gas composition, directly after the thermal runaway, is summarized for the three NCR18650B experiments.

Table 4: Gas composition of the three distinctive gas analysis experiments of the NCR18650B cell, each sample was taken immediately after the thermal runaway event.

experiment	N_2 / %	CO_2 / %	CO / %	H_2 / %	CH_4 / %	C_2H_2 / %	C_2H_4 / %	C_2H_6 / %
NCR18650B 1	33.43	6.34	42.87	15.73	1.07	0.00	0.51	0.04
NCR18650B 2	24.95	7.90	53.81	11.77	0.86	0.28	0.33	0.10
NCR18650B 3	22.08	10.93	52.06	12.98	1.13	0.28	0.45	0.09

Additionally to the thermal and gas analysis test a separate experiment was conducted to determine the amount of gas evolving in the course of the thermal ramp test. During the heating phase of the cell only small quantities of gas were released. This is mostly because of the expansion of the cummulative reactor gas volume with rising temperatures. Immediately at the first venting of the cell a significant gas evolution can be seen as a steep surge of the volume curve can be seen which accounts for a gas volume of 245 mL. At height of the thermal runaway event abruptly 4750 mL of gas evolved from the cell. Combined with the venting event and the thermal expansion an absolut gas volume of 5250 mL was generated during the whole experiment.

3.3 NCR18650BF

The NCR18650BF cell is very similar to the NCR18650B cell. The main difference between the two cells is the small amount of silicon oxide (SiO) with which the high density graphite of the anode is blended. This leads in combination with the high density $Li(Ni_{0.8}Co_{0.15}Al_{0.05})O_2$ cathode to a relatively low averaged weight of 44.88 ± 0.10 g. The nominal capacity is rated as 3350 mAh at a nominal voltage of 3.60 V. Therefore the calculated volumetric energy density was 729.1 Wh L^{-1} and the gravimetric energy density was 268.7 Wh g^{-1}.

3.3.1 Differential cell test NCR18650BF

The differential cell test of the NCR18650BF cell gave basic information about the thermal and the open circuit voltage performance of the cell during a thermal ramp experiment and is presented in Figure 19. The voltage of the charged cell remained constant at the typical OCV voltage of 4.15 V until the cell reached a temperature of 102.97 °C. At this point the cell voltage seceded to a value under 1 V. It began to rise with increasing degree and reached a value as high as 2.16 V until the 1st venting event of the cell were it decreased again and fluctuated around a value of 0.50 V. Right before the thermal runaway event the cell voltage rose to roughly 2 V and immediately after the thermal runaway no voltage was measurable anymore.
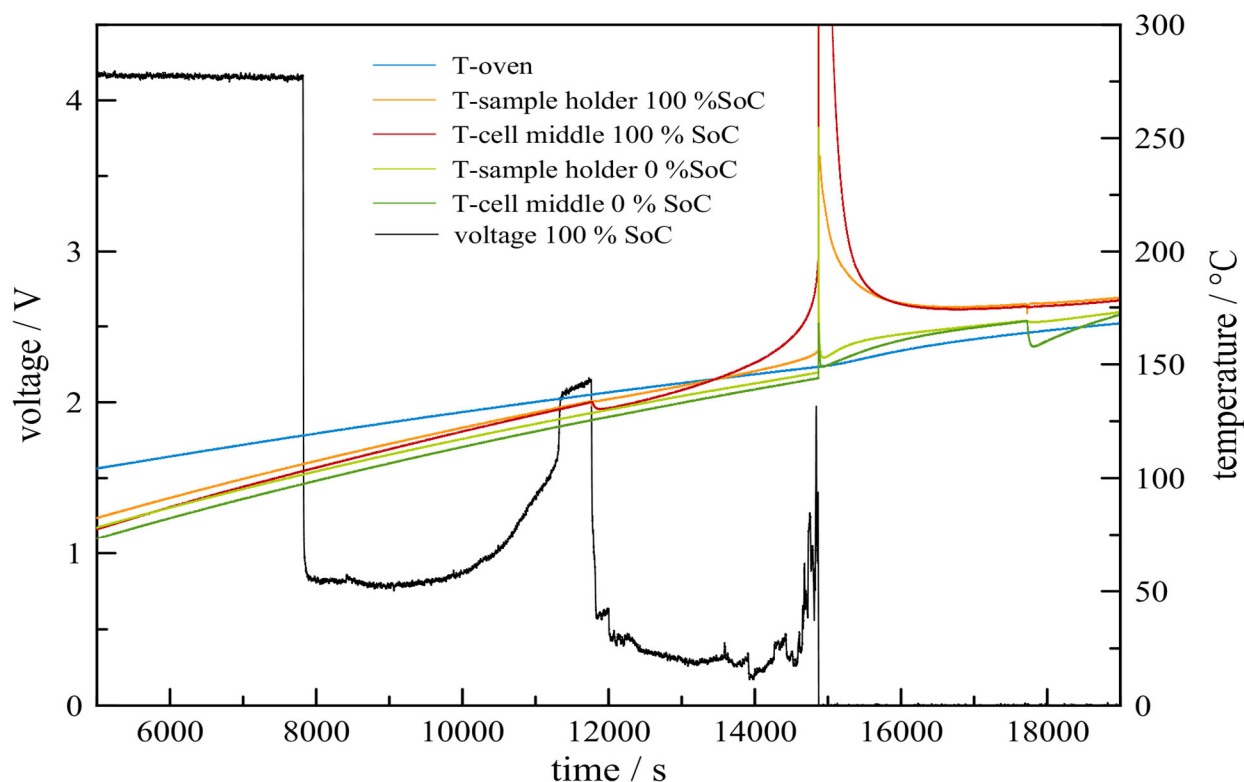
Figure 19: Temperature vs. time plot of the differential cell test experiment of the NCR18650BF cell, the cell and sample holder temperatures of each cell as well as the oven temperature and the cell voltage of the charged cell are plotted over the time.

The temperatures of the charged cell as well as the uncharged cell were rising with an offset of 4 K between them. This offset increased during the thermal ramp experiment to ≈ 8 K until the 1st venting of the charged cell reduced it's temperature from 133.32 °C to 130.16 °C. Shortly after the endothermic cooling due to the venting the 100 % SoC cell temperature sped up it's advance and the cell went into thermal runaway at 14840 s. The uncharged cell showed no accelerated heating until the thermal runaway event of the charged cell whereby it gained ≈ 5 K from that exothermic reaction. After that also the uncharged cell's temperature rose steadily until it vented at a temperature of 168.20 °C at 17700 s after the beginning of the experiment. The venting lowered the temperature to 157.10 °C. After that no further deviations could be observed.

3.3.2 Thermal investigation NCR18650BF

The temperature vs. time plot of one of the three identically performed thermal ramp experiments is illustrated in Figure 20. With the initiation of the experiment the oven temperature started at roughly 80 °C while the cell temperatures were still at room temperature around 25 °C. With ongoing heating the cell temperature converged toward the oven temperature. At 140.97 °C cell temperature the venting of the cell took place and lowered the temperature to 136.81 °C. After further heating the cell experienced thermal runaway and deflagrated whereby it reached an averaged temperature of 598.53 °C. The specific thermal parameters of the NCR18650BF cell are summarized in Table 5.
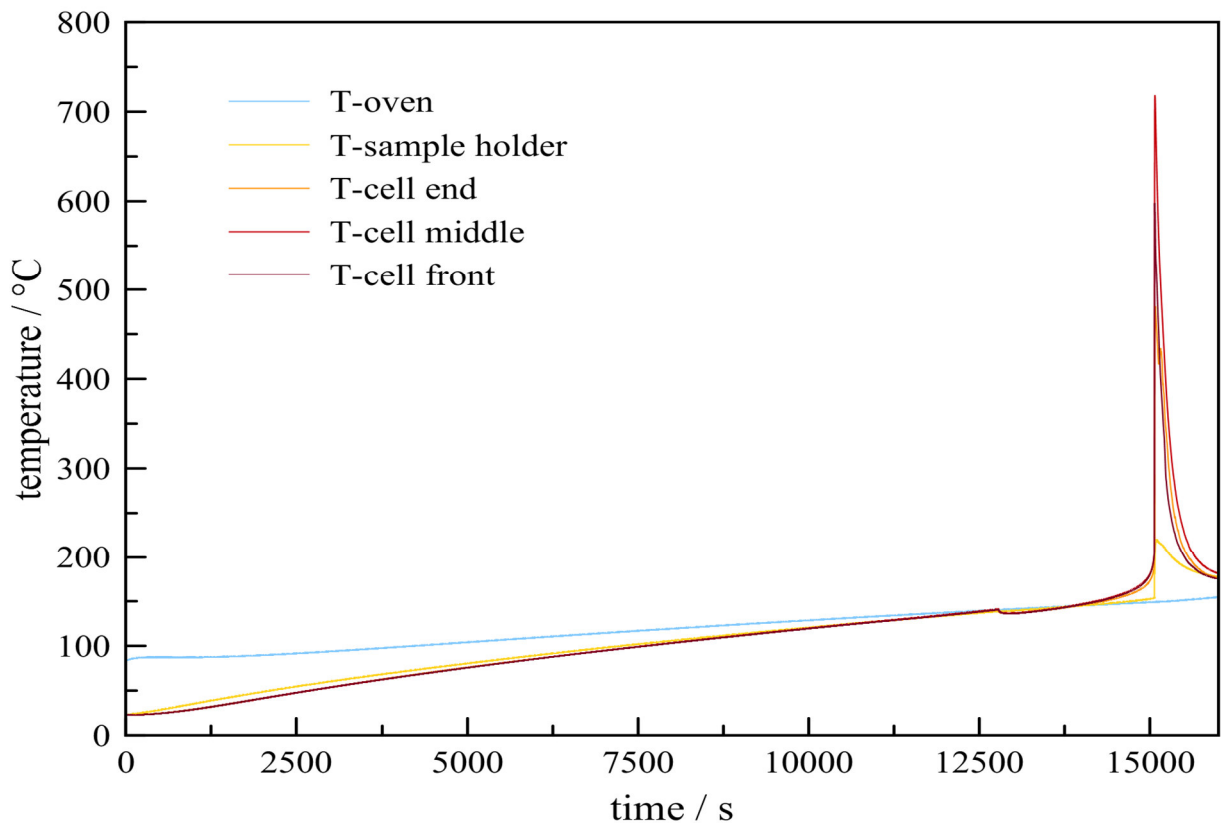
Figure 20: Temperature vs. time plot of the NCR18650BF 1 thermal ramp experiment.

Table 5: Summary of the key thermal indicators of three identical thermal ramp experiments of the NCR18650BF Li-ion cell.

experiment	Δm / g	T_{vent} / °C	Q_{vent} / KJ	T_{onset} / °C	T_{TR} / °C	T_{max} / °C	TR_{Rate} / °C min^{-1}	Q_{TR} / kJ
NCR18650BF 1	25.95	140.97	0.20	139.05	160.11	598.53	61.23	20.44
NCR18650BF 2	28.86	141.00	0.16	140.13	159.13	565.23	71.73	18.92
NCR18650BF 3	25.18	136.73	0.18	135.87	160.80	781.47	97.64	28.95

3.3.3 Gas analysis NCR18650BF

The results of the gas analysis for the NCR18650BF 1 experiment are displayed in Figure 21. The samples were taken at the specific points outlined in 3.1. While the samples taken before the runaway of the cell showed little other gases than N_2 and CO_2 the samples afterwards showed a diverse gas composition. Sample 3 was taken 120 s after the 1st venting of the cell and had a higher proportion of CO_2 than sample 2 which was taken immediately after venting. This suggested that the desintegration of the electrolyte continued after the venting incident. Also the sample 4 which was withdrawn shortly before the thermal runaway showed more than 2 % CO_2 in the off-gas. After the thermal runaway the evolved gases displaced most of the inert gas from the reactor. With increasing time the reactor gases were diluted by flushing and the sample 8 (300 s after thermal runaway) had a nitrogen fraction of almost 90 % as can be seen in Figure 21.

	1	2	3	4	5	6	7	8
N2 / %	100.00	98.96	97.67	97.53	41.39	52.82	64.61	89.44
CO2 / %	0.00	1.04	2.20	2.08	7.41	8.61	10.29	3.71
CO / %	0.00	0.00	0.00	0.00	28.79	17.36	11.57	3.47
H2 / %	0.00	0.00	0.00	0.16	20.64	19.23	12.05	3.35
CH4 / %	0.00	0.00	0.00	0.00	1.55	1.63	1.22	0.00
C2H2 / %	0.00	0.00	0.00	0.00	0.00	0.00	0.00	0.00
C2H4 / %	0.00	0.00	0.00	0.13	0.14	0.26	0.15	0.03
C2H6 / %	0.00	0.00	0.13	0.11	0.09	0.09	0.11	0.00
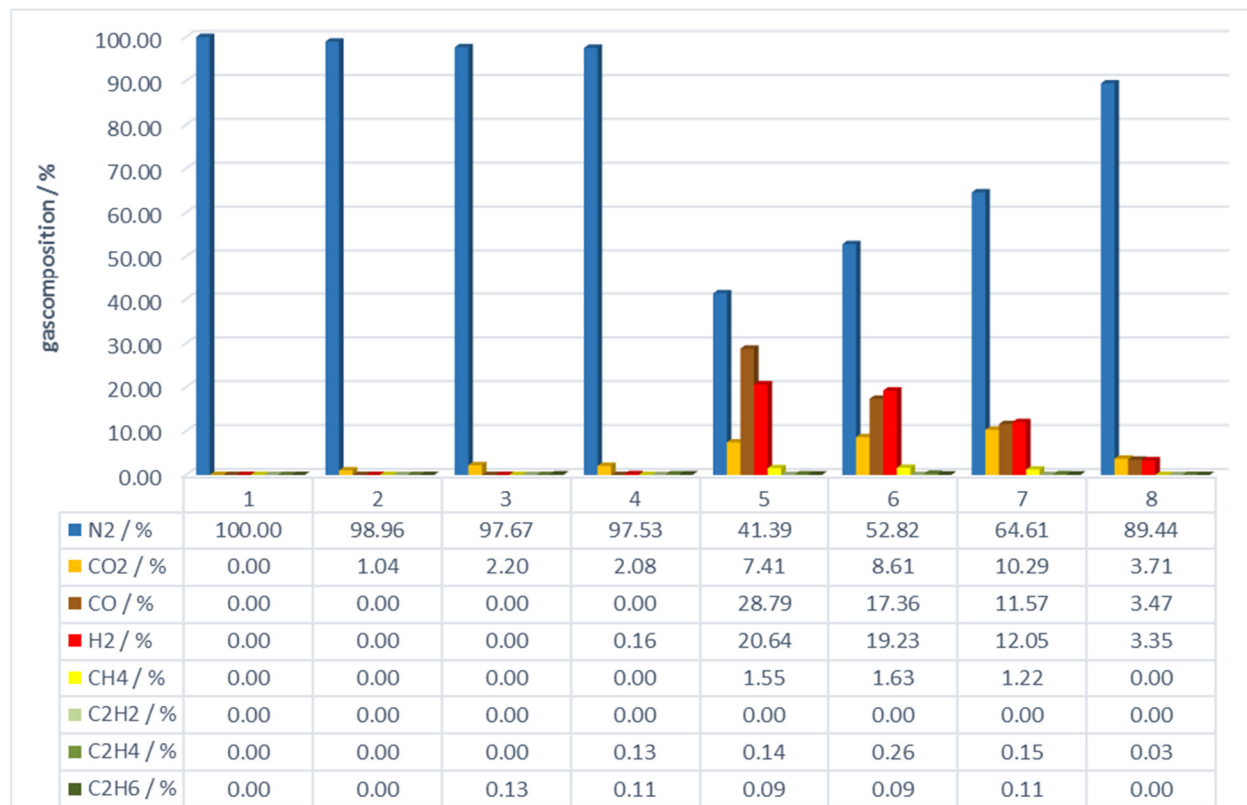
Figure 21: Gas composition of the eight samples taken from the reactor at specific moments during the NCR18650BF 1 experiment.

The gas analysis results of the three individual experiments for the NCR18650BF cell are summarized in Table 6. Each sample was taken immediately after the thermal runaway. The experiments 1 and 2 showed similar compositions while the experiment 3 showed lower values for the inert gas N_2 and higher values for almost all other gas constituents. This might indicate a higher gas volume development by the thermal runaway process.

Table 6: Gas composition of the three distinctive gas analysis experiments of the NCR18650BF cell, each sample was taken immediately after the thermal runaway event.

experiment	N_2 / %	CO_2 / %	CO / %	H_2 / %	CH_4 / %	C_2H_2 / %	C_2H_4 / %	C_2H_6 / %
NCR18650BF 1	41.39	7.41	28.79	20.64	1.55	0.00	0.14	0.09
NCR18650BF 2	46.85	5.60	23.54	22.27	1.60	0.00	0.05	0.09
NCR18650BF 3	29.62	13.62	36.09	18.08	1.87	0.31	0.33	0.09

The gas volume development was investigated in a separate experiment using the water displacement system described under 2.4. During the slow heating of the cell the gas volume slowly ascended to 199 mL until the venting of the cell at a temperature of 134.75 °C after 12000 s since the beginning of the experiment. The net gas evolved during the spontaneous venting was 326 mL after 300 s. The cell temperature climbed again and the cell went into thermal runaway around 195 °C and contributed to a net gas volume of 5593 mL which evolved instantly at 15000 s of test duration. The gross amount of gas was 6260 mL at the end of the experiment.

3.4 NCR18650GA

The NCR18650GA cell has a rated capacity of 3300 mAh at a nominal voltage of 3.60 V. Therefore the calculated nominal volumetric energy density is 718.3 Wh L^{-1}. The investigated cells had an average weigth of 46.75 ± 0.04 g. The gravimetric energy density was calculated to be 254.1 Wh kg^{-1}. The maximum, continuous discharge current is rated at 10 A which, in combination with the high capacity, makes the cell a good choice for high power applications.

3.4.1 Differential cell test NCR18650GA

The differential cell test for the NCR18650GA cell (Figure 22) again showed a strong decline of the cell voltage at a cell temperature around 100 °C. The cell voltage fell from 4.13 V to under 1 V and remained there until it rapidly rose again to 2.25 V at a cell temperature of 117.70 °C. At 128.17 °C cell temperature the voltage dropped again to under 1 V and oscillated around 0.5 and 1 V until the thermal runaway event when the cell voltage was reduced to zero.
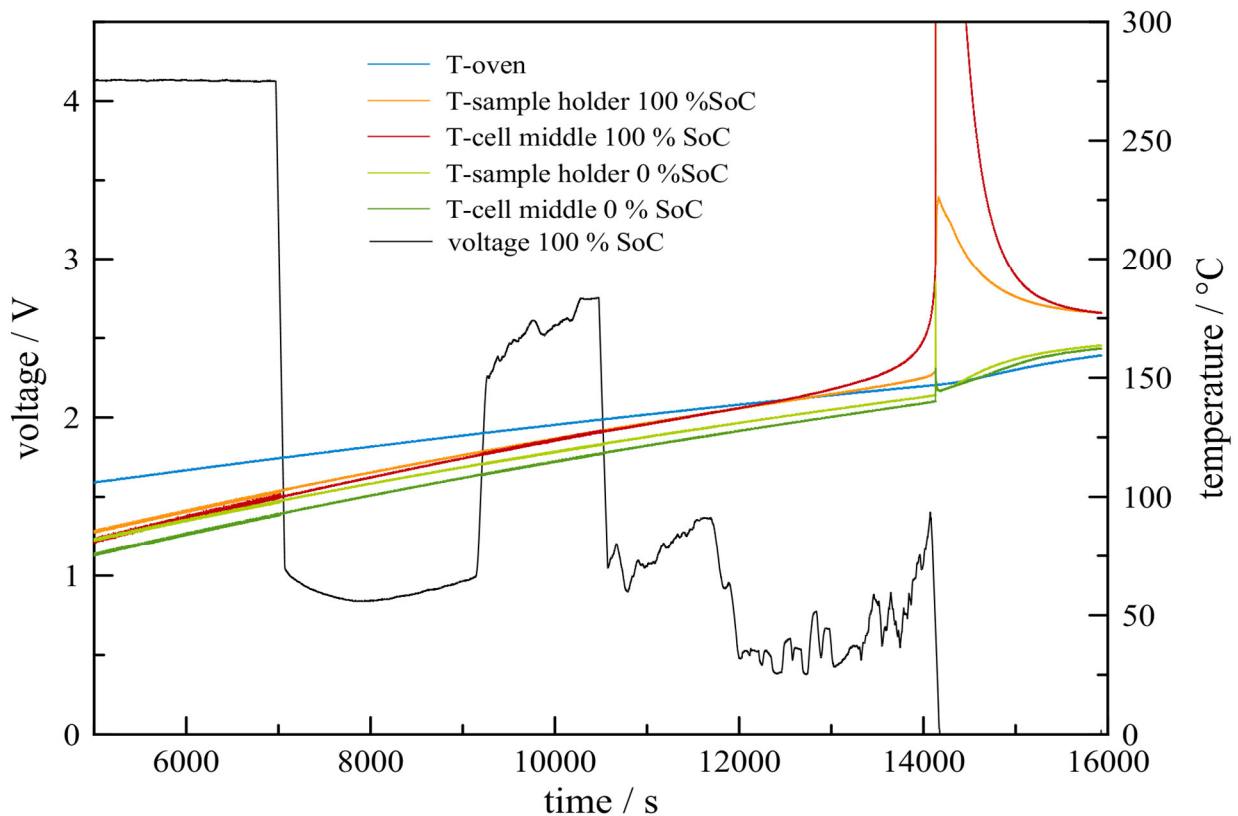
Figure 22: Temperature vs. time plot of the differential cell test experiment of the NCR18650GA cell, the cell and sample holder temperatures of each cell as well as the oven temperature and the cell voltage of the charged cell are plotted over the time.

The temperature of the charged and the uncharged cell slowly increased with ongoing test duration and the charged cell exceeded the oven temperature after 12500 s at a temperature of 140.65 °C. The charged cell went into thermal runaway after 14130 s since the start of the experiment and reached a maximum temperature of 741.34 °C. The developed heat from the thermal runaway of the charged cell increased the uncharged cell temperature from 140 °C to 144.52 °C. Neither the charged nor the uncharged cell showed any sign of venting during the whole test duration.

3.4.2 Thermal analysis NCR18650GA

The temperature of the NCR18650GA cell slowly increased with progressively heating. When the offset between oven and cell temperatures was big, the rate of which the cell heated up from room temperature was also higher. The closer the cell temperature was approaching the oven temperature the slower the increase. This can be seen in Figure 23. At a time of 13000 s and a cell temperature of 142.11 °C the cell equaled the oven temperature and slowly overtook it. After a runtime of 14505 s the cell went into thermal runaway and the temperature signal indicated 635.01, 676.29 and 411.01 °C in the front, middle and end position of the cell as the maximum temperatures. Again no venting could be identified in any of the three thermal ramp experiments.
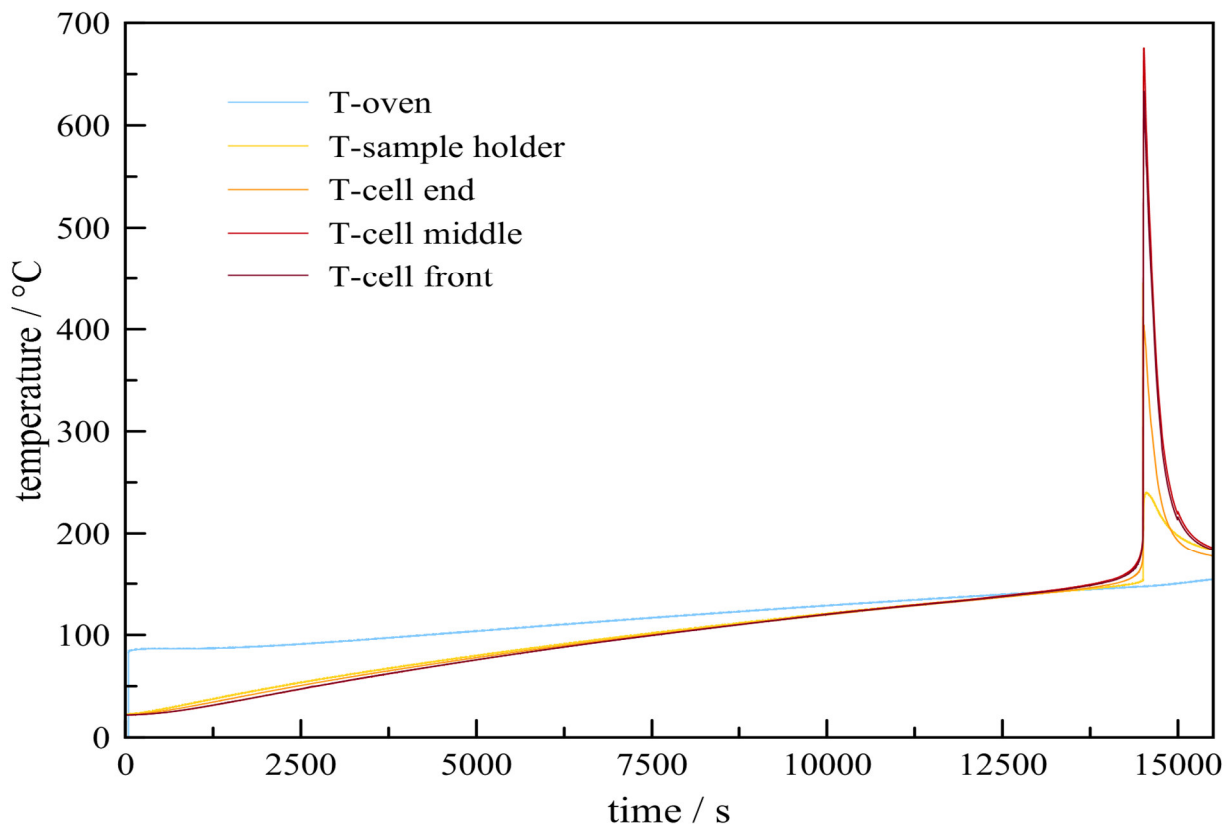
Figure 23: Temperature vs. time plot of the NCR18650GA 1 thermal ramp experiment.

As can be seen in Table 7 no venting event could be detected in the three individual thermal ramp experiments. Nevertheless each cell experienced thermal runaway and the individual experiments showed similar results.

Table 7: Summary of the key thermal indicators of three identical thermal ramp experiments of the NCR18650GA Li-ion cell.

experiment	Δm / g	T_{vent} / °C	Q_{vent} / KJ	T_{onset} / °C	T_{TR} / °C	T_{max} / °C	TR_{Rate} / °C min^{-1}	Q_{TR} / kJ
NCR18650GA 1	24.34	-	-	141.07	155.53	569.47	80.67	20.11
NCR18650GA 2	28.18	-	-	139.23	157.07	573.53	73.48	20.27
NCR18650GA 3	22.16	-	-	131.93	156.83	607.84	81.52	21.92

3.4.3 Gas analysis NCR18650GA

Since no 1st venting could be observed by the temperature signals from the NCR18650GA cell, the samples 1, 2 and 3 where taken at defined cell temperatures. Sample 1 at an averaged cell temperature of 120 °C, sample 2 at 135 °C and sample 3 at 150 °C. Again sample 4 was drawn from the reactor shortly before the deflagration of the cell. This was done equally for all three experiments. Even though the thermal signal showed no indication of a venting event an increasing amount of CO_2 was identified in the samples taken before the deflagration (Figure 24). It is likely that the cell vent opened partly and small quantities of electrolyte boiled out of the cell.

	1	2	3	4	5	6	7	8
N2 / %	99.99	99.82	98.55	96.10	27.64	44.41	67.29	88.62
CO2/ %	0.01	0.18	1.35	3.67	12.84	12.53	8.30	3.12
CO / %	0.00	0.00	0.00	0.00	36.31	24.08	12.47	4.22
H2 / %	0.00	0.00	0.00	0.03	20.16	16.24	10.06	3.33
CH4 / %	0.00	0.00	0.00	0.00	2.21	2.07	1.44	0.54
C2H2 / %	0.00	0.00	0.00	0.00	0.22	0.00	0.00	0.00
C2H4 / %	0.00	0.00	0.00	0.11	0.61	0.65	0.40	0.07
C2H6 / %	0.00	0.00	0.10	0.08	0.01	0.00	0.05	0.10
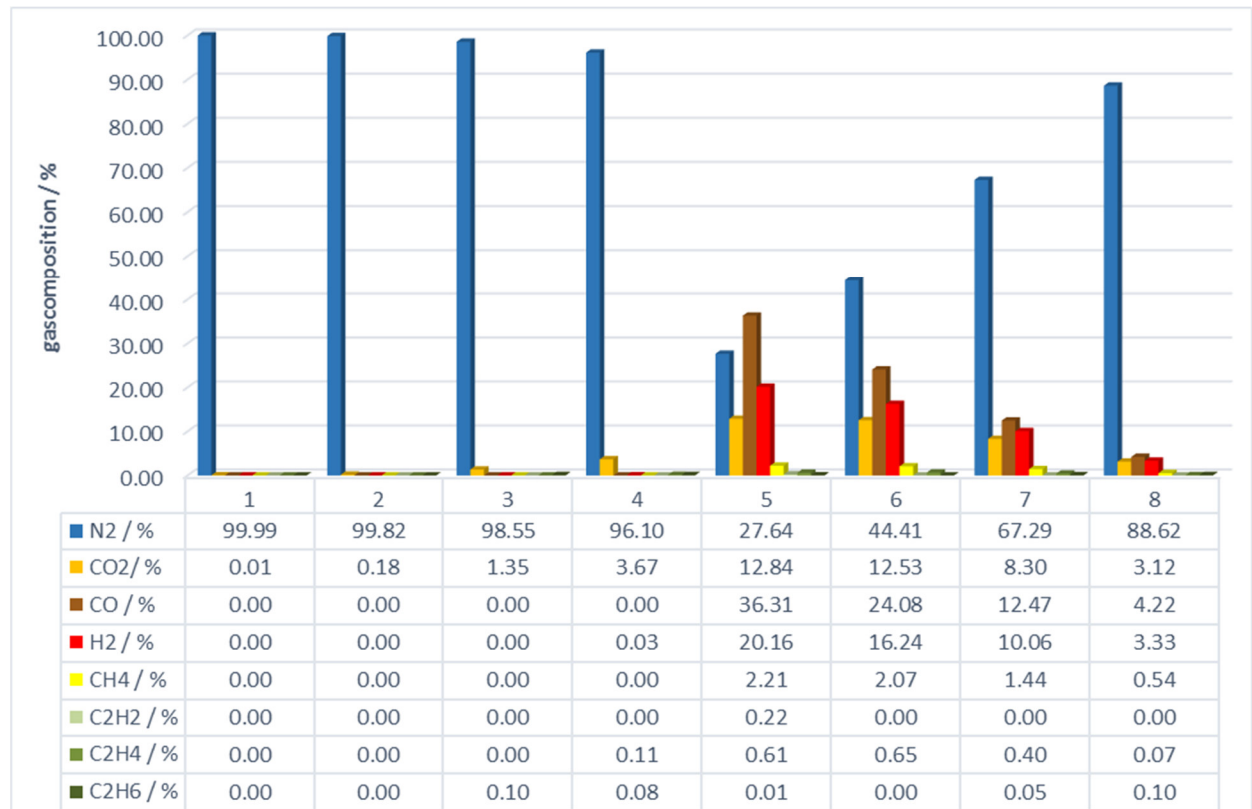
Figure 24: Gas composition of the eight samples taken from the reactor at specific moments during the NCR18650GA 1 experiment.

The sample 5 showed a diverse composition of the gas emitted during thermal runaway. With 36.31 % (CO), 20.16 % (H$_2$), 12.84 % (CO$_2$) and 2.21 % (CH$_4$) as the main detected gases. Also C$_2$-hydrocarbons were detected in minor proportions. The constant flushing with nitrogen displaced the emitted gas from the reactor and their amount decreased with time. The gascomposition of the sample 5 from the three individual thermal ramp experiments is summarized in Table 8.

Table 8: Gas composition of the three distinctive gas analysis experiments of the NCR18650GA cell, each sample was taken immediately after the thermal runaway event.

experiment	N$_2$ / %	CO$_2$ / %	CO / %	H$_2$ / %	CH$_4$ / %	C$_2$H$_2$ / %	C$_2$H$_4$ / %	C$_2$H$_6$ / %
NCR18650GA 1	27.64	12.84	36.31	20.16	2.21	0.22	0.61	0.01
NCR18650GA 2	32.37	6.96	31.14	27.30	2.17	0.00	0.00	0.06
NCR18650GA 3	36.21	13.03	30.42	17.98	1.84	0.00	0.48	0.03

Also in the gas volume experiment no venting was detected. After a runtime of 12000 s a gasvolume of 208 mL was measured at a cell temperature of 137.98 °C. This was mostly due to the temperature dependent expansion of the gas within the reactor. Before the thermal runaway at a runtime of 14000 s the gas volume increased to 490 mL. This steep increase in volume suggested that small proportions of electrolyte evaporated from the cell, decomposed and increased the gasvolume. This gas was also detected by the gas chromatograph. The thermal runaway event led to an additional gas development of 5904 mL. The absolut gas volume evolved during the whole experiment added up to 6394 mL.

3.5 ICR18650-32A

The ICR18650-32A features a nominal capacity of 3200 mAh at a nominal voltage of 3.75 V. The investigated cells had an averaged weight of 48.46 ± 0.10 g. The gravimetric energy density was calculated to be 247.6 Wh kg^{-1} and the volumetric energy density was 725.5 Wh L^{-1}. The maximum, continuous discharge current of 6.4 A combined with the relatively high capacity makes this cell suitable for a wide range of applications.

3.5.1 Differential experiment ICR18650-32A

Figure 25 illustrates the differential cell test for the ICR18650-32A cell. A slow decrease of the cell voltage can be observed with increasing temperature. At a cell temperature of 113.75 °C the voltage was reduced to 1.13 V until it quickly broke down to zero at the 1st venting of the cell at 129.95 °C after 10250 s of experimental runtime. The voltage signal showed inconstancy and increased again to 1.7 V until it completely collapsed at the thermal runaway after 15100 s.
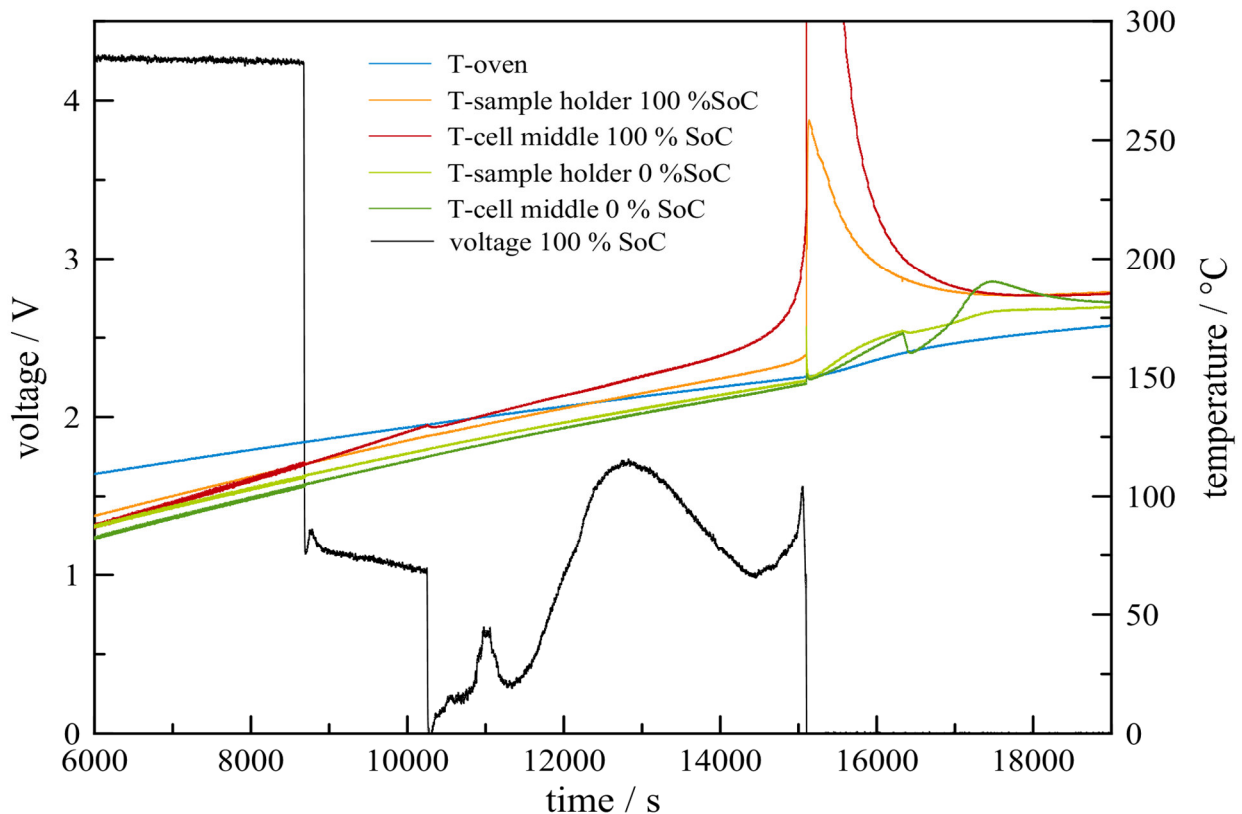
Figure 25: Temperature vs. time plot of the differential cell test experiment of the ICR18650-32A cell, the cell and sample holder temperatures of each cell as well as the oven temperature and the cell voltage of the charged cell are plotted over the time.

The thermal signals of the cells examined in the differential cell test steadily increased with the charged cell's temperature progressively exceeding the temperature of the discharged cell. At a cell temperature of 129.95 °C the 100 % SoC cell vented and it's temperature dropped about 0.9 K. It steadily increased afterwards until it experienced thermal runaway after 15100 seconds

since the start of the trial. The excess heat from the charged cell's thermal runaway supported the uncharged cell's temperature increase and it also vented at 168.74 °C which reduced it's temperature to 160.21 °C. The uncharged cell also showed an exothermic behavior which led to a strong increase of the cell temperature after the venting event. This slope flattened at a maximum temperature of 190.44 °C and the cell temperature resembled the sample holder temperature around 180 °C again and no further thermic events were observed.

3.5.2 Thermal analysis ICR18650-32A

The temperature vs. time plot of one of the three identical thermal ramp experiments is illustrated in Figure 26. With the initiation of the experiment the oven temperature started at roughly 80 °C while the cell temperatures were still around 28 °C. With ongoing heating the cell and sample holder temperatures converged toward the oven temperature. At 130.79 °C averaged cell temperature a mild venting of the cell was observed and lowered the temperature by 1.06 K to 129.73 °C. With ongoing heating the first exothermic behaviour of the cell was observed at the onset temperauture of 144.53 °C. After a runtime of 13795 s the cell reached a heating rate of 2 °C min^{-1} at a thermal runaway initiation temperature of 166.38 °C. During thermal runaway the cell reached an average, maximum temperature of 719.60 °C between the 3 thermocouples before it cooled down towards the oven temperature again.
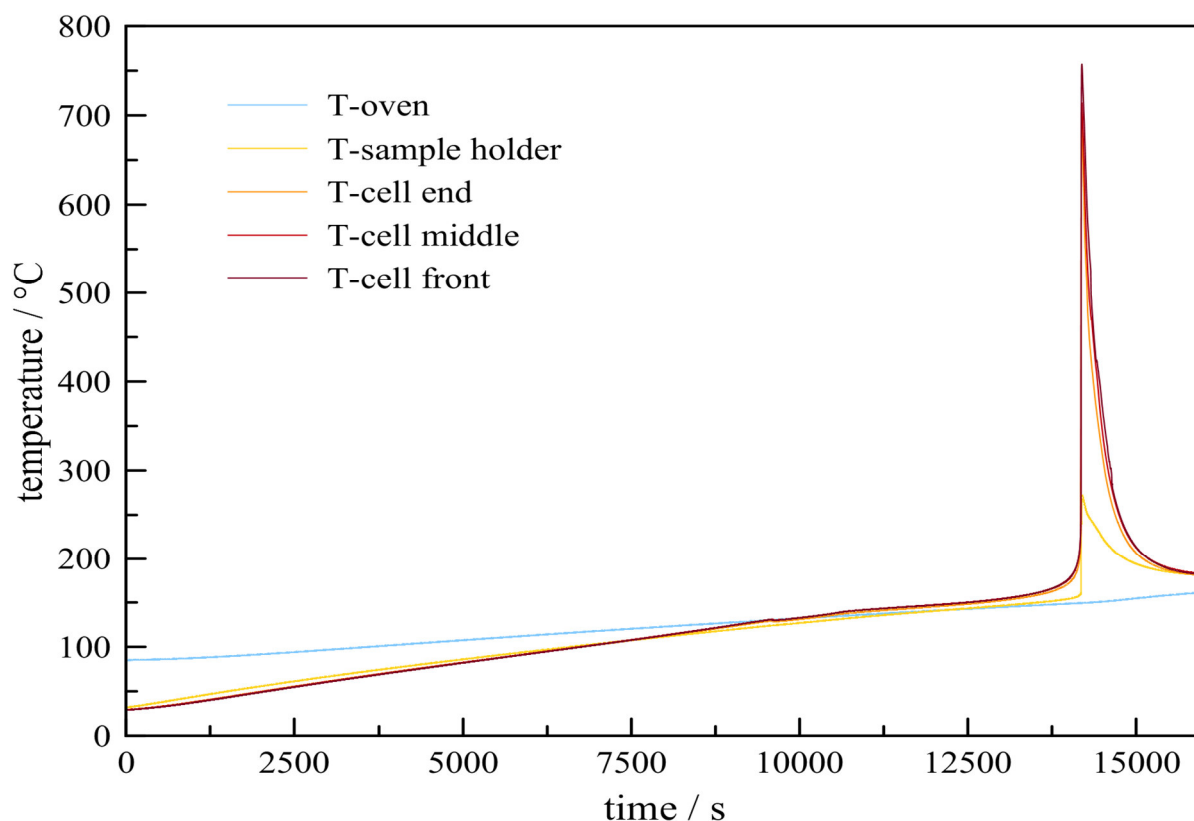
Figure 26: Temperature vs. time plot of the ICR18650-32A 1 thermal ramp experiment.

The specific thermal parameters of the three ICR18650-32A experiments are summarized in Table 9. Compared to the previously investigated cells the venting event of the ICR18650-32A cell was quite unremarkable. This could be seen by the low temperature difference and consequently the low dissipated heat of 50 and 40 J for the experiments 1 and 2. For the experiment 3 no venting was observed in the thermal survey.

Table 9: Summary of the key thermal indicators of three identically excecuted thermal ramp experiments of the ICR18650-32A Li-ion cell.

experiment	Δm / g	T_{vent} / °C	Q_{vent} / KJ	T_{onset} / °C	T_{TR} / °C	T_{max} / °C	TR_{Rate} / °C min^{-1}	Q_{TR} / kJ
ICR18650-32A 1	19.06	130.79	0.05	144.53	166.38	719.60	83.36	27.95
ICR18650-32A 2	26.76	128.46	0.04	144.69	166.92	557.97	58.27	19.80
ICR18650-32A 3	12.30	-	-	144.45	165.50	739.12	87.30	29.02

The onset temperature (T_{onset}) and the initiation of the thermal runaway temperature (T_{TR}) showed a low temperature difference of roughly 22 K. The magnitude of the thermal runaway can be defined as the maximum averaged cell temperature and the heat that got produced during the event. Here a less severe thermal runaway could be observed for the second experiment when compared to the other two tests.

3.5.3 Gas analysis ICR18650-32A

	1	2	3	4	5	6	7	8
N2 / %	100.00	99.64	99.44	97.78	45.40	57.33	68.68	85.84
CO2 / %	0.00	0.26	0.46	2.13	14.53	12.40	9.62	4.57
CO / %	0.00	0.00	0.00	0.00	29.45	20.56	13.69	5.37
H2 / %	0.00	0.00	0.00	0.08	7.37	6.51	5.21	2.59
CH4 / %	0.00	0.00	0.00	0.00	1.49	1.45	1.28	0.71
C2H2 / %	0.00	0.00	0.00	0.00	0.22	0.21	0.21	0.22
C2H4 / %	0.00	0.00	0.00	0.01	1.54	1.53	1.30	0.64
C2H6 / %	0.00	0.10	0.10	0.00	0.02	0.02	0.00	0.05
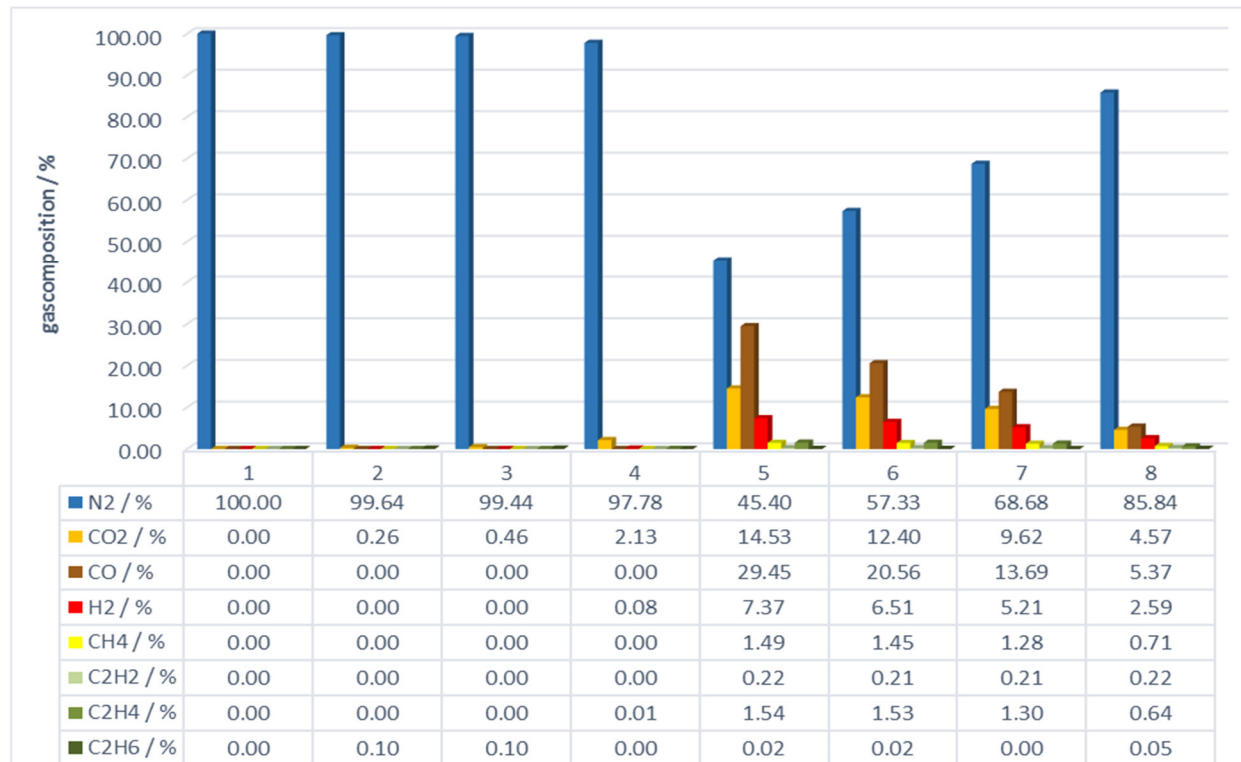
Figure 27: Gas composition of the eight samples taken from the reactor at specific moments during the ICR18650-32A 1 experiment.

Figure 27 illustrates the progression of the reactor gas composition during the ICR18650-32A 1 experiment. The low value for CO_2 of the venting samples 2 and 3 corresponds to the weak venting observed in the temperature plot. Sample 4 was taken prior the thermal runaway of the cell and had a CO_2 composition of more than 2 %. This indicated the ongoing boiling of electrolyte from the cell interior after the venting until the thermal runaway. The samples taken after the thermal runaway again showed a diverse composition of gases that got slowly diluted by the inert gas. In Table 10 the three individual gas samples taken directly after the thermal runaway are summarized. The high CO percentage in the ICR18650-32A 3 experiment is notable.

Table 10: Gas composition of the three distinctive gas analysis experiments of the ICR18650-32A cell, each sample was taken immediately after the thermal runaway event.

experiment	N_2 / %	CO_2 / %	CO / %	H_2 / %	CH_4 / %	C_2H_2 / %	C_2H_4 / %	C_2H_6 / %
ICR18650-32A 1	45.40	14.53	29.45	7.37	1.49	0.22	1.54	0.02
ICR18650-32A 2	29.11	9.60	36.37	19.21	2.85	0.00	2.77	0.10
ICR18650-32A 3	12.26	18.48	61.43	6.34	0.66	0.24	0.52	0.07

The gas volume determination also showed a relatively small gas volume development during the weak 1st venting of the cell. After a runtime of 10134 s the cell vented and the gasvolume increased from 200 mL to 305 mL after the venting. While the cell temperature declined from 132.69 °C to 131.54 °C. Prior the thermal runaway event, the gas volume had grown to 625 mL and increased during the thermal runaway by 3133 mL to an absolut volume of 3758 mL at the end of the thermal ramp experiment.

3.6 INR18650-35E

The INR18650-35E cell is equipped with a Li(Ni$_{0.8}$Co$_{0.15}$Al$_{0.05}$)O$_2$ cathode and has a nominal cell capacity of 3500 mAh and a nominal voltage of 3.60 V. The tested cells had a medium weight of 47.68 ± 0.10 g. The volumetric energy density of the cell is 761.8 Wh L^{-1} while the gravimetric energy density was calculated to 264.3 Wh kg^{-1}. With the high capacity and a high continuous discharge current of 8 A it is well suited for high power applications which also have high energy needs.

3.6.1 Differential cell test INR18650-35E

The differential cell test of the INR18650-35E cell gave basic information about the thermal and the open circuit voltage performance of the cell during a thermal ramp experiment. The outcome is presented in Figure 28. The voltage of the charged cell was 4.19 V at the beginning of the experiment and slowly declined to 4.11 V during the heat up. After 9370 s runtime the voltage quickly dropped to 1.20 V at a cell temperature of 116.50 °C. It rose again to 1.81 V before decreasing with the venting of the cell at a temperature of 135.16 °C where it dropped again to 1.22 V. Afterwards the cell regained it's voltage to 2.75 V until it dropped to 0 V with the thermal runaway of the cell.
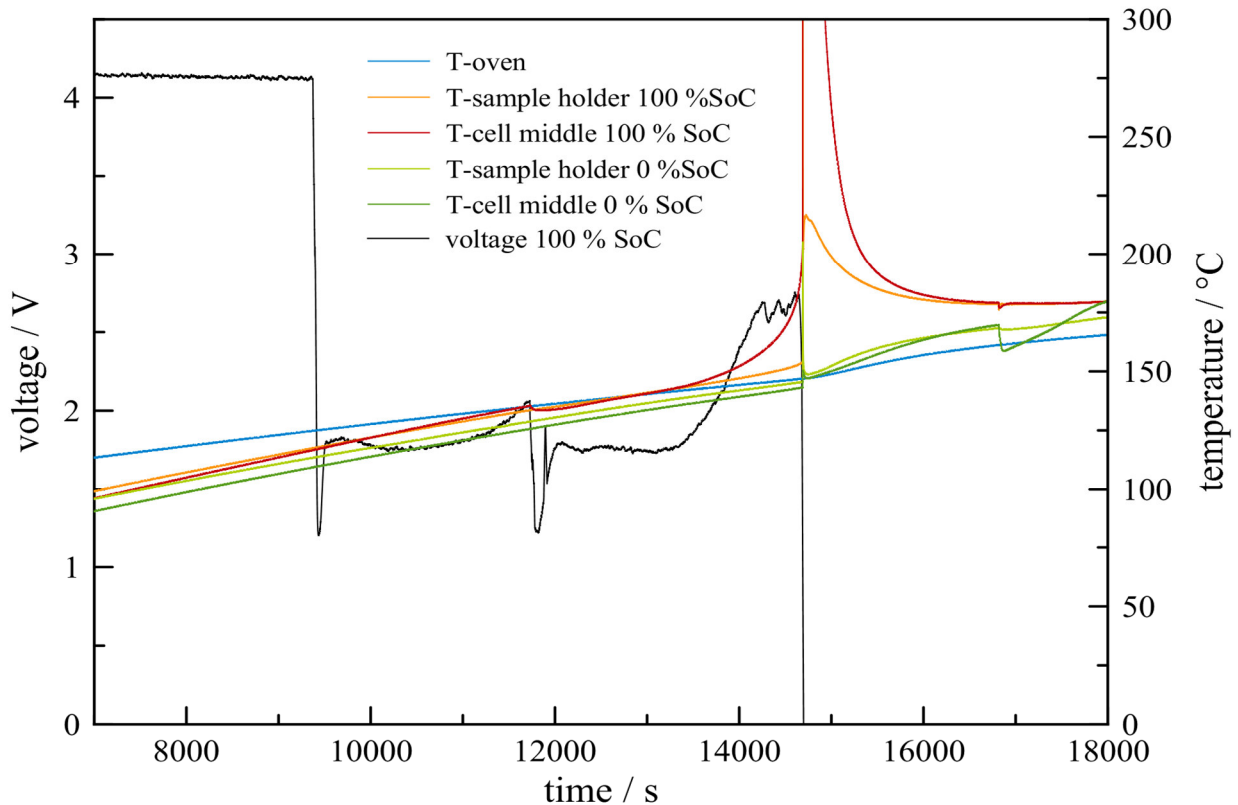
Figure 28: Temperature vs. time plot of the differential cell test experiment of the INR18650-35E cell, the cell and sample holder temperatures of each cell as well as the oven temperature and the cell voltage of the charged cell are plotted over the time.

As mentioned above the charged cell vented at a runtime of 11736 s where its temperature decreased from 135.16 °C to 133.39 °C. Thermal runaway occurred after 14279 s test duration and the cell reached 645.95 °C averaged maximum temperature. The discharged cell's temperature substantially increased by 4 K and the rate at which the cell heated up increased as well which could be observed as higher gradient in the temperature vs. time plot. The discharged cell afterwards experienced a venting event which lowered it's temperature from 169.57 to 158.77 °C. The discharged cell also showed an exothermic behavior which led to a strong increase of the cell temperature after the venting event which flattened at 182.5 °C and the cell temperature resembled the sample holder temperature again. The experiment was ended after no further thermal responses of both cells could be observed.

3.6.2 Thermal analysis INR18650-35E

Figure 29 displays a standard thermal ramp experiment of one of the three thermal experiments conducted for the INR18650-35E cell. The oven temperature is almost linear ascending over the whole experiment duration. The cell is mainly exposed to heat by the sample holder and therefore the temperatures of the cell advanced similar to that of the sample holder with a slight backlog. The three temperature signals ascended similar and no real offset was noticed for the heat up phase until the 1st venting event.
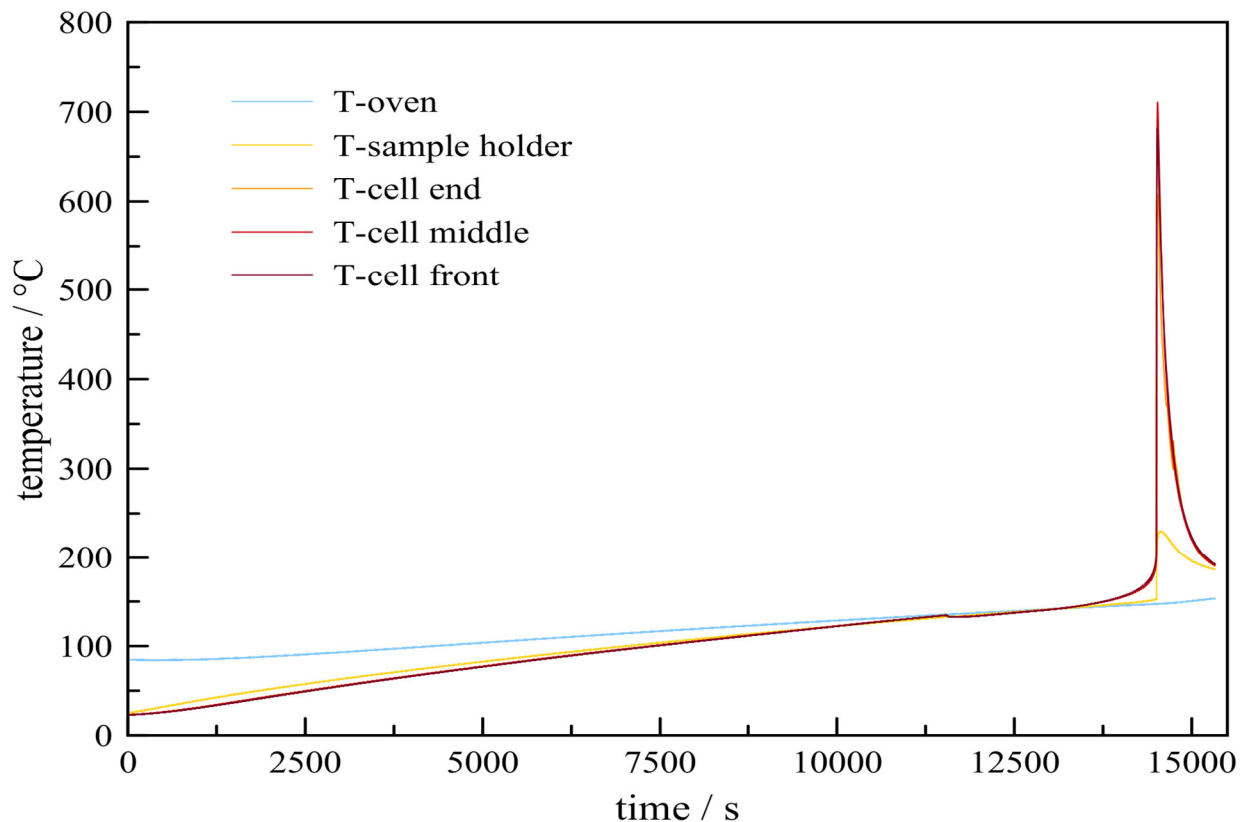
Figure 29: Temperature vs. time plot of the INR18650-35A 1 thermal ramp experiment.

The cell vented at an averaged temperature of 134.63 °C after 11537 s runtime. The venting lowered the cells temperature by 1.75 K and as a consequence dissipated 90.0 J of heat. The heating rate of the cell constantly increased after the onset temperature of 139.36 °C and at the cell temperature of 158.08 °C the spontaneous, highly exothermic thermal runaway initiated a steep temperature increase up to a maximum temperature (T_{max}) of 682.03, 711.97 and 670.25 °C at the end, middle and front position of the cell. This heat generation between the thermal runaway temperature (T_{TR}) and the maximum cell temperature was taking place with an averaged rate of 77.70 °C min^{-1} and was responsible for a heat generation of 26.28 kJ. This experimental results as well as the results of the two other thermal ramp tests of the same cell type are summarized in Table 11.

Table 11: Summary of the key thermal indicators of three identical thermal ramp experiments of the INR18650-35E Li-ion cell.

experiment	Δm / g	T_{vent} / °C	Q_{vent} / KJ	T_{onset} / °C	T_{TR} / °C	T_{max} / °C	TR_{Rate} / °C min^{-1}	Q_{TR} / kJ
INR18650-35E 1	26.54	134.63	0.09	139.36	158.08	688.08	77.70	26.28
INR18650-35E 2	28.15	134.82	0.10	139.42	158.11	582.65	74.16	21.06
INR18650-35E 3	21.10	132.93	0.07	138.55	157.28	712.15	102.19	27.53

3.6.3 Gas analysis INR18650-35E

	1	2	3	4	5	6	7	8
N2 / %	100.00	98.61	98.48	44.52	60.72	73.36	92.19	99.31
CO2/ %	0.00	1.39	1.52	8.61	8.59	6.65	2.20	0.32
CO / %	0.00	0.00	0.00	27.44	17.47	11.16	3.35	0.00
H2 / %	0.00	0.00	0.00	16.18	10.87	7.36	2.19	0.26
CH4 / %	0.00	0.00	0.00	1.70	1.25	0.90	0.00	0.00
C2H2 / %	0.00	0.00	0.00	0.24	0.25	0.00	0.00	0.00
C2H4 / %	0.00	0.00	0.00	1.24	0.77	0.48	0.06	0.11
C2H6 / %	0.00	0.00	0.00	0.06	0.08	0.09	0.00	0.00
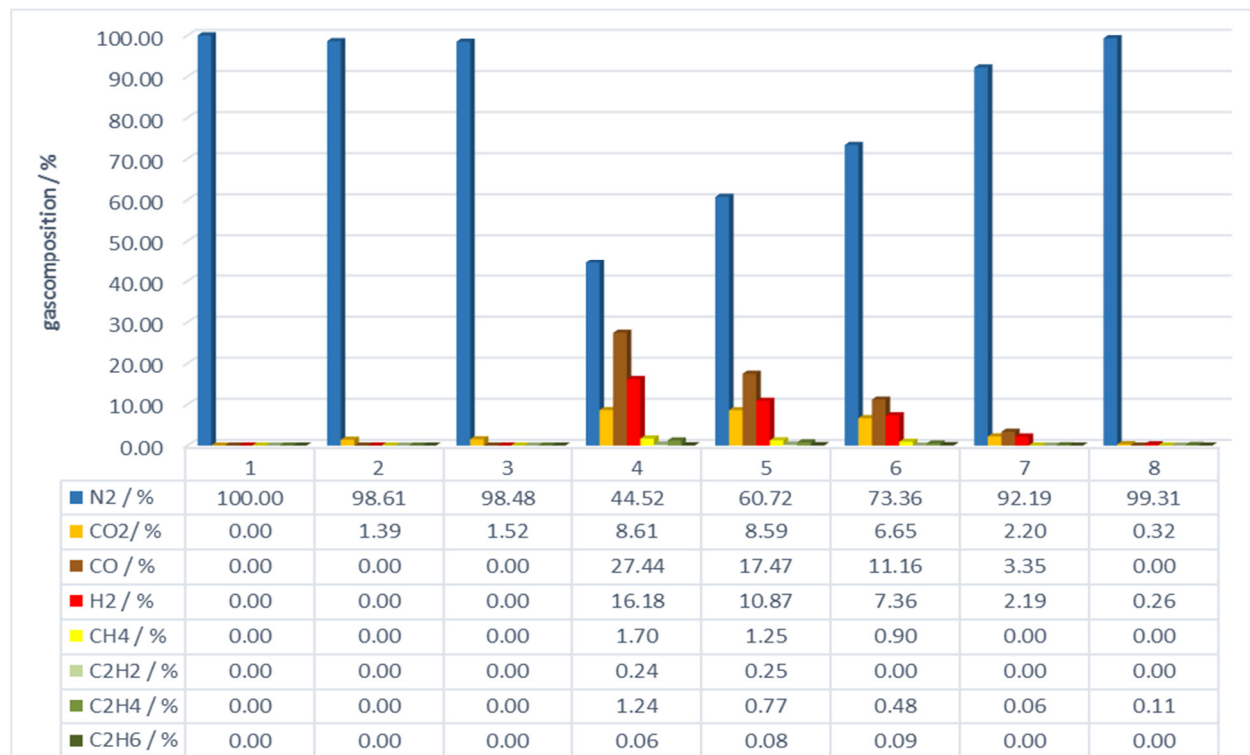
Figure 30: Gas composition of the eight samples taken from the reactor at specific moments during the INR18650-35E 3 experiment.

Figure 30 illustrates the gas composition of the eight gas samples taken during the thermal ramp test for the INR18650-35E cell. Sample 1 was taken before the first venting of the cell and only consisted of pure nitrogen gas. Therefore the cell still remained sealed. In the samples 2 and 3 small quantities of CO_2 were measured which exemplifies that the venting released gaseous emissions. After the thermal runaway a gas mixture was identified which got progressively diluted by the inert gas. In the experiment 3 the sample 4 was already taken after the thermal runaway event and no sample was taken prior the event. This was done because also a sample 10 minutes after the thermal runaway event was used to investigate the gas evolution after the thermal runaway event. No newly produced gases were measured and the reactor gas composition was further diluted by the inert gas. This gives rise to the assumption that after the thermal runaway all cell constituents were consumed and no further reactions took place.

The gas composition of the three INR18650-35E experiments is summarized in Table 12 for the samples taken immediately after the thermal runaway event.

Table 12: Gas composition of the three distinctive gas analysis experiments of the INR18650-35E cell, each sample was taken immediately after the thermal runaway event.

experiment	N_2 / %	CO_2 / %	CO / %	H_2 / %	CH_4 / %	C_2H_2 / %	C_2H_4 / %	C_2H_6 / %
INR18650-35E 1	41.44	11.94	22.00	21.29	2.26	0.00	1.04	0.03
INR18650-35E 2	31.84	5.18	30.65	28.29	2.76	0.00	1.27	0.00
INR18650-35E 3	44.52	8.61	27.44	16.18	1.70	0.24	1.24	0.06

The volume of the evolving gases during a thermal ramp experiment was investigated with the water displacement apparatus described under 2.4. At a cell temperature of 134.97 °C the scale showed a value of 128 g which equaled the gasvolume of 128 mL. After the venting 388 mL of absolut gas amount was measured which indicated an evolved gas volume during venting of 260 mL. Before the thermal runaway of the cell the developed gas volume was 619 mL which quickly increased to 6230 mL after the exothermic event. Therefore 5610 mL of gaseous emissions were evolved by the thermal runaway process.

3.7 INR18650MJ1

The INR18650MJ1 cell has a nominal voltage of 3.64 V and a nominal capacity of 3500 mAh. The tested cells had an averaged weight of 46.31 ± 0.13 g. The high capacity in combination with the high continuous discharge current of 10 A makes the cell suitable for a wide range of high power and high energy applications. The gravimetric energy density of the cell is 274.7 Wh g^{-1} and the volumetric energy density is 769.2 Wh L^{-1}.

3.7.1 Differential experiment INR18650MJ1

Figure 31 illustrates the voltage and temperature curves of the INR18650MJ1 differential experiment over the test duration. The open circuit voltage remained around 4.15 V until it diminished to 1.25 V at a cell temperature of 113.08 °C. Shortly after at a cell temperature of 122.36 °C the cell vented and the voltage increased from 1.52 V to 2.11 V. After the venting of the charged cell the voltage slowly declined until it collapsed with the thermal runaway of the cell.
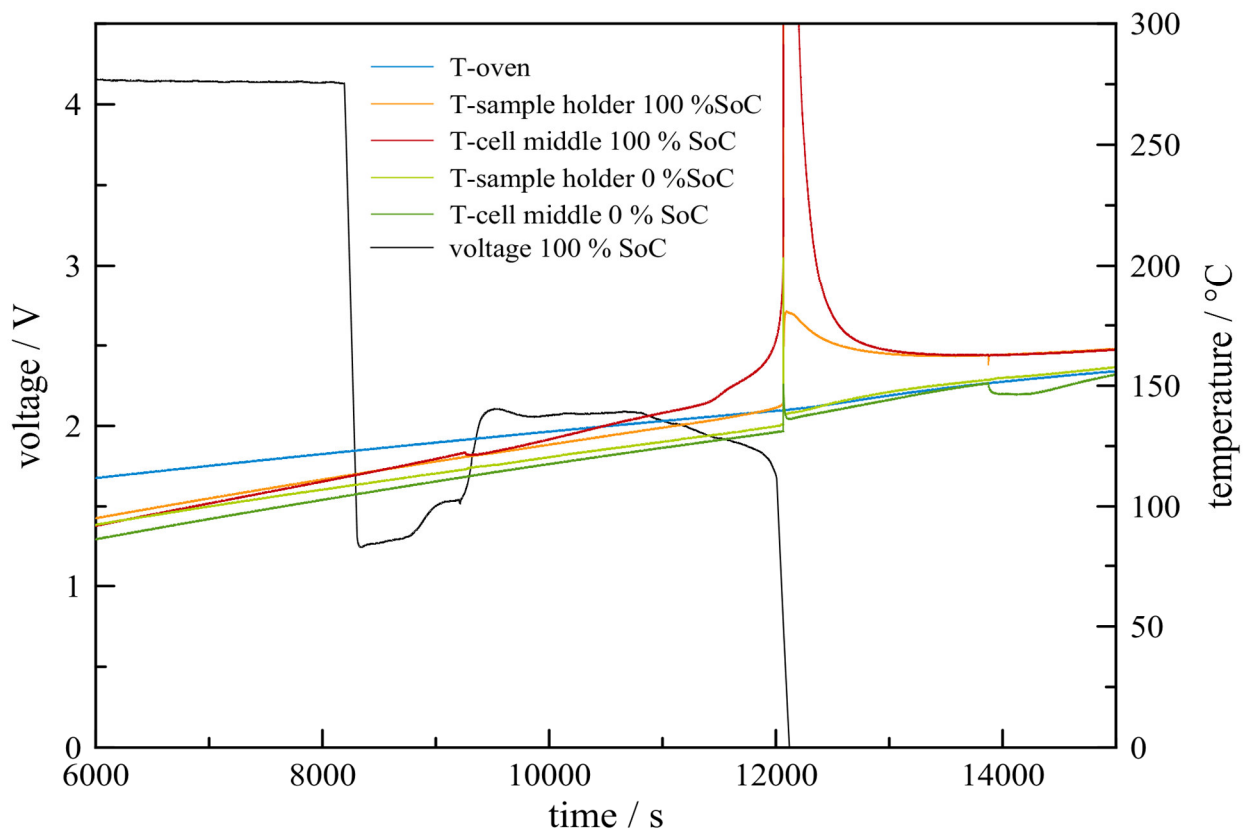
Figure 31: Temperature vs. time plot of the differential cell test experiment of the INR 18650 MJ1 cell, the cell and sample holder temperatures of each cell as well as the oven temperature and the cell voltage of the charged cell are plotted over the time.

The differential cell test showed a venting of the charged cell after 9863 s when the cell had an averaged temperature of 122.74 °C. The venting reduced this temperature to 121.31 °C. The ongoing heating increased this temperature further and after a runtime of 12490 s the cell experienced thermal runaway with a maximum temperature of 578.23 °C. This event produced a heat amount of 20.72 kJ which also increased the discharged cell temperature by ≈ 5 K. The uncharged cell vented at a temperature of 151.16 °C.

3.7.2 Thermal analysis INR18650MJ1

After the differential cell test the INR18650MJ1 cell was further investigated for its response to thermal ramp heating. As with the experiments of the previously tested cells the oven was pre-heated to 80 °C and the test was started. With ongoing heating the cell and sample holder temperatures approached the temperature of the oven. After 9332 s since the start of the test a venting of the cell took place. The cell temperature was 121.50 °C and got reduced by 0.83 K during the venting. At 138.47 °C cell temperature the onset temperature was reached. From there on the cell's heating rate increased continuously and a significant knee can be seen in Figure 32 at 143.44 °C when the heating gradient increased furthermore. Soon afterwards the cell experienced thermal runaway after 12140 s. This lead to a maximum cell temperature of 393.90, 519.10 and 470.40 °C at the end, middle and front position of the cell.
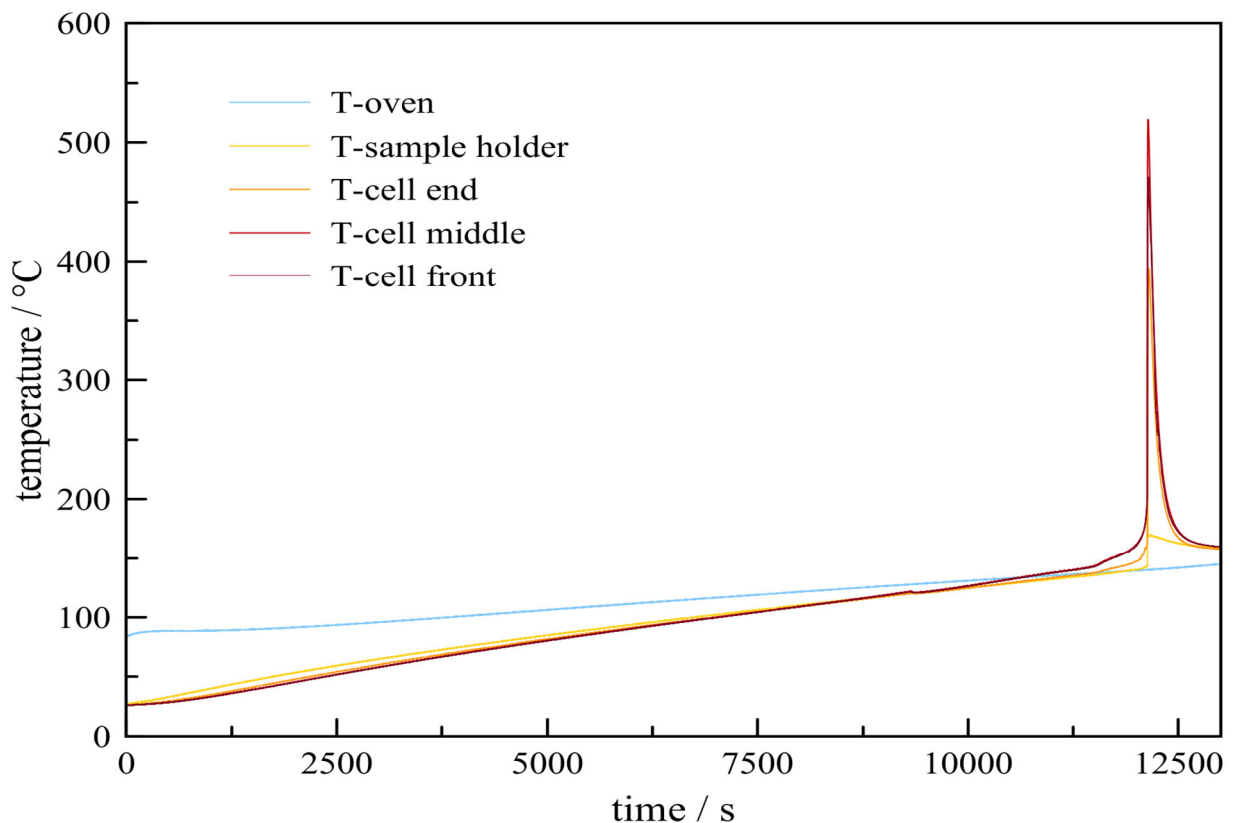
Figure 32: Temperature vs. time plot of the INR18650MJ1 1 thermal ramp experiment.

The specific thermal parameters of the three INR18650MJ1 experiments are summarized in the Table 13.

Table 13: Summary of the key thermal indicators of three identical thermal ramp experiments of the INR18650MJ1 Li-ion cell.

experiment	Δm / g	T_{vent} / °C	Q_{vent} / KJ	T_{onset} / °C	T_{TR} / °C	T_{max} / °C	TR_{Rate} / °C min^{-1}	Q_{TR} / kJ
INR18650MJ1 1	33.56	121.80	0.05	139.30	151.13	424.57	44.76	13.17
INR18650MJ1 2	35.23	121.50	0.04	138.47	149.33	461.13	57.03	14.98
INR18650MJ1 3	30.90	122.57	0.04	138.77	151.98	515.50	69.89	17.47

3.7.3 Gas analysis INR18650MJ1

Figure 33 presents the gas composition development of the INR18650MJ1 1 experiment graphically. After the venting increasing proportions of CO_2 were measured. Sample 5 was taken immediately after the thermal runaway event and showed a diverse composition of detected gases with relatively high H_2 concentration which even increased in the sample 6 which was taken 60 seconds after the thermal runaway.

	1	2	3	4	5	6	7	8
N2 / %	100.00	99.56	99.14	96.94	36.71	49.24	62.22	87.49
CO2 / %	0.00	0.44	0.86	3.06	8.56	4.20	4.44	3.15
CO / %	0.00	0.00	0.00	0.00	21.17	8.94	7.49	2.64
H2 / %	0.00	0.00	0.00	0.00	27.62	31.25	21.48	5.08
CH4 / %	0.00	0.00	0.00	0.00	4.50	4.70	3.31	1.03
C2H2 / %	0.00	0.00	0.00	0.00	0.00	0.00	0.00	0.31
C2H4 / %	0.00	0.00	0.00	0.00	1.42	1.60	1.04	0.20
C2H6 / %	0.00	0.00	0.00	0.00	0.01	0.07	0.01	0.10
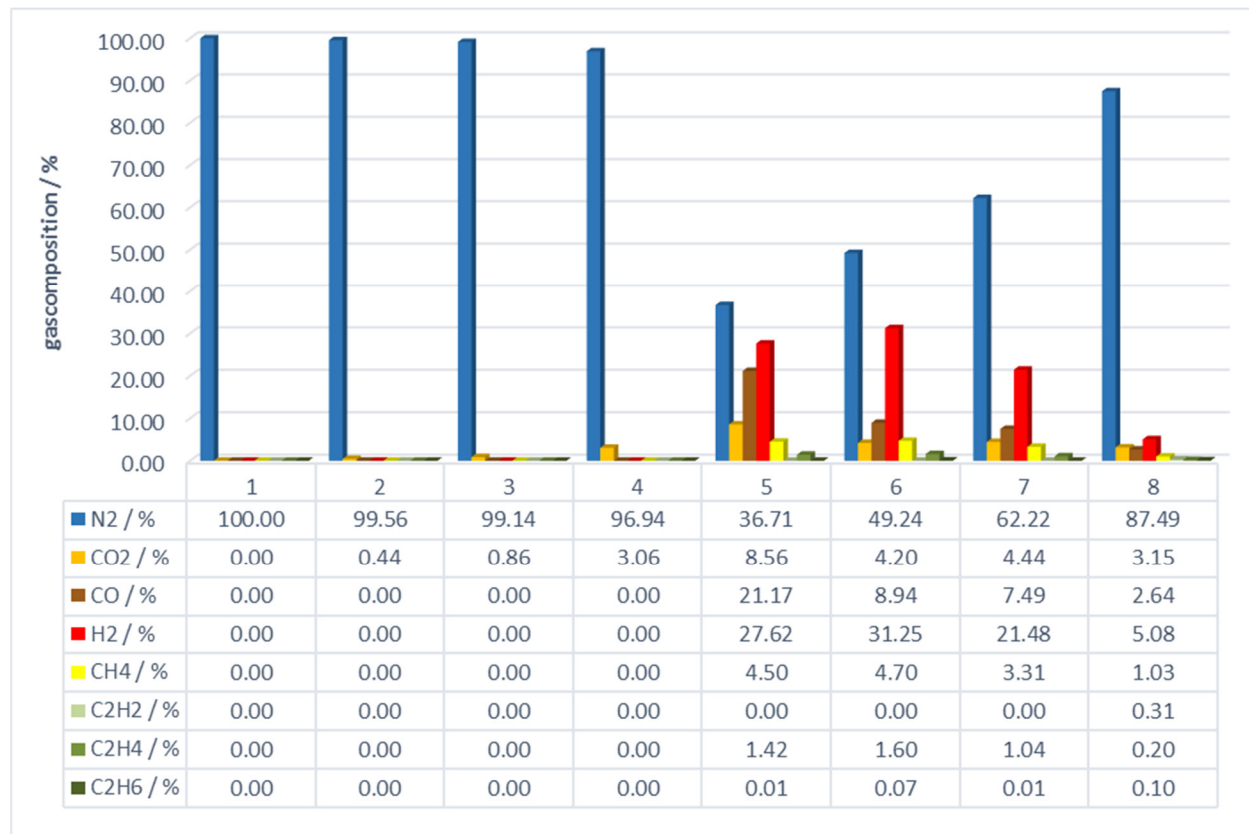
Figure 33: Gas composition of the eight samples taken from the reactor at specific moments during the INR18650MJ1 1 experiment.

The sample 5 which was taken immediately after the thermal runaway event had the most informative value. The compositon of this sample is summarized in Table 14 for the three individual thermal ramp experiments of the INR18650MJ1 cell.

Table 14: Gas composition of the three distinctive gas analysis experiments of the INR18650MJ1 cell, each sample was taken immediately after the thermal runaway event.

experiment	N_2 / %	CO_2 / %	CO / %	H_2 / %	CH_4 / %	C_2H_2 / %	C_2H_4 / %	C_2H_6 / %
INR18650MJ1 1	36.71	8.56	21.17	27.62	4.50	0.00	1.42	0.01
INR18650MJ1 2	32.44	6.66	29.50	25.42	3.88	0.32	1.74	0.04
INR18650MJ1 3	52.65	5.51	14.29	22.49	3.52	0.27	1.26	0.02

After the differential cell test and the thermal investigation of the cells, which also incorporated the gas analysis, the gas volume emitted by the cell was measured. During the slow heating of the cell the gas volume slowly ascended to 71 mL until the venting of the cell at a temperature of 124.79 °C after 9780 s since the beginning of the experiment. The net gas volume evolved during the spontaneous venting was 87 mL after 300 s. The temperature climbed again, the cell went into thermal runaway after 13030 s and contributed to a net gasvolume increase of 5261 mL which evolved instantely after the thermal runaway event. The gross amount of gas was 5636 mL at the end of the experiment.

3.8 18650HE4

The 18650HE4 features a Li(NiMnCo)O_2 cathode, a nominal capacity of 2500 mAh and a nominal voltage of 3.60 V. The evaluated cells had an average weight of 45.48 ± 0.16 g. The gravimetric energy density was calculated to be 197.9 Wh kg^{-1} and a volumetric energy density of 544.1 Wh L^{-1}. The low capacity and the very high continuous discharge current of 20 A make it a designated cell for short term, high power applications.

3.8.1 Differential cell test 18650HE4

The differential cell test for the 18650HE4 cell is displayed in Figure 34. Initially the cell voltage started at a value of 4.17 V and slowly decreased with ongoing heating. After 7764 s it rapidly dropped from 4.11 V to as low as 0.77 V at a respective cell temperature of 105.78 °C. The venting of the charged cell led to a steep rise of the voltage to 2.58 V. The cell voltage went to 2.09 V before it rose to 2.58 V again and started a slow decline. During this steady decline of the cell voltage, several events were observed where the voltage dropped for a very short period of time but regained its former value quickly after. After a runtime of 17600 s, when no runaway had taken place yet, the voltage was still measurable but remained under 0.10 V.
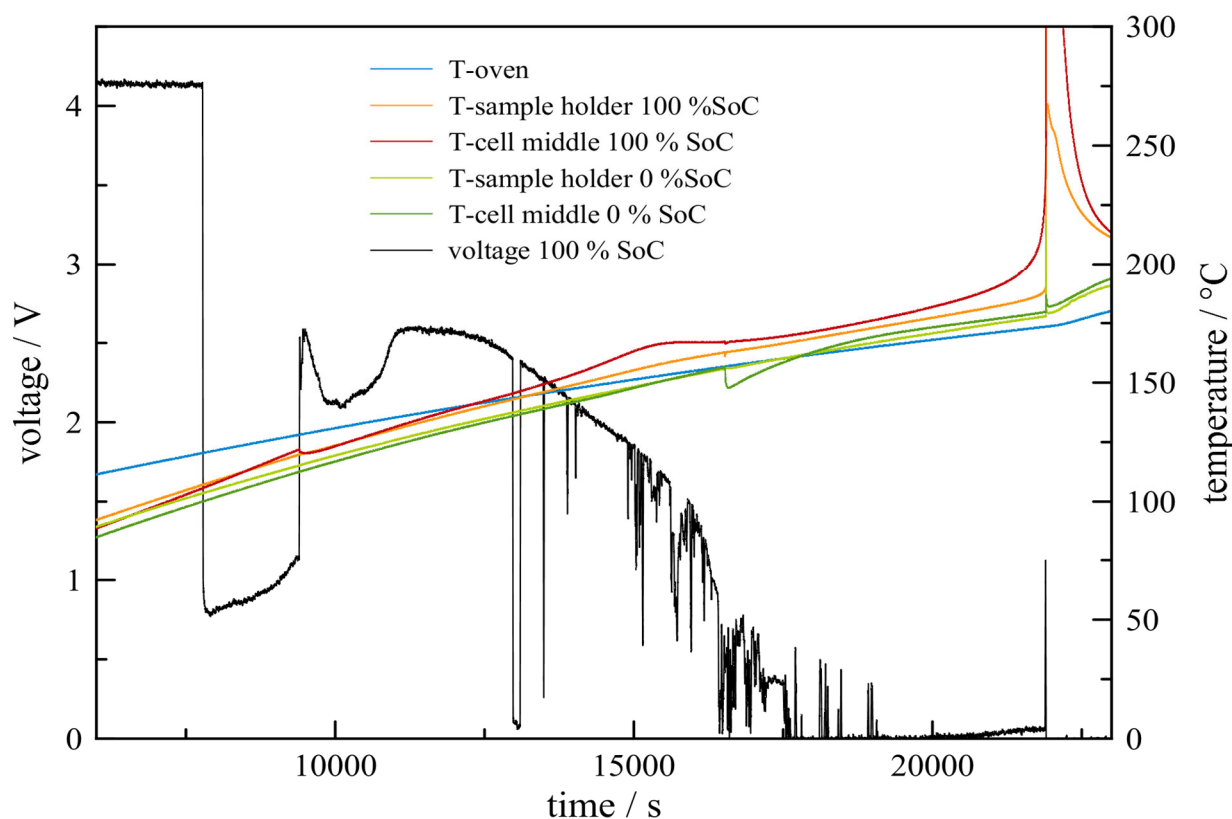
Figure 34: Temperature vs. time plot of the differential cell test experiment of the 18650HE4 cell, the cell and sample holder temperatures of each cell as well as the oven temperature and the cell voltage of the charged cell are plotted over the time.

After the start of the experiment the cell temperatures slowly increased accoarding to the respective sample holder temperature. At a cell temperature of 121.68 °C the 100 % SoC cell vented and it's temperature dropped by 1.61 K. It remained higher than the discharged cell and steadily increased afterwards which increased the offset between charged and discharged cell. A clear exothermic behavior was observed as a steadily increasing offset between sample holder and cell temperature which peaked around 15500 s before the cell temperature approached the sample holder temperature again. After 21880 s runtime the charged cell went into the exothermic runaway and reached an averaged cell temperature of 578.23 °C. The discharged cell vented after 16530 s. This was long before the 100 % SoC cell thermal runaway event.

3.8.2 Thermal analysis 18650HE4

For the thermal ramp experiments of the 18650HE4 the oven started at the set temperature of roughly 80 °C when the test was started. Constant heating of the oven slowly increased the sample holder and consequently the cell temperatures. The venting of the cell can be seen in the Figure 35 as a decrease of the cell temperature at 8975 s. This endothermic cooling reduced the cell temperature from 116.51 °C to 115.44 °C. The dissipated heat by the venting event amounted to 50.8 J.
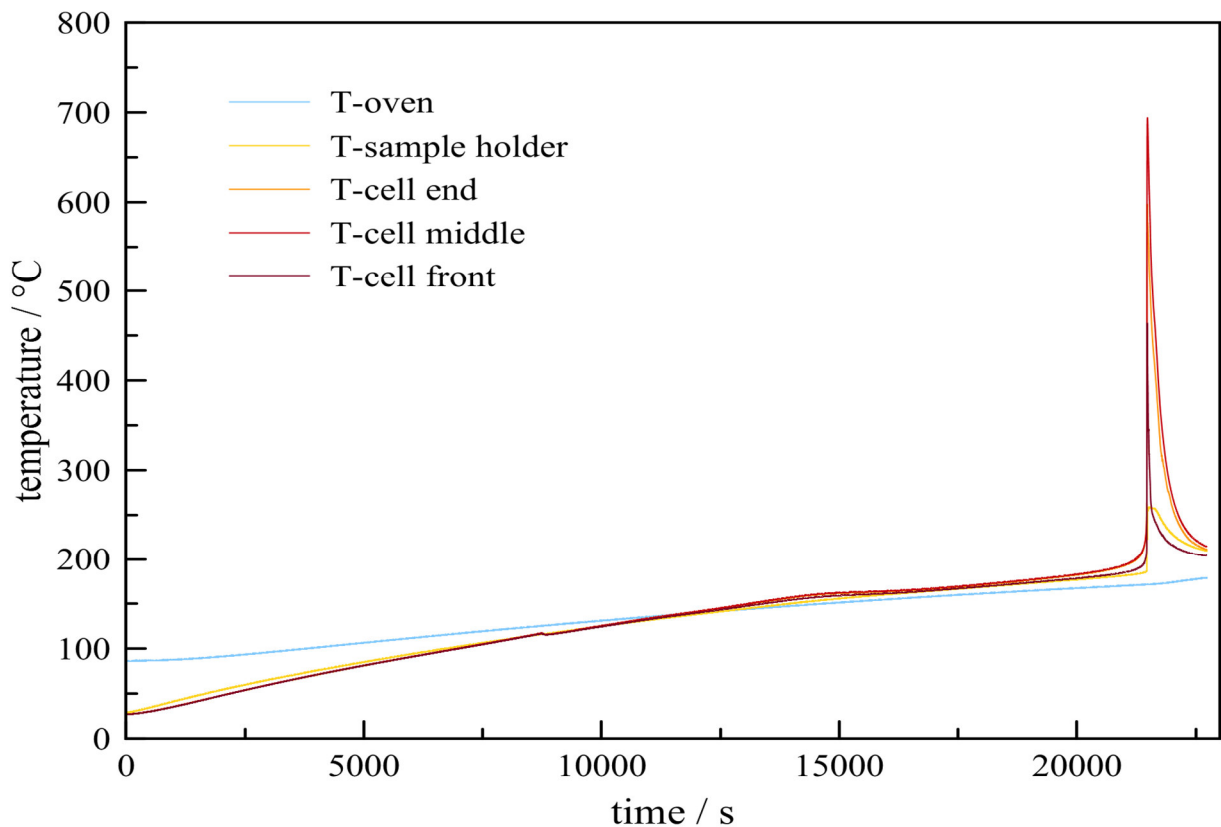
Figure 35: Temperature vs. time plot of the 18650HE4 1 thermal ramp experiment.

After the venting the cell regained its former temperature and showed a clear exothermic behavior which raised it's temperature significantly over the oven and sample holder temperature. This can be observed as a shallow peak around 15000 s. This peak flattened and the cell temperature ascended towards the sample holder temperature again. The thermal runaway of the cell resulted in an abrupt increase of the cell temperature to an averaged value of 563.83 °C. After the cell material was consumed in this exothermic event the cell cooled down to the oven temperature again. In the Table 15 the key thermal parameters of the three distinctive thermal ramp experiments are summarized.

Table 15: Summary of the key thermal indicators of three identical thermal ramp experiments of the 18650HE4 Li-ion cell.

experiment	Δm / g	T_{vent} / °C	Q_{vent} / KJ	T_{onset} / °C	T_{TR} / °C	T_{max} / °C	TR_{Rate} / °C/min^{-1}	Q_{TR} / kJ
18650HE4 1	28.63	116.51	0.05	165.63	196.82	661.02	91.55	21.89
18650HE4 2	13.23	117.19	0.06	162.38	194.36	584.91	79.83	18.58
18650HE4 3	12.99	118.26	0.11	163.02	196.25	556.26	78.58	16.99

3.8.3 Gas analysis 18650HE4

	1	2	3	4	5	6	7	8
N2 / %	99.67	99.75	99.79	95.87	22.03	50.13	71.10	91.35
CO2 / %	0.29	0.21	0.13	3.89	14.07	9.05	6.20	2.24
CO / %	0.00	0.00	0.00	0.00	45.84	24.53	11.99	2.58
H2 / %	0.03	0.04	0.07	0.14	15.36	14.63	9.78	3.68
CH4 / %	0.00	0.00	0.00	0.00	1.18	0.86	0.60	0.00
C2H2 / %	0.00	0.00	0.00	0.00	0.22	0.31	0.00	0.00
C2H4 / %	0.00	0.00	0.00	0.10	1.27	0.45	0.26	0.04
C2H6 / %	0.00	0.00	0.00	0.00	0.03	0.04	0.06	0.11
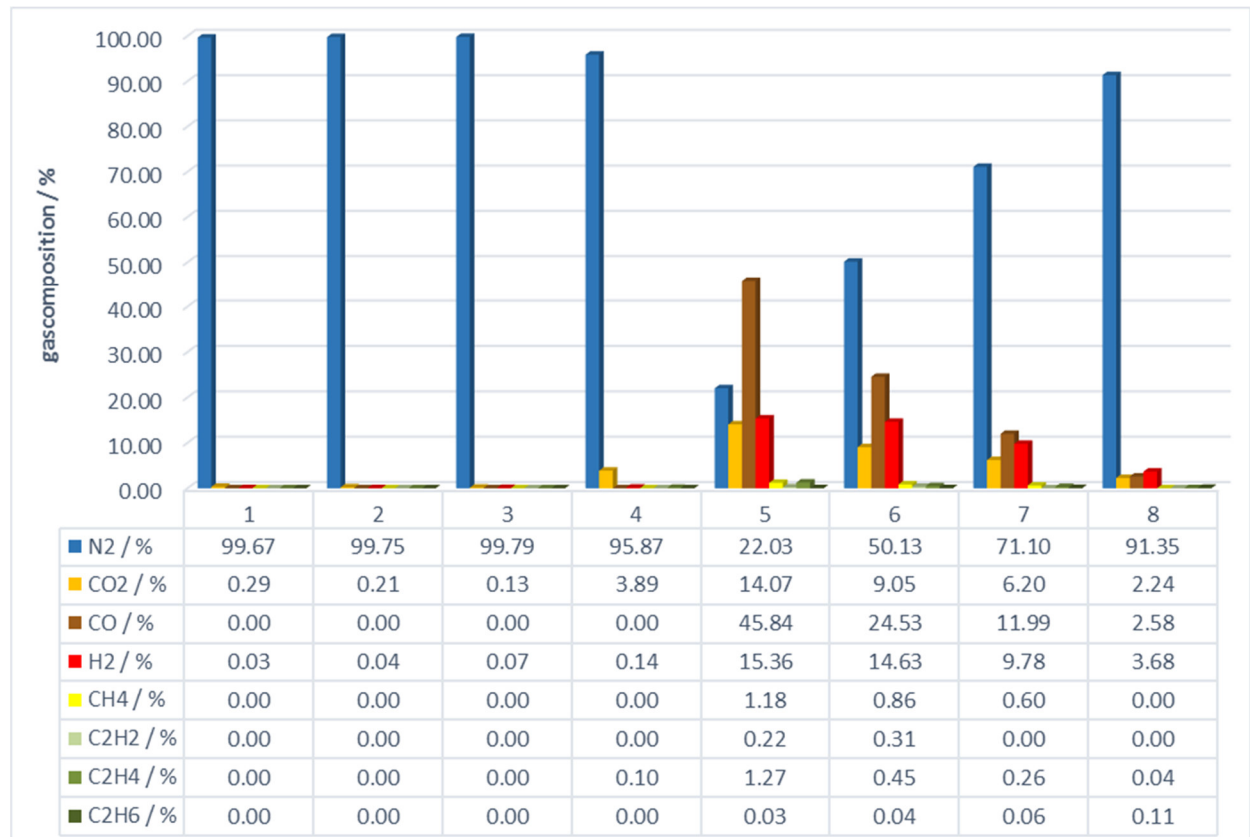
Figure 36: Gas composition of the eight samples taken from the reactor at specific moments during the 18650HE4 3 experiment.

Figure 36 illustrates the gas composition of the eight gas samples taken during the thermal ramp test for the 18650HE4 cell. Sample 1 was taken before the first venting of the cell and already showed small proportions of CO_2 and H_2 besides the flushing gas N_2. This might indicate electrolyte degradation prior the thermally identified venting of the cell. Samples 2 and 3 were taken after the venting of the cell was indicated by a decrease in cell temperature. But they did not show increasing amounts of gas components which would have indicated electrolyte degradation. Sample 4 was taken shortly before the runaway event and showed almost 4 % of CO_2 which clearly indicates a boiling of the electrolyte and its degradation products from the cell. After the thermal runaway a gas mixture was identified which got progressively diluted by the inert gas.

The gas composition of the sample 5 from the three individual thermal runaway experiments are summarized in Table 16.

Table 16: Gas composition of the three distinctive gas analysis experiments of the 18650HE4 cell, each sample was taken immediately after the thermal runaway event.

experiment	N_2 / %	CO_2 / %	CO / %	H_2 / %	CH_4 / %	C_2H_2 / %	C_2H_4 / %	C_2H_6 / %
18650HE4 1	26.25	16.88	23.61	30.01	2.46	0.00	0.62	0.17
18650HE4 2	24.90	14.62	43.08	14.54	1.17	0.24	1.43	0.02
18650HE4 3	22.03	14.07	45.84	15.36	1.18	0.22	1.27	0.03

For the 18650HE4 cell several gas volume measurement experiments were conducted. The heating power of 74.27 W, which was used for all other experiments, was alternated to investigate the influence of the heat input on the cells thermal response and gas development. The heating of the oven was increased to 272 W which led to an quicker heat up of the cells. The results of this alternated experiments are summarized in Table 17.

Table 17: Summarized resutls of the alternated gasvolume measurements of the 18650HE4 cell.

experiment	heating power / W	T_{vent} / °C	t_{vent} / s	gas volume venting / mL	T_{onset} / °C	T_{TR} / °C	gas volume TR / mL	t_{TR} / s
18650HE4 4	74.27	116.05	8266	155	162.13	192.29	2930	22524
18650HE4 5	74.27	118.27	9210	128	164.10	198.68	2888	23534
18650HE4 6	272	137.76	3922	274	143.47	160.96	4430	4940
18650HE4 7	272	143.33	4235	369	147.48	156.1	3955	5070

3.9 ICR18650-26F

The ICR18650-26F cell is composed of a Li(NiMnCo)O$_2$ cathode and possesses a capacity of 2600 mAh at a nominal voltage of 3.7 V. The cells of interest had an average weight of 44.14 ± 0.05 g. A low capacity and a low maximum discharge current of 5.2 A is limiting this cell to low power applications with small energy consumption. The gravimetric energy density of the cell is 218 Wh g^{-1} and the volumetric energy density is 581.6 Wh L^{-1}.

3.9.1 Differential analysis ICR18650-26F

The differential cell test of the NCR18650-26F cell gave basic information about the thermal and the open circuit voltage performance of the cell during a thermal ramp experiment and is presented in Figure 37. The voltage of the charged cell remained constant at the typical OCV of 4.15 V until the cell reached a temperature of 116.25 °C. At this point the cell voltage quickly decreased to a value of 1.43 V. The 1st venting event of the cell reduced the voltage from 2.00 V to 0.44 V from where it increased again to 1.44 V until it began to drop at a cell temperature of 160.70 °C With the thermal runaway of the cell the voltage fell to zero after 14780 s.
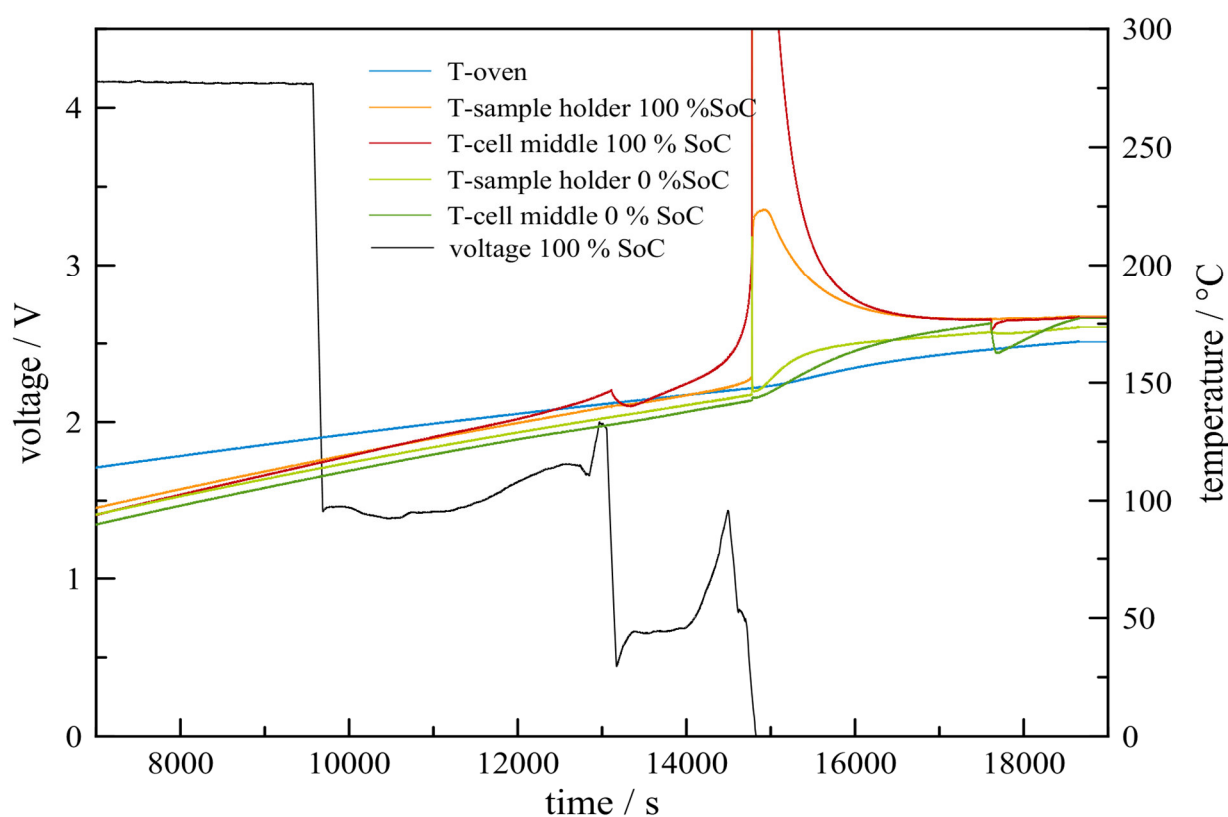
Figure 37: Temperature vs. time plot of the differential cell test experiment of the ICR18650-26F cell, the cell and sample holder temperatures of each cell as well as the oven temperature and the cell voltage of the charged cell are plotted over the time.

The charged cell vented at a cell temperature of 147.01 °C which reduced the temperature to 139.91 °C. The thermal runaway of the cell raised its temperature to 601.32 °C. With the thermal runaway event of the charged cell the temperature slope of the uncharged cell experienced an significant upswing. At a cell temperature of 175.32 °C the cell vented and its temperature declined to 162.56 °C. After this event the temperatures of the cells approached the sample holder temperature and no further reactions were observed.

3.9.2 Thermal analysis ICR18650-26F

The temperature vs. time plot of one of the three identically performed thermal ramp experiments for the ICR18650-26F cell is illustrated in Figure 38. With ongoing heating the cell and sample holder temperatures converged towards the oven temperature which started around 80 °C. At 147.80 °C an intense venting of the cell was observed and lowered the temperature by 7.89 K to 139.9 °C. The 1st venting dissipated 384 J of heat. The onset temperature of the ICR18650-26F was reached quickly after the venting when the cell regained a temperature of 147.43 °C. After a runtime of 14253 s the cell reached a heating rate of 2 °C min^{-1} at a thermal runaway onset temperature of 158.07 °C. During thermal runaway the cell reached an averaged, maximum temperature between the 3 thermocouples of 580.26 °C which generated 19.4 kJ of heat before it cooled down towards the oven temperature again.
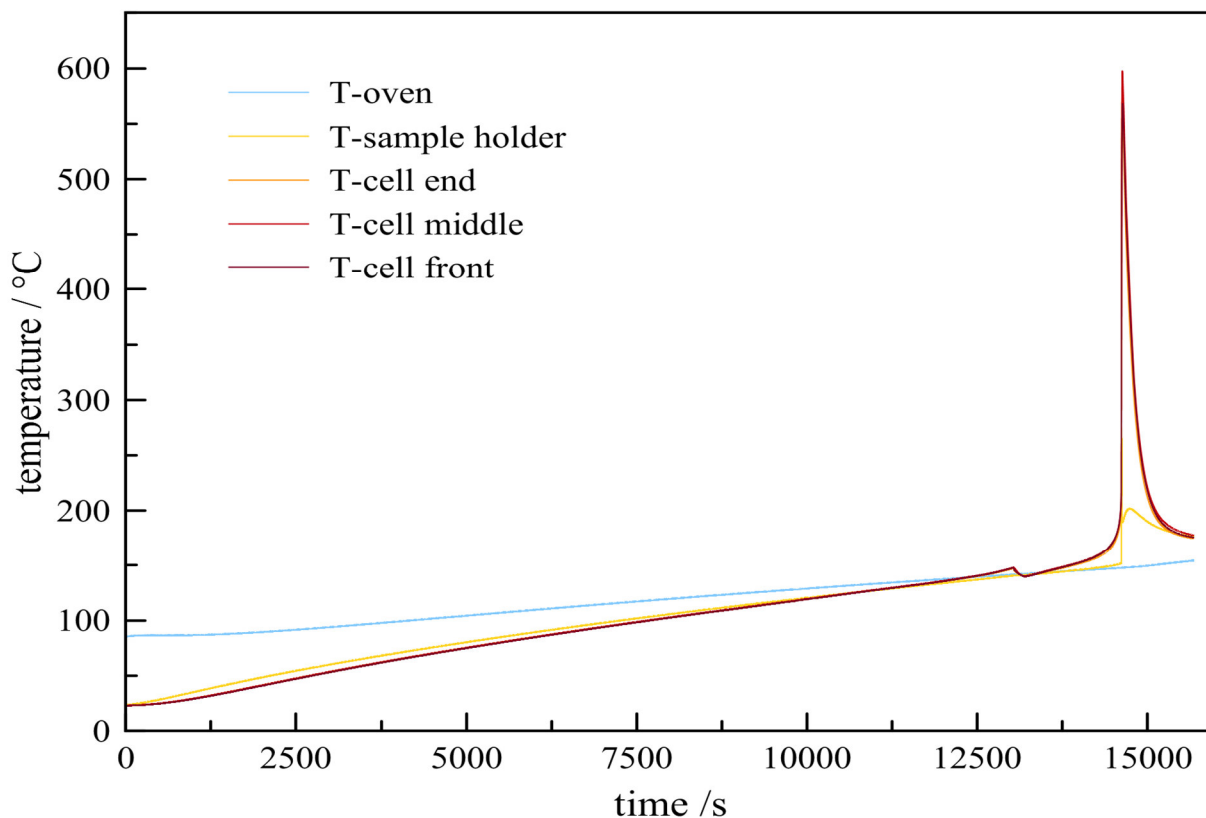
Figure 38: Temperature vs. time plot of the ICR18650-26F 3 thermal ramp experiment.

The values for the thermal experiments of the ICR18650-26F cells were summarized in the Table 18. The experiments 2 and 3 showed a significant cell venting, but no venting was observed by the thermal behavior in the experiment 1.

Table 18: Summary of the key thermal indicators of three identical thermal ramp experiments of the ICR18650-26F Li-ion cell.

experiment	Δm / g	T_{vent} / °C	Q_{vent} / kJ	T_{onset} / °C	T_{TR} / °C	T_{max} / °C	TR_{Rate} / °C min^{-1}	Q_{TR} / kJ
INR18650-26F 1	26.22	-	-	147.45	151.96	392.33	45.75	11,05
INR18650-26F 2	12.60	146.49	0.36	146.35	157.39	753.60	96.47	27,34
INR18650-26F 3	29.86	147.80	0.36	147.43	158.07	580.26	66.76	19,40

3.9.3 Gas analysis ICR18650-26F

The development of the gas composition inside the reactor by the ICR18650-26F cell is illustrated in Figure 39 for one of the three individual experiments. Sample 1 was taken before the first venting and solely consisted of the inert gas. A very small amount of CO_2 was identified in the sample 2 which was drawn from the reactor immediately after the 1st venting event. Sample 3 was drawn 120 s later and had a higher proportion of CO_2 which increased in sample 4 which was taken shortly before the thermal runaway. The samples 5 to 8 were taken immediately, 60, 120 and 300 s after the runaway. A dilution of the evolved gases by the flushing gas is illustrated by the ongoing increase of nitrogen in that samples.

	1	2	3	4	5	6	7	8
N2 / %	100.00	99.92	97.33	94.46	31.49	38.53	56.69	85.28
CO2 / %	0.00	0.08	2.67	5.51	9.14	7.80	6.81	3.20
CO / %	0.00	0.00	0.00	0.00	17.01	11.46	6.86	2.07
H2 / %	0.00	0.00	0.00	0.03	32.46	32.38	23.16	7.41
CH4 / %	0.00	0.00	0.00	0.00	4.47	4.72	3.23	1.11
C2H2 / %	0.00	0.00	0.00	0.00	0.00	0.00	0.00	0.00
C2H4 / %	0.00	0.00	0.00	0.00	4.80	4.34	2.80	0.89
C2H6 / %	0.00	0.00	0.00	0.00	0.64	0.77	0.45	0.04
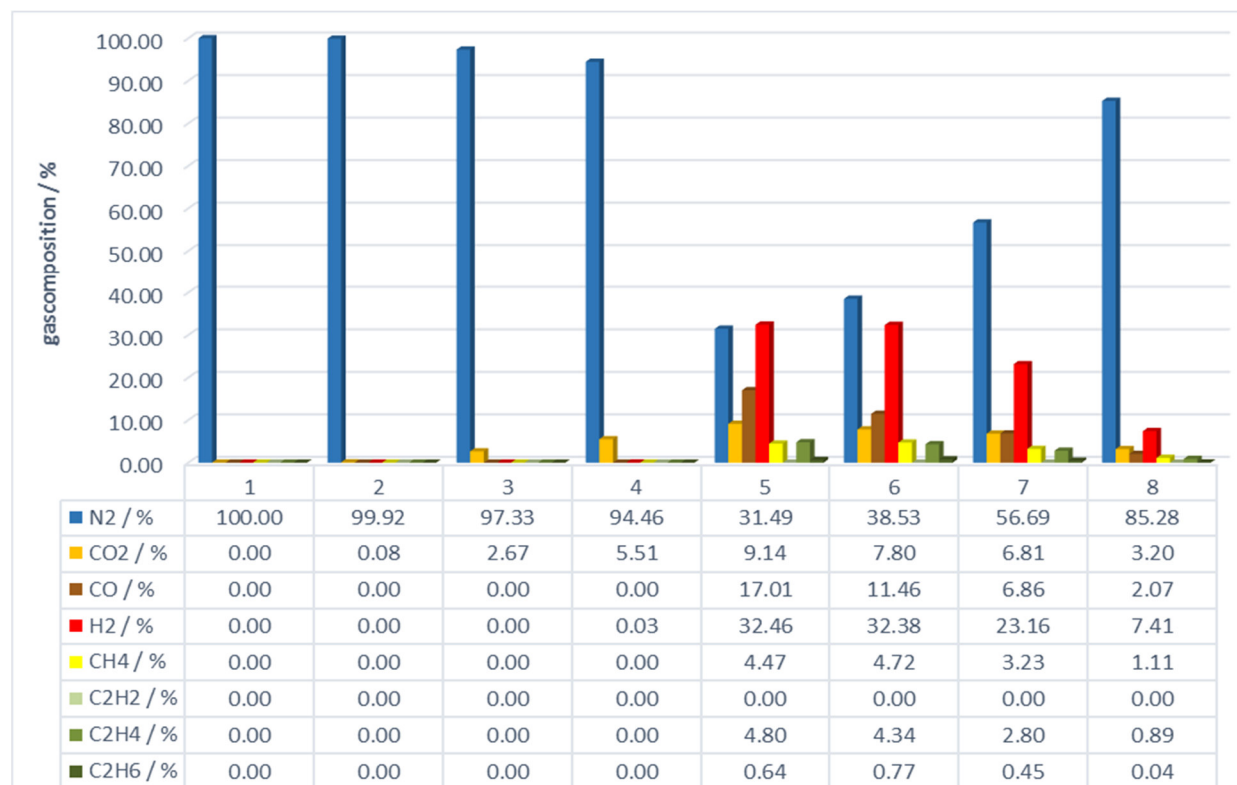
Figure 39: Gas composition of the eight samples taken from the reactor at specific moments during the ICR18650-26F 1 experiment.

The gas analysis results of the three individual experiments for the ICR18650-26F cell are summarized in Table 19. Each sample was taken immediately after the thermal runaway. The experiments 1 and 3 showed similar compositions while the experiment 2 showed significantly lower values of H_2 and CH_4 but higher values for CO_2 and CO.

Table 19: Gas composition of the three distinctive gas analysis experiments of the ICR18650-26F cell, each sample was taken immediately after the thermal runaway event.

experiment	N_2 / %	CO_2 / %	CO / %	H_2 / %	CH_4 / %	$C2H_2$ / %	$C2H_4$ / %	C_2H_6 / %
ICR18650-26F 1	31.49	9.14	17.01	32.46	4.47	0.00	4.80	0.64
ICR18650-26F 2	25.67	12.84	44.50	14.44	1.03	0.39	1.13	0.00
ICR18650-26F 3	21.25	8.88	28.53	35.06	3.26	0.00	2.69	0.33

As for the other cells also the gas volume for the ICR 18650-26F cell was determined in an individual water displacement experiment. During the slow heating of the cell the gas volume constantly grew with increasing temperature. Similar to the thermal experiment 1, mentioned above, no venting event was observed and the gasvolume reached 278 mL after a runtime of 12250 s. Afterwards the cell temperature started to increase intensively and generated a gas volume of 580 mL. At this point the cell experienced thermal runaway and contributed to a net gas volume of 3765 mL. The absolut amount of gas emitted during the whole experiment therefore was 4345 mL.

3.10 US18650VTC5A

The US18650VTC5A features a Li(NiMnCo)O_2 cathode and the investigated cells had an averaged weight of 47.48 ± 0.07 g. The cells nominal voltage is 3.6 V and its nominal capacity is rated at 2500 mAh. This translates to a gravimetric energy density of 189.6 Wh kg^{-1} and a volumetric energy density of 544.1 Wh L^{-1}. Of all the investigated cells the VTC5A had one of the smallest capacities but the highest continuous discharge current of 30 A. Therefore it is particularly adapted for high power applications with short run-times.

3.10.1 Differential cell experiment US18650VTC5A

The results of the differential cell test for the US18650VTC5A cells are plotted in Figure 40. The voltage curve showed a slow decline during the heat up of the 100 % SoC cell until it dropped from 4.17 V to a value as low as 0.02 V. This breakdown of the voltage happened after a experimental runtime of 8690s when a cell temperature of 110.75 °C was detected. The voltage remained low but slowly increased to 0.30 V when it quickly rose to 2.29 V after 10418 s at a cell temperature of 126.81 °C. The venting of the charged cell decreased the OCV again to 1.48V. It quickly increased afterwards and reached 2.75 V before it diminished. The thermal runaway of the cell induced a short increase to 0.83 V before the cell voltage wasn't measurable anymore.
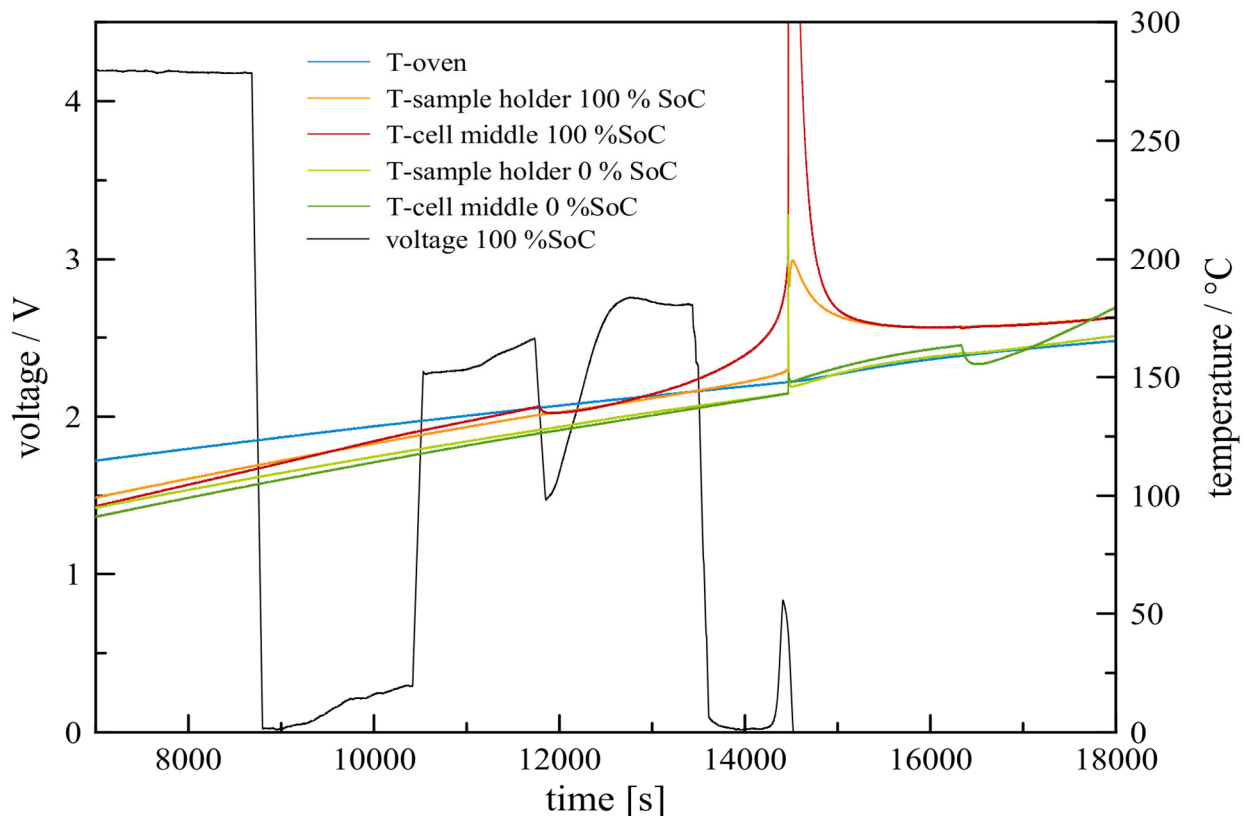
Figure 40: Temperature vs. time plot of the differential cell test experiment of the US18650 VTC5A cell, the cell and sample holder temperatures of each cell as well as the oven temperature and the cell voltage of the charged cell are plotted over the time.

The venting of the charged cell took place after 11788 s and reduced the temperature from 137.37 °C to 134.60 °C. The thermal runaway took place after 14490 s which increased the cell to a maximum temperature of 547.83 °C. The uncharged cell experienced an increase in temperature from the excess heat of the thermal runaway and vented after 16325 s and the cell temperature was reduced from 163.22 °C to 154.85 °C.

3.10.2 Thermal analysis US18650VTC5A

A typical temperature pathway of a thermal ramp experiment for the US18650VTC5A cell is displayed in Figure 41. Again the oven started at the pre-heated temperature of roughly 80 °C when the test was started. Constant heating of the oven slowly increased the sample holder and consequently the cell temperatures. After 11850 s a venting of the cell took place which can be seen in the plot as a quick cooling of the cell. This endothermic cooling reduced the cell temperature from 136.17 °C to 133.78 °C. The dissipated heat amounted to 120.0 J. After the venting the cell regained its former temperature and soon the cell temperature exceeded that of the sample holder and the oven. The thermal runaway of the cell resulted in an abrupt increase of the cell temperature to an averaged value of 563.83 °C. After the cell material was consumed in this exothermic event the cell cooled down to the oven temperature again.
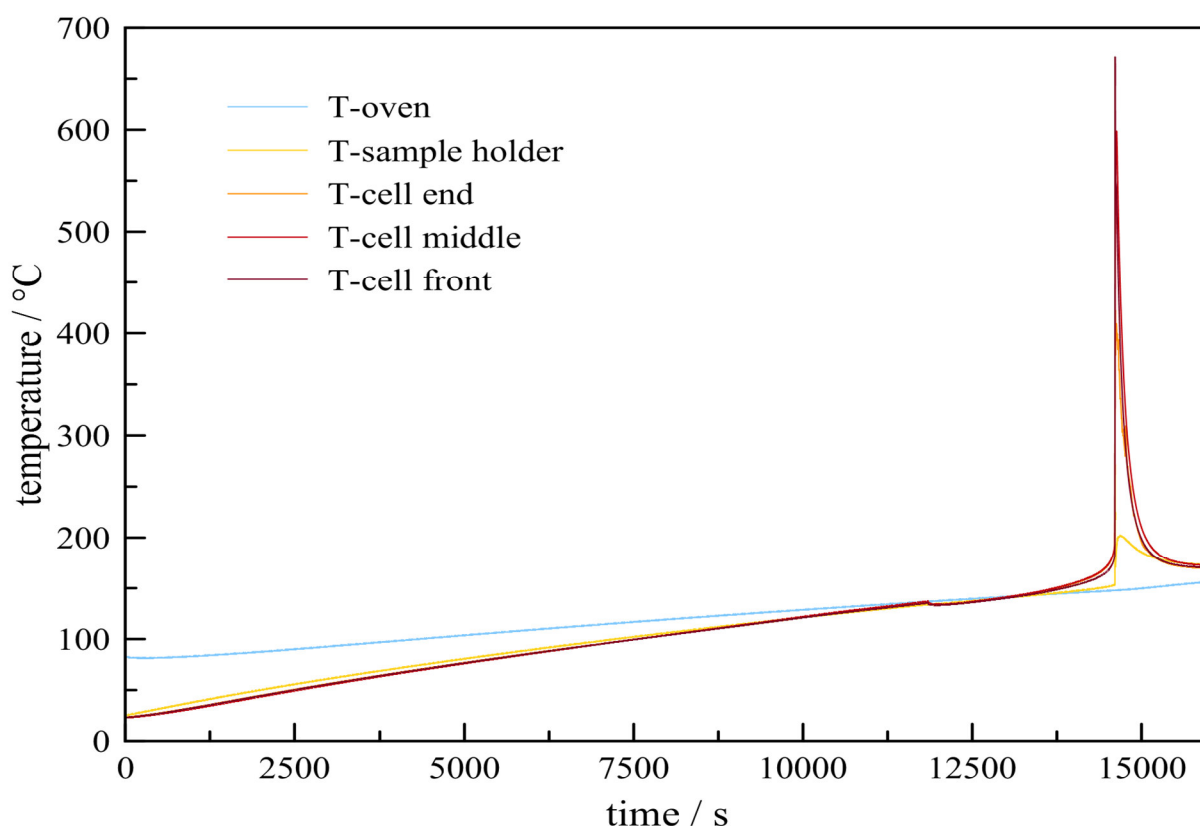
Figure 41: Temperature vs. time plot of the US18650VTC5A 2 thermal ramp experiment.

In the Table 20 the key thermal parameters of the three distinctive thermal ramp experiments are summarized.

Table 20: Summary of the key thermal indicators of three identical thermal ramp experiments of the US18650VTC5A Li-ion cell.

experiment	Δm / g	T_{vent} / °C	Q_{vent} / KJ	T_{onset} / °C	T_{TR} / °C	T_{max} / °C	TR_{Rate} / °C min^{-1}	Q_{TR} / kJ
US18650VTC5A 1	25.69	135.71	0.14	138.70	161.78	712.71	89.26	27.19
US18650VTC5A 2	29.28	136.17	0.12	137.00	160.87	563.83	74.24	19.89
US18650VTC5A 3	23.71	134.72	0.10	138.07	158.87	540.30	82.18	18.83

3.10.3 Gas analysis US18650VTC5A

	1	2	3	4	5	6	7	8
N2 / %	100.00	97.36	96.78	98.31	32.74	48.88	71.38	95.62
CO2 / %	0.00	2.49	3.05	1.41	9.01	6.62	6.17	1.62
CO / %	0.00	0.00	0.00	0.00	24.34	15.66	8.11	0.90
H2 / %	0.00	0.15	0.07	0.16	29.93	25.91	12.67	1.74
CH4 / %	0.00	0.00	0.00	0.00	2.43	1.96	1.11	0.00
C2H2 / %	0.00	0.00	0.00	0.00	0.27	0.00	0.00	0.00
C2H4 / %	0.00	0.00	0.00	0.09	1.26	0.94	0.51	0.01
C2H6 / %	0.00	0.00	0.10	0.03	0.02	0.03	0.06	0.11
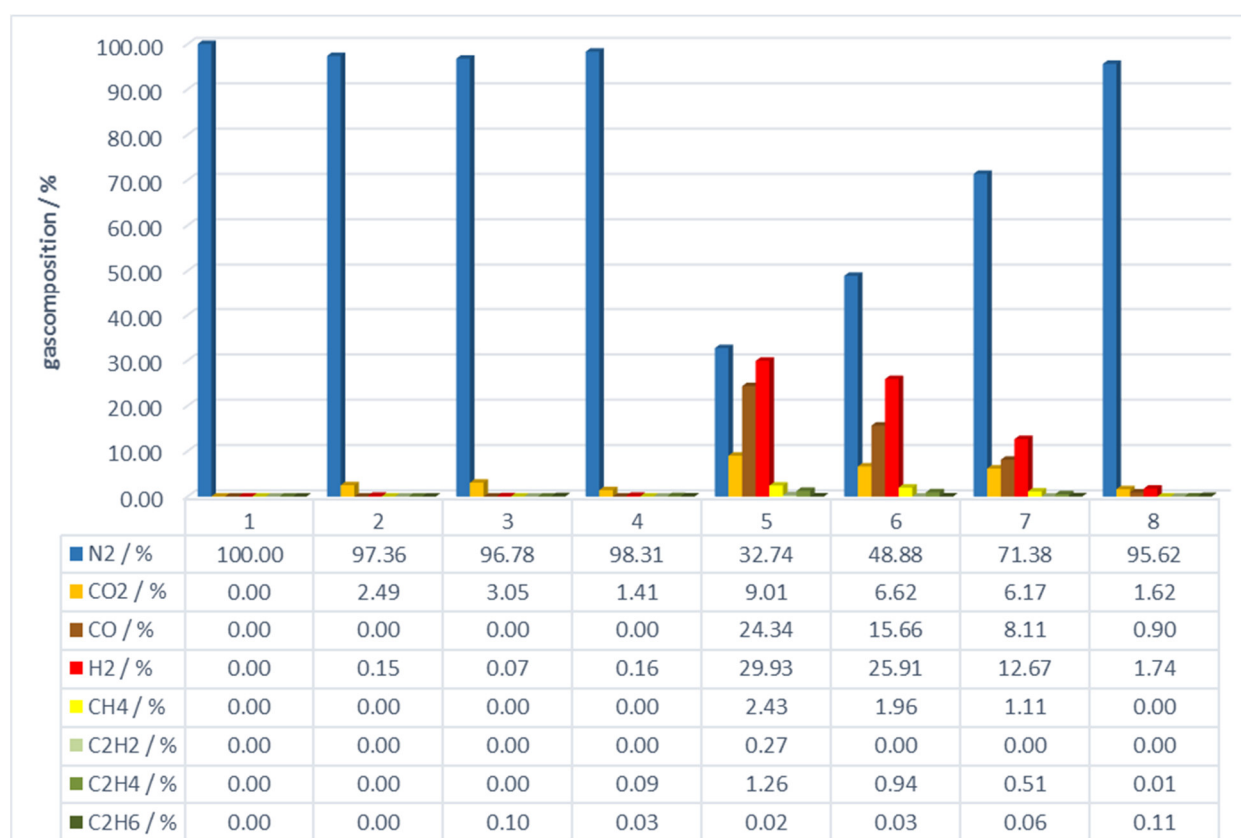
Figure 42: Gas composition of the eight samples taken from the reactor at specific moments during the US18650VTC-5A 2 experiment.

Figure 42 illustrates the gas composition of the eight gas samples taken during the thermal ramp test for the US18650VTC5A cell. Sample 1 was taken before the first venting of the cell and only consisted of pure nitrogen gas. Therefore the cell is still considered sealed and no electrolyte was released from the cell cap. Carbon dioxide and small quantities of hydrogen were detected in the samples 2 and 3. In the sample 3 which was taken 120 seconds after the venting also 0.10% of C_2H_6 was measured. Sample 4 was taken shortly before the runaway event and showed a similar composition. After the thermal runaway a gas mixture was identified which got progressively diluted by the inert gas.

The gas composition of the three US18650VTC5A experiments is summarized in Table 21 for the samples taken immediately after the thermal runaway event.

Table 21: Gas composition of the three distinctive gas analysis experiments of the US18650VTC5A cell, each sample was taken immediately after the thermal runaway event.

experiment	N_2 / %	CO_2 / %	CO / %	H_2 / %	CH_4 / %	C_2H_2 / %	C_2H_4 / %	C_2H_6 / %
US18650VTC5A 1	28.45	11.18	34.29	22.10	2.53	0.18	1.21	0.05
US18650VTC5A 2	32.74	9.01	24.34	29.93	2.43	0.27	1.26	0.02
US18650VTC5A 3	38.31	12.50	26.59	18.82	2.02	0.26	1.49	0.01

The amount of gaseous emissions during the thermal ramp experiments was also investigated for the US18650VTC5A. Before the venting of the cell an amount of 174 mL gas was displaced from the reactor. This was mostly due to the heat related expansion of the inert gas in the reactor. After the venting event the displaced gasvolume had increased to 560 mL. Therefore 386 mL of gas got released by the cell during the 1st venting event. With ongoing heating of the reactor, more inert gas got displaced due to the evaporation of minor amounts of remaining electrolyte and the gas expansion. Before the runaway this displaced gas volume was 638 mL and the thermal runaway event added 4358 mL which in the end amounted to 4996 mL of absolute gas displaced during the thermal ramp experiment of the US18650VTC5A.

4   DISCUSSION OF THE EXPERIMENTAL DATA

Thermal ramp experiments were conducted on nine different types of lithium ion batteries. The thermal behavior and gaseous emissions of the 18650 format cells were investigated.

The open circuit voltage of the charged cells investigated in the differential experiment showed a diverse behavior for the different cell types. However with the start of the heating a slow decline of the voltage was measured in all cells. This was due to a slow rise of the impedance of the cell with increasing temperature [19]. In a temperature range between 100 °C and 117 °C all cells experienced a strong decrease of the open circuit voltage. This progression of the voltage curve suggested an strong impedance jump and was associated with the positive temperature current disk. The PTC is designed to limit the current at temperatures around 110 °C and was responsible for this significant decrease of cell voltage [20, 21]. Sharp fluctuations of the cell voltage were observed after the first drop of the cell voltage around 110 °C. In this temperature range several effects and reactions took place and contributed to this fluctuating voltage behavior. The breakdown of the solid electrolyte interface (SEI) on the anode slowly initiated at temperatures around 90 – 120 °C [20, 6]. The breakdown of the protective SEI layer leads to the reduction of electrolyte with the lithiated carbon on the anode and is one of the first exothermic reactions that increases the cells temperature. However the thermal ramp experiments conducted in this work did not provide enough thermal sensibility to identify this low self heating reactions. Another strong decrease of the cell voltage was observed during the venting of the cells, except the 18650 HE4 cells which showed an increase of the cell voltage during the venting event. In all experiments performed on the NCR18650GA cell no venting was indicated by the typical endothermic cooling due to the expansion of the vent gases. However the gas analysis showed significant proportions of CO_2 before the actual thermal runaway event. This gives rise to the assumption that an opening of the cell vent occurred but did not happen in the spontaneous way as in the other cells. It is believed that all of the investigated cells rely on shutdown separators which are composed of polyethylene and polypropylene layers. This separators typically shows a steep increase in impedance at a cell temperature of 130 °C because the endothermic melting of the polyethylene membrane blocks the ion conducting pores. The separator itself remains mechanically stable until the melting of the polypropylene stability layer at 160 °C [5, 20]. Once the separator lost its stability it is very likely that internal short circuits between the electrodes occur which lead to a break down of the voltage. This break down of the open circuit voltage at cell temperatures around 160 °C was observed for the US18650VTC-5A, the ICR1865026-F, the 18650HE4 and the NCR18650B cells. For the other investigated cells, this expected behavior of the separator could not be manifested by the open current voltage measurements. Separators with ceramic coatings do not lose their stability until temperatures as high as 250 °C [19]. It is therefore assumed that the cells which showed no signs of internal short circuits were equipped with such a separator.

In none of the cells an open circuit voltage was measurable after the thermal runaway. It is believed that the measurement of the open circuit voltage without an electrical load is not a sufficient method to investigate the electrochemical behavior during the thermal runaway experiments. The combination of open circuit voltage and impedance measurement should give better information on the internal reactions and is part of further research activities.

A strong dependence of the cells thermal behavior on their state of charge was observed during the differential cell tests. None of the discharged cells experienced thermal runaway. However all discharged cells experienced venting except the NCR18650GA cells which did not vent unrelated to the state of charge. A sustainable temperature increase of the discharged cells was observed due to the thermal runaway of the charged cell in the differential cell tests. The discharged cells showed an accelerated temperature increase and vented in a temperature range around 160 °C. When compared to the charged cells a significantly higher amount of heat was dissipated by the discharged cells venting event. Because the electrolyte itself breaks down above 160 °C enough gas was generated for the venting of the discharged cells [23].

All of the charged cells experienced a highly exothermic thermal runaway event during the thermal ramp experiments. The averaged values for the venting temperature (T_{vent}), the onset temperature (T_{onset}), the initiation temperature of the thermal runaway (T_{TR}) and the maximum temperature of the cell (T_{max}) are summarized Table 22.

Table 22: Summarized parameters for the thermal investigations, averaged values with standard deviation of the three individual experiments.

	Tvent / °C	Tonset / °C	TTR / °C	Tmax / °C
NCR18650B	131.01 ± 0.53	157.69 ± 0.94	173.06 ± 0.78	685.80 ± 44.2
NCR18650BF	139.57 ± 2.01	138.35 ± 1.81	160.01 ± 0.69	648.41 ± 95.06
NCR18650GA	-	137.41 ± 3.95	156.48 ± 0.68	583.61 ± 17.22
ICR18650-32A	129.63 ± 1.17	144.56 ± 0.10	166.27 ± 0.59	672.23 ± 81.19
INR18650-35E	134.13 ± 0.85	139.11 ± 0.40	157.82 ± 0.38	660.96 ± 56.24
INR18650MJ1	121.96 ± 0.45	138.85 ± 0.34	150.81 ± 1.10	467.10 ± 37.36
18650HE4	117.32 ± 0.72	163.68 ± 1.41	195.81 ± 1.05	600.73 ± 44.21
ICR18650-26F	147.15 ± 0.66	147.10 ± 0.51	155.81 ± 2.73	575.40 ± 147.21
US18650VTC-5A	135.53 ± 0.60	137.92 ± 0.70	160.51 ± 1.21	605.61 ± 76.34

The thermal parameters of the individual cell tests were found to be very consistent for the individually performed thermal ramp experiments. The identification of the onset and thermal runaway temperature based on the heating rate had proven to be an adequate method to determine the self heating process of the cell.

After the above described first exothermic degradation reactions of the solid electrolyte interface which initiated at temperatures around 90 °C the breakdown significantly increased at 120 °C with the reduction of electrolyte at the exposed lithiated carbon anode [14]. The breakdown of the separator and the resulting short circuits can further increase the self heating [24]. With increasing temperatures of the cell, first reactions are initiated at the cathode around 140 – 160 °C, depending on its active material composition [19]. Oxygen is released from the metal oxide cathode during its decomposition. This leads to the oxidation of the electrolyte and is by far the most energetic runaway reaction [7]. In this work the first exothermic reactions were observed in a temperature range from 137 °C to 164 °C. With the onset of the self heating the cell temperature quickly rose and the cells experienced thermal runaway. The averaged thermal parameters for each cell types are illustrated in Figure 43. During the thermal investigations conducted for this work no apparent coherences could be found between the thermal properties of the different cell types and their cathode compositon or their nominal capacity.
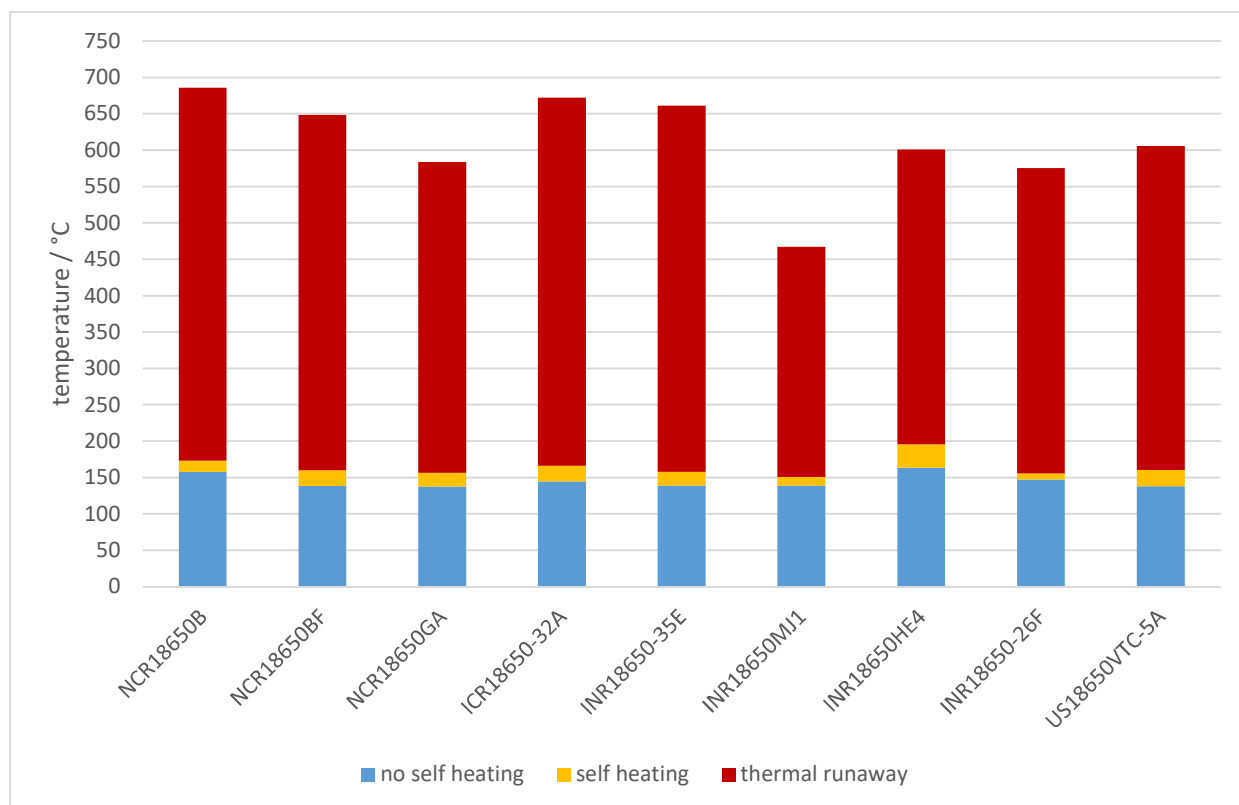
Figure 43: Thermal mapping of the 9 investigated cells, the respective thermal parameters are the averaged values of the three individual thermal ramp experiments.

Some cells experienced a violent rupturing of the cell can during thermal runaway and the cell constituents got partly ejected form the cell. It is believed that the maximum temperatures reached during the thermal runaway event are higher in the inside of the cell than the values measured with the thermocouples on the outside of the cell can. In several experiments the cell can violently bursted and the thermocouples on this positions showed higher values or even got destroyed. Investigations of the cells after the thermal runaway event showed a melting of the positive

electrode aluminum current collector foil. However the copper foil of the negative electrode was chipped but did not melt in any of the experiments. Therefore the internal temperature has been somewhere in between the melting point of aluminum (660 °C) and copper (1085 °C) [24, 25]. The three thermocouples on the cell can were used to evaluate the spatial distribution over the cell surface. The temperature signals showed similar temperature behavior during the thermal ramp experiments and it is believed that the metal can distributed the temperature uniformly over the cell surface. Only for the actual thermal runaway event temperature signals showed an inhomogeneous temperature distribution over the cell can surface. It is estimated that the temperature in the inner regions of the cell is higher than in the outer regions which are in contact with the cell can and that the thermal decomposition of the electrodes is procceding from the inside towards the outer layers [24].

The gas composition of each cell type was investigated at least three times in individual thermal ramp experiments. All cells remained sealed and released no gases until the venting of the cell whereby small quantities of mainly CO_2 gas, were released through the venting openings in the cell cap. Also the samples, taken between the venting and the thermal runaway event, contained gaseous emissions which gives rise to the assumption that the venting of gases sustained after the venting and that the cell vents were not blocked after the initial venting event. The venting of gases dissipated an amount of heat in the range of 50 to 360 J. The thermal runaway event emitted gases of very diverging compositions and generated an amount of heat in the range of 15.20 kJ to 25.59 kJ. Even for the same cell type the gas emissions of the individual experiments and the generated heat showed no coherences.

The samples taken after the thermal runaway event suggested that the evolution of the gases took place rapidly and after the maximum temperature was reached no further gases were released. This circumstance was also seen in the gas volume measurement were the evolution of gases during thermal runaway happened within a few seconds.

The volume emitted by the venting event ranged from 87 mL to 292 mL and from 2888 mL to 5904 mL for the thermal runaway event, depending on the cell type. A good coherence was found for repeated measurements of the same cell type. Therefore it is concluded that the gas volume emissions depend on the cell type and its composition. Additionally it was experimentally proven that an increase in the heating of the cells leads to an increase of gaseous emissions during the venting and the thermal runaway event.

5   LIST OF FIGURES

6   LIST OF TABELS

7 REFERENCES

[1] T. F. Stocker, D. Qin, G. K. Plattner, L. V. Alexander, S. K. Allen, N. L. Bindoff, F. M. Breon, J. A. Church, U. Cubasch, S. Emori, P. Forster, P. Friedlingstein, N. Gillett, J. M. Gregory, D. L. Hartmann, E. Jansen, B. Kirtman, R. Knutti , K. Krishna Kumar, P. Lemke, J. Marotzke, V. Masson-Delmotte, G. A. Meehl, I. I. Mokhov, S. Piao, V. Ramaswamy, D. Randall, M. Rhein, M. Rojas, C. Sabine, D. Shindell, L. D. Talley, D. G. Vaughan und S. P. Xie, „Technical Summary in Climate Change 2013: The Physical Science Basis," Cambridge University Press, Cambridge, 2013.

[2] C. Pillot, „Future trends in the rechargeable battery market," Montreux, Switzerland, 2015.

[3] A. Dinger, R. Martin, X. Mosquet, M. Rabl, D. Rizoulls, M. Russo und G. Sticher, „Batteries for Electric Cars," Boston Consulting Group, Boston, 2010.

[4] R. J. Brodd, Batteries for Sustainability: Selected Entries from the Encyclopedia of Sustainability and Technology, New York: Springer Science +Business Media, 2013.

[5] D. H. Doughty und A. A. Pesaran, „Vehicle Battery Safety Roadmap Guidance," National Renewable Energy Laboratory, Denver, Colorado, 2012.

[6] Q. Wang, P. Ping, X. Zhao, G. Chu, J. Sun und C. Chen, „Thermal runaway caused fire and explosion of lithium ion battery," *Journal of Power Sources,* pp. 210-224, 2012.

[7] D. Doughty und P. E. Roth, „ A General Discussion on Li Ion Battery Safety," The Electrochemical Society, New Jersey, USA, 2012.

[8] L. H. Saw, Y. Ye und A. A. Tay, „Integration issues of lithium-ion battery into electric vehicle battery pack," *Journal of Cleaner Production,* pp. 1032-1045, 2016.

[9] J. Tübke , „ict.fraunhofer.de," fraunhofer institut für chemische Technologie, 2016. [Online]. Available: http://www1.ict.fraunhofer.de/deutsch/scope/ae/ion.html. [Zugriff am 23 11 2016].

[10] P. T. Moseley und J. Garche, Electrochemical Energy Storage for Renewable Sources and Grid Balancing, Oxford: Elsevier, 2015.

[11] A. W. Golubkov, S. Scheikl, R. Planteu, G. Voitic, H. Wiltsche, C. Stangl, G. Fauler, A. Thaler und V. Hacker , „Thermal runaway of commercial 18650 Li-ion batteries with LFP and NCA cathodes - impact of state of charge and overcharge," *Royal Society of Chemistry,* pp. 57171-57186, 2015.

[12] D. P. Abraham, E. P. Roth, R. Kostecki, K. McCarthy, S. MacLaren und D. H. Doughty, „Diagnostic examination of thermally abused high-power lithium-ion cells," *Journal of Power Sources 161,* pp. 648-657, 2006.

[13] C. J. Orendorff, J. Lamb, L. A. M. Steele, S. W. Spangler und J. Langendorf, „Quantification of Lithium-ion Cell Thermal Runaway Energetics," Sandia National Laboratories, Albuquerque, 2016.

[14] E. P. Roth und D. H. Doughty, „Thermal abuse performance of high-power 18650 Li-ion cells," *Journal of Power Sources 128,* pp. 308-318, 2004.

[15] C.-Y. Jhu, Y.-W. Wang, C.-M. Shu, J.-C. Chang und J.-C. Wu, „Thermal explosion hazards on 18650 lithium ion batteries with a VSP2 adiabatic calorimeter," *Journal of Hazardous Materials 192,* pp. 99-107, 2011.

[16] P. T. Coman, S. Rayman und R. E. White, „A lumped model of venting during thermal runaway in a cylindrical Lithium Cobalt Oxide lithium-ion cell," *Journal of Power Sources,* pp. 56-62, 2016.

[17] A. W. Golubkov, D. Fuchs, J. Wagner, H. Wiltsche, C. Stangl, G. Fauler, G. Voitic, A. Thaler und Hacker Viktor, „Thermal-runaway experiments on consumer Li-ion batteries with metal-oxide and olivin-type cathodes," *Royal Society of Chemistry Advances,* pp. 3633-3642, 4 2014.

[18] H. Maleki, S. Al Hallaj, J. R. Selman, R. B. Dinwiddie und H. Wang, „Thermal Properties of Lithium-Ion Battery and Components," *Journal of The Electrochemical Society 146,* pp. 947-954, 1999.

[19] X. Feng, M. Fang, X. He, M. Ouyang, L. Lu, H. Wang und M. Zhang, „Thermal runaway features of large format prismatic lithium ion battery using extended volume accelerating rate calorimetry," *Journal of Power Sources,* pp. 294-301, 2014.

[20] G. Venugopal, „Characterization of thermal cut-off mechanisms in prismatic lithium-ion batteries," *Journal of Power Sources,* pp. 231-237, 2001.

[21] D. D. MacNeil, T. D. Hatchard und J. R. Dahn, „A Comparison Between the High Temperature Electrode/Electrolyte Reactions of LixCoO2 and LixMn2O4," *Journal of the Electrochemical Society,* pp. 755-761, 2001 July.

[22] M. N. Richard und J. R. Dahn, „Accelerating Rate Calorimetry Study on the Thermal Stability of Lithium Intercalated Graphite in Electrolyte I. Experimental," *Journal of The Electrochemical Society,* pp. 2068-2077, 1999.

[23] R. P. E., „Abuse Response of 18650 Li-Ion Cells with Different Cathodes Using EC:EMC/LiPF6 and EC:PC:DMC/LiPF6 Electrolytes," *Electrochemical Society Transactions,* pp. 19-41, 2008.

[24] E. P. Roth, D. H. Doughty und D. L. Pile, „Effects of separator breakdown on abuse response of 18650 Li-ion cells," *Journal of Power Sources,* pp. 579-583, 2007.

[25] D. P. Finegan, M. Scheel, J. B. Robinson, B. Tjaden, I. Hunt, T. J. Mason, J. Millichamp, M. D. Michiel, G. J. Offer, G. Hinds, D. J. Brett und P. R. Shearing, „In-operando high-speed tomography of lithium-ion batteries during thermal runaway," *Nature communications,* p. DOI:10.1038/ncomms7924, 2015.

[26] M. Buser und J. Mählß, „Lithium Batteries Fire and Safety Hazards Efficient loss prevention and fire fighting," Batteryuniversity GmbH, Karlstein, 2016.

[27] D. D. MacNeil, D. Larcher und J. R. Dahn, *Journal of Electrochemical Society,* pp. 3596-3602, 1999.

[28] D. D. MacNeil, Z. Lu, Z. Chen und J. R. Dahn, „A comparison of the electrode/electrolyte reaction at elevated temperatures for various Li-ion battery cathodes," *Journal of Power Sources,* pp. 8-14, June 2002.

[29] O. S. Mendoza-Hernandez, H. Ishikawa, Y. Nishikawa, Y. Maruyama und M. Umeda, „Cathode material comparison of thermal runaway behabior of Li-ion cells at different state of charges including over charge," *Journal of Power Sources 280,* pp. 499-504, 2015.